

AN ABSTRACT OF THE THESIS OF

Mary Jane N. Shroyer for the degree of Master of Science in Microbiology presented on August 31, 1999. Title: *Escherichia coli* Uracil-DNA Glycosylase: DNA Binding, Catalysis, and Mechanism of Action.

Redacted for Privacy

Abstract approved: _____

Dale W. Mosbaugh

The role of the conserved histidine-187 located in the leucine loop of *Escherichia coli* uracil-DNA glycosylase (Ung) was investigated. The vector pUngH187D containing the *ungH187D* gene was unstable in *E. coli ung* and *ung recA* strains; thus, the protein was overproduced in wild type *E. coli*, purified to apparent homogeneity, and characterized relative to wild type Ung. Ung H187D differed with respect to specific activity, pH optimum, substrate specificity, DNA binding, inhibition by uracil analogs, and enzyme kinetics. Most notably, Ung H187D exhibited a 55,000-fold lower specific activity and a shift in pH optimum from pH 8.0 to 7.0. Under reaction conditions optimal for wild type Ung (pH 8.0), the substrate preference of Ung H187D on oligonucleotide substrates was U/G-25-mer > U-25-mer > U/A-25-mer. However, Ung H187D processed these substrates at comparable rates at pH 7.0 with ~3-fold stimulation in activity relative to the U-25-mer at pH 8.0. Ung H187D was less susceptible than Ung to inhibition by uracil, 6-amino uracil, and 5-fluorouracil but retained the ability to bind uracil-DNA glycosylase inhibitor (Ugi) protein. Using UV-catalyzed protein/DNA crosslinking to measure DNA binding affinity, the efficiency of Ung H187D binding to thymine-, uracil-, and apyrimidinic site-containing DNA was $(dT_{20}) = (dT_{19}-U) \geq (dT_{19}-AP)$. Measurements of reaction kinetics at pH 8.0 with [uracil-³H] DNA indicated the k_{cat} of Ung H187D was reduced 48,000-fold relative to Ung, while V_{max}/K_m was essentially unchanged. Steady state

fluorescence measurements using a duplex 2-aminopurine-containing oligonucleotide (27-mer) demonstrated a ~870-fold reduction in k_{cat} for Ung H187D relative to Ung at pH 7.4. Based on the biochemical properties and X-ray crystallographic structure of Ung H187D, a reaction mechanism was proposed wherein His-187 stabilizes the developing negative charge on the uracil ring and polarization of the N1-C1' glycosidic bond.

Additionally, polyclonal antisera to Ung and Ugi were raised which were capable of inhibiting enzyme and inhibitor function. The Ung antiserum was also immunoreactive with mitochondrial uracil-DNA glycosylases from pig and rat. Rat liver mitochondrial extracts were subjected to Ugi-affinity purification, yielding a single polypeptide (M_r 25,000) similar in size to *E. coli* Ung which cross-reacted with Ung antibody.

Escherichia coli Uracil-DNA Glycosylase:
DNA Binding, Catalysis, and Mechanism of Action

by

Mary Jane N. Shroyer

A THESIS

submitted to

Oregon State University

in partial fulfillment of
the requirements for the
degree of

Master of Science

Completed August 31, 1999
Commencement June 2000

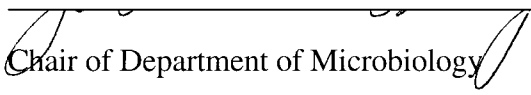
Master of Science thesis of Mary Jane N. Shroyer presented on August 31, 1999

APPROVED:

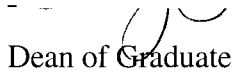
Redacted for Privacy

Major Professor, representing Microbiology

Redacted for Privacy


Chair of Department of Microbiology

Redacted for Privacy


Dean of Graduate School

I understand that my thesis will become part of the permanent collection of Oregon State University libraries. My signature below authorizes release of my thesis to any reader upon request.

Redacted for Privacy



Mary Jane N. Shroyer, Author

TABLE OF CONTENTS

	<u>Page</u>
1. INTRODUCTION.....	1
1.1 Uracil Residues in DNA.....	1
1.1.1 Incorporation of Uracil Residues During DNA Synthesis	1
1.1.2 Deamination of Cytosine.....	1
1.1.2.1 Spontaneous Cytosine Deamination	1
1.1.2.2 Induced Cytosine Deamination.....	2
1.1.3 The Effects of Uracil in DNA	2
1.2 Uracil-DNA Glycosylase	3
1.2.1 <i>Escherichia coli</i> Uracil-DNA Glycosylase.....	4
1.2.2 Mammalian Uracil-DNA Glycosylase.....	4
1.2.2.1 Nuclear and Mitochondrial Uracil-DNA Glycosylase.....	4
1.2.2.2 Cyclin-Like Uracil-DNA Glycosylase.....	6
1.2.3 Other Enzymes Exhibiting Uracil-DNA Glycosylase Activity.....	8
1.2.3.1 Thymine-DNA Glycosylase.....	8
1.2.3.2 Mismatch-Specific Uracil-DNA Glycosylase.....	10
1.2.3.3 Single-Strand-Selective Monofunctional Uracil-DNA Glycosylase.....	12
1.2.3.4 Thermostable Uracil-DNA Glycosylases.....	14
1.2.4 Structure of Uracil-DNA Glycosylase	15
1.3 Uracil-Initiated Base Excision Repair	17
1.3.1 Prokaryotic Uracil-Initiated Base Excision Repair	17
1.3.1.1 Removal of Uracil from DNA.....	17
1.3.1.2 AP-Site Incision and Removal of 5'-Deoxyribose Phosphate.....	20
1.3.1.3 DNA Synthesis and Ligation.....	21
1.3.2 Eukaryotic Uracil-Initiated Base Excision Repair.....	23
1.4 Bacteriophage PBS2 Uracil-DNA Glycosylase Inhibitor Protein.....	27
1.4.1 Bacteriophage PBS2	27
1.4.2 PBS2 Uracil-DNA Glycosylase Inhibitor.....	27
1.4.3 Structure of Uracil-DNA Glycosylase Inhibitor Protein.....	28
1.5 Research Objectives.....	29

TABLE OF CONTENTS (Continued)

	<u>Page</u>
2. MATERIALS AND EXPERIMENTAL PROCEDURES	31
2.1 Materials	31
2.1.1 Chemicals	31
2.1.2 Radionucleotides	32
2.1.3 Bacterial Growth Media	32
2.1.4 Bacterial Strains and Bacteriophage	32
2.1.5 Plasmids	34
2.1.6 Chromatographic Resins	34
2.1.7 Oligonucleotides	34
2.1.8 Enzymes	35
2.2 Experimental Procedures	35
2.2.1 Preparation of Chromatographic Resins	35
2.2.1.1 Preparation of DEAE-Cellulose, Sephadex G-25 and G-75, Bio-Gel P-4, and Poly(U) Sepharose	35
2.2.1.2 Preparation of Hydroxylapatite	36
2.2.1.3 Preparation of Single-Stranded DNA-Agarose	36
2.2.1.4 Preparation of Dowex 1-X8	37
2.2.1.5 Preparation of Ung- and Ugi-Sepharose	37
2.2.2 Preparation of Dialysis Tubing	38
2.2.3 Protein Concentration Measurements	39
2.2.3.1 Concentration Determination by Bradford Assay	39
2.2.3.2 Concentration Determination by Spectrophotometric Measurements	39
2.2.4 Small-Scale Preparation of Plasmid DNA	39
2.2.5 Restriction Enzyme Digestion of Plasmid DNA	40
2.2.6 Oligonucleotide Purification	41
2.2.7 5'-end ³² P-Phosphorylation of Oligonucleotides	41
2.2.8 Generation of Abasic Site-Containing Oligonucleotide	42
2.2.9 Hybridization of Oligonucleotides	42
2.2.10 Electroporation of <i>E. coli</i> with Plasmid DNA	43
2.2.11 Transduction of <i>E. coli</i> BW310 by P1vir	44
2.2.12 Preparation of Crude Cell Extracts	44
2.2.13 Purification of <i>E. coli</i> Uracil-DNA Glycosylase	45
2.2.13.1 Large Scale Purification of Ung	45
2.2.13.2 Purification of [³ H-Leu]Ung	47
2.2.13.3 Purification of Ung H187D	47
2.2.13.4 Rechromatography of Ung and Ung H187D	47

TABLE OF CONTENTS (Continued)

	<u>Page</u>
2.2.14 Purification of PBS2 Uracil-DNA Glycosylase Inhibitor Protein	48
2.2.14.1 Large Scale Purification of Ugi	48
2.2.14.2 Purification of [³⁵ S-Met]Ugi	49
2.2.15 Ung- and Ugi-Sepharose Chromatography	49
2.2.16 Isolation of Liver Mitochondria	50
2.2.17 Purification of Mitochondrial Ung	51
2.2.18 Polyacrylimide Gel Electrophoresis	52
2.2.18.1 Sodium Dodecyl Sulfate Polyacrylamide Gel Electrophoresis	52
2.2.18.2 Nondenaturing Polyacrylamide Gel Electrophoresis	53
2.2.18.3 Polyacrylamide Sequencing-Gel Electrophoresis	53
2.2.19 Agarose Gel Electrophoresis	53
2.2.20 Quantitation of Radiolabeled Proteins and DNA from Polyacrylimide Gels	54
2.2.21 Synthesis of [<i>uracil</i> - ³ H] DNA	54
2.2.22 Enzyme Assays	55
2.2.22.1 Ugi Assay	55
2.2.22.2 Ung Assay	56
2.2.22.3 Assay for pH Optima	56
2.2.22.4 Substrate Titration and Uracil Inhibition Assays	57
2.2.22.5 Assay for Substrate Specificity	57
2.2.22.6 Ung/Ugi Binding Assay	58
2.2.22.7 Assay of DNA Binding by Ung Using UV-Catalyzed Crosslinking Reactions	58
2.2.23 Steady-State Fluorometry	59
2.2.24 Polyclonal Antiserum Production	59
2.2.25 Functional Assay of Serum	60
2.2.26 Immunoassay of Serum and Affinity Purified Antibody	60
2.2.27 Western Blot Analysis of Ung-Containing Samples	61
2.2.28 Antibody Purification	62
 3. RESULTS	 65
 3.1 Overproduction and Characterization of Uracil-DNA Glycosylase H187D	 65
3.1.1 Verification of Ung and Ung H187D Overexpression Vectors	65
3.1.2 Transformation of <i>E. coli</i> BD2314 (<i>ung</i> -152::Tn10) and BW310 (<i>ung</i> -1) with pKK223-3, pSB1051 and pUngH187D	70

TABLE OF CONTENTS (Continued)

	<u>Page</u>
3.1.3 Construction of <i>E. coli</i> <i>recA ung</i> Strains for Overexpression of the <i>ungH187D</i> Gene.....	73
3.1.4 Transformation of <i>E. coli</i> MJS100 with pSB1051 and pUngH187D	73
3.1.5 Overproduction of the Ung H187D Protein	78
3.1.6 Purification of the Ung H187D Protein.....	78
3.1.7 Rechromatography of Ung H187D on Single-Stranded DNA Agarose	90
3.1.8 Ability of Ung and Ung H187D to Bind the Uracil-DNA Glycosylase Inhibitor	93
3.1.9 pH Optimum of Ung H187D Activity.....	93
3.1.10 Substrate Specificity of Ung and Ung H187D	93
3.1.11 Effect of Uracil on Ung and Ung H187D Activity	98
3.1.12 Ability of Ung and Ung H187D to Bind DNA	107
3.1.13 Effect of Uracil on DNA Binding.....	112
3.1.14 Enzyme Kinetics of Ung and Ung H187D.....	112
3.2 Ugi-Affinity Purification of Mitochondrial Uracil-DNA Glycosylases	126
3.2.1 Production of Polyclonal Antisera to Uracil-DNA Glycosylase and Uracil-DNA Glycosylase Inhibitor	126
3.2.2 Preparation of Ugi- and Ung-Sepharose	126
3.2.3 Affinity Chromatography of Uracil-DNA Glycosylase	129
3.2.4 Affinity Purification of Polyclonal Antibody to Uracil-DNA Glycosylase.....	139
3.2.5 Purification of Ung from Mitochondrial Extracts.....	144
4. DISCUSSION	154
4.1 Overproduction and Characterization of Uracil-DNA Glycosylase H187D	154
4.2 Ugi-Affinity Purification of Mitochondrial Uracil-DNA Glycosylases	168
BIBLIOGRAPHY.....	173

LIST OF FIGURES

<u>Figure</u>	<u>Page</u>
1. Restriction maps of pSB1051 and pUngH187D overexpression vectors	66
2. Restriction site analysis of overexpression vectors isolated from <i>E. coli</i> strain JM105.....	68
3. <i>BamH</i> I restriction site analysis of overexpression vectors from <i>E. coli</i> strains BD2314 and BW310.....	71
4. UV light sensitivity of <i>E. coli</i> BW310, JC10289, and MJS100.....	74
5. <i>BamH</i> I restriction site analysis of <i>ung</i> overexpression vectors isolated from <i>E. coli</i> MJS100.....	76
6. Overproduction of Ung and Ung H187D.....	79
7. Scheme for purification of Ung and Ung H187D from <i>E. coli</i> JM105	81
8. Sephadex G-75 chromatography of Ung H187D.....	84
9. Hydroxylapatite chromatography of Ung H187D.....	86
10. Single-stranded DNA agarose and Poly(U) Sepharose chromatography of Ung H187D	88
11. Rechromatography of Ung H187D on single-stranded DNA agarose	91
12. Binding of Ung and Ung H187D by uracil-DNA glycosylase inhibitor protein.....	94

LIST OF FIGURES (Continued)

<u>Figure</u>	<u>Page</u>
13. Comparison of pH optima of wild type Ung and Ung H187D activity	96
14. Substrate specificity of Ung and Ung H187D at pH 8.0	99
15. Substrate specificity of Ung and Ung H187D at pH 7.0	102
16. Effect of uracil on wild type Ung and Ung H187D activity	105
17. Relative ability of Ung and Ung H187D to form UV-catalyzed cross-links with dT ₂₀	108
18. Effect of uracil- and AP-sites on UV-catalyzed cross-linking of Ung and Ung H187D to dT ₂₀	110
19. Effect of free uracil on UV-catalyzed cross-linking of Ung and Ung H187D to dT ₂₀	113
20. Effect of substrate concentration on Ung and Ung H187D activity	115
21. Steady state kinetics of Ung with a 2-aminopurine-containing double-stranded oligonucleotide.....	119
22. Steady state kinetics of Ung H187D with a 2-aminopurine-containing double-stranded oligonucleotide.....	122
23. Double reciprocal plots of Ung and Ung H187D hydrolysis of a 2-aminopurine-containing double-stranded oligonucleotide	124
24. Binding capacity of Ugi-Sepharose.....	130

LIST OF FIGURES (Continued)

<u>Figure</u>	<u>Page</u>
25. Binding capacity of Ung-Sepharose	132
26. Recovery of Ung from <i>E. coli</i> cell extracts by Ugi-Sepharose chromatography	135
27. Elution of <i>E. coli</i> Ung from Ugi-Sepharose.....	137
28. Determining elution conditions for affinity purification of polyclonal antibody to Ung using Ung-Sepharose.....	140
29. Affinity purification of anti-Ung polyclonal antibody.....	142
30. Detection of Ung in mitochondrial extracts using Western blot analysis	145
31. Scheme for purification of rat or pig liver mitochondrial Ung.....	147
32. Purification of uracil-DNA glycosylase from rat liver mitochondrial extracts.....	150
33. Purification of uracil-DNA glycosylase from pig liver mitochondrial extracts.....	152
34. Model of <i>E. coli</i> Ung binding to uracil-containing DNA.....	157
35. Scheme of the reaction mechanism for cleavage of the N1-C1' glycosylic bond by <i>E. coli</i> Ung.....	164

LIST OF TABLES

<u>Table</u>	<u>Page</u>
1. <i>DNA Interactions and Amino Acid Homology of Human Uracil-DNA Glycosylase</i>	19
2. <i><u>E. coli</u> Strains and Genotypes</i>	33
3. <i>Buffer Conditions for Ung-Sepharose Affinity Chromatography</i>	63
4. <i>Kinetic Parameters for Wild Type and H187D Mutant Uracil-DNA Glycosylases on Calf Thymus [uracil-³H] DNA Substrate</i>	117
5. <i>Inhibition of Uracil-DNA Glycosylase by Polyclonal Antisera to <u>E. coli</u> Uracil-DNA Glycosylase</i>	127
6. <i>Inhibition of Uracil-DNA Glycosylase Inhibitor by Polyclonal Antisera to PBS2 Uracil-DNA Glycosylase Inhibitor</i>	128

***Escherichia coli* Uracil-DNA Glycosylase: DNA Binding, Catalysis, and Mechanism of Action.**

1. INTRODUCTION

1.1 Uracil Residues in DNA

1.1.1 Incorporation of Uracil Residues During DNA Synthesis

Uracil is introduced into genomic DNA at low levels because deoxyuridine triphosphate (dUTP) is utilized efficiently by DNA polymerases in place of deoxythymidine triphosphate (dTTP) during DNA synthesis (12, 28, 99). The incorporation of dUMP in place of dTMP results in U·A basepairs (99). The level of uracil residue incorporation is dependent on the intracellular concentration of dUTP relative to dTTP (147). It is estimated that the concentrations of dUTP and dTTP in *Escherichia coli* are 0.5 μ M and 150 μ M, respectively, resulting in the introduction of about 1 uracil nucleotide for every 300 thymine nucleotides incorporated (120). In bacteria, accumulation of dUTP results from phosphorylation of dUDP or deamination of dCTP by deoxycytidine triphosphate (dCTP) deaminase (98). Deoxyuridine 5'-triphosphate nucleotidohydrolase (dUTPase) minimizes the intracellular dUTP pool by hydrolyzing dUTP to dUMP, which is used in dTTP biosynthesis, and pyrophosphate (120). The small amount of dUMP that becomes incorporated into DNA is rapidly excised by uracil-DNA glycosylase (Ung) in the first step of uracil-initiated base excision repair (20, 66, 69).

1.1.2 Deamination of Cytosine

1.1.2.1 Spontaneous Cytosine Deamination

Deamination of cytosine residues results in the introduction of U·G mispairs into DNA (32, 34). Deamination may be spontaneous or

environmentally induced (17, 40, 70). The rate of spontaneous cytosine deamination is estimated to be 7×10^{-13} and $1 \times 10^{-10} \text{ sec}^{-1}$ for double- and single-stranded DNA, respectively (40). Because the rate of deamination is more than 100 times greater for single-stranded DNA, the genome may be more susceptible to deamination during transcription and replication, which involve transient denaturation of double-stranded DNA (70).

1.1.2.2 Induced Cytosine Deamination

Cytosine deamination may be induced by ultraviolet (UV) irradiation (132) or chemical modification (81, 119). Sodium bisulfite (18, 50), nitrous acid (78, 118), and strong alkali (139) are capable of promoting deamination reactions. Nitrous acid acts non-specifically, deaminating adenine and guanine as well as cytosine residues in single- and double-stranded DNA (118). In contrast, unpaired cytosine is exclusively targeted by sodium bisulfite (50). In addition, the rate of cytosine deamination increases with temperature, suggesting that uracil-DNA repair may pose a greater challenge for thermophilic organisms (70).

1.1.3 The Effects of Uracil in DNA

The introduction of uracil into DNA has negative biological consequences. Although uracil and thymine are structurally similar, the methyl group of thymine projects into the major groove of duplex DNA. This structural feature is absent when uracil replaces thymine in DNA. Thus, substitution of uracil for thymine may result in the disruption of protein-DNA interactions required for normal cell processes. For example, substitution of uracil for thymine at position 13 of the *lac* operator reduces the *in vitro* binding affinity of the *lac* repressor (37). This is also observed in *E. coli dut ung* where uninduced β -galactosidase is overproduced 20-fold when uracil residues accumulate in the bacterial genome (29). Similarly, the incorporation of uracil residues into restriction endonuclease recognition sites has been shown to reduce rates of cleavage by *HpaI*, *HindII* and *HindIII* endonucleases (11). In

addition to altering protein-DNA interactions and gene expression, the introduction of uracil residues into DNA may lead to mutagenesis. Duncan *et al.* observed ~5-fold increase in mutation frequency of *E. coli ung* mutants by screening for resistance to nalidixic acid and rifampin, indicating that the *ung* allele is a weak mutator in *E. coli* (33). Studies of *trpA* reversion frequencies in *ung* mutants revealed a ~30-fold increase in G·C→A·T transitions relative to *ung*⁺ *E. coli* (34).

Although uracil is not a normal constituent of DNA, notable exceptions are the *Bacillus subtilis* bacteriophages PBS1 and PBS2. The double-stranded genomes of PBS1 and PBS2 contain uracil in place of thymine (131). In order for their AU-rich genomes to be replicated in a bacterial host containing mechanisms for eliminating uracil-containing DNA, the production of phage-encoded uracil-DNA glycosylase inhibitor protein (Ugi) is induced upon infection to inactivate *B. subtilis* uracil-DNA glycosylase (41).

1.2 Uracil-DNA Glycosylase

Uracil-DNA glycosylase is a ubiquitous DNA repair enzyme that catalyzes the first step of uracil-initiated base excision repair (BER) (16, 26, 27, 61, 65, 69). The enzyme hydrolyzes the N-glycosylic bond linking the uracil base to the deoxyribose phosphate backbone of DNA, resulting in free uracil and an apyrimidinic (AP) site (66, 69). *E. coli* uracil-DNA glycosylase shares significant amino acid sequence homology with its counterparts isolated from a wide range of biological sources, including human cells (85, 100, 110, 140). A comparison of the sequence between *E. coli* and human uracil-DNA glycosylase reveals 55.7% identical residues with 73.3% polypeptide similarity when conservative amino acid substitutions are considered (100). This striking degree of homology suggests structural and functional conservation as well.

1.2.1 *Escherichia coli* Uracil-DNA Glycosylase

E. coli uracil-DNA glycosylase was the first DNA glycosylase to be identified and purified to apparent homogeneity (66, 69). The *ung* gene was subsequently cloned and purification of overexpressed Ung allowed for extensive biochemical characterization (7, 31, 141, 142). Uracil-DNA glycosylase is a 229 amino acid protein with a deduced molecular weight of 25,694 (7, 141). The enzyme does not require divalent cations or other cofactors for activity (69). Ung is specific for uracil in DNA and does not act on dUMP, dUTP, uracil in RNA, or 3'-terminal uracil residues in oligonucleotide DNA (69, 142). *E. coli* Ung also catalyzes the removal of 5-fluorouracil from DNA; however, thymine and 5-bromouracil contain larger modifying groups which are sterically excluded from the uracil-binding pocket (68, 80).

Uracil residues in single-stranded DNA are removed about twice as efficiently as those in double-stranded DNA substrate and U·G mispairs are preferred 2.4-fold over U·A base pairs in oligonucleotide DNA (9, 69). Sequence context affects the rate of catalysis. In general, uracils within AT-rich sequences are recognized more efficiently than in GC-rich sequences (96). Consensus sequences for good and poor removal were 5'-(A/T)UA(A/T)-3' and 5'-(G/C)U(T/G/C)-3', respectively (96). The enzyme has a broad pH range with maximal activity detected at pH 8.0 (69). Ung has a K_m value for dUMP residues in PBS1 DNA of $\sim 4 \times 10^{-8}$ M (69). The enzyme is inhibited by free uracil and AP sites in DNA by noncompetitive and competitive mechanisms, respectively (69, 133). Glycerol at a concentration of 200 mM is reported to inhibit the Ung reaction rate by $\sim 50\%$ (153).

1.2.2 Mammalian Uracil-DNA Glycosylase

1.2.2.1 Nuclear and Mitochondrial Uracil-DNA Glycosylase

Uracil-DNA glycosylase activity has been isolated from nuclear and mitochondrial extracts of human cells (1, 16, 26, 27, 61). There has been

some controversy as to the number, identity, and subcellular localization of mammalian uracil-DNA glycosylase (UDG).

UDG activities have been purified to apparent homogeneity from rat liver nuclei and mitochondria (26, 27). The nuclear UDG was shown to have an apparent molecular weight of ~33,000 while the mitochondrial form was smaller with a molecular weight of ~20,000 (26). Furthermore, distinct biochemical properties were reported for the nuclear and mitochondrial forms of rat liver UDG. The apparent K_m of the nuclear species for uracil in DNA was 0.5 μ M with a turnover rate of approximately 10 uracils/min (27). In contrast, the mitochondrial species had an apparent K_m of 1.1 μ M and turnover rate of 1000 uracils/min (27). Similar to their *E. coli* counterpart, both enzymes show a 2-fold preference for uracil residues contained in single-stranded over double-stranded DNA, cleave uracil from U·G mispairs about twice as efficiently as from U·A base pairs, and display end product inhibition (27).

Despite these kinetic differences, polyclonal antibody to human UDG recognized nuclear, mitochondrial, and cytosolic forms of the enzyme, indicating that the three forms share antigenic determinants (89, 125, 126). Cellular localization studies utilizing immunostaining and a cDNA clone of uracil-DNA glycosylase from human placenta suggested the mitochondrial and nuclear UDG were encoded by a single gene (126). Mitochondrial translocation was dependent upon a 77 amino acid N-terminal pre-sequence (126).

Cloning of the full length human *UNG* gene revealed the presence of 7 exons which code for the nuclear (UNG2) and mitochondrial (UNG1) forms of UDG (95, 100). The two forms are generated from unique promoters and are the result of alternative splicing (95). UNG2 (313 amino acids) is generated from the promoter P_A and requires splicing of exon 1A into a consensus splice site located after codon 35 in exon 1B. UNG1 (304 amino acids) is initiated from promoter P_B at codon 1 of exon 1B and does not require alternative splicing (95). Thus the two forms differ in their N-termini, which target UNG1

and UNG2 for mitochondrial and nuclear translocation, respectively (95, 101). Their C-terminal 269 amino acids are identical and constitute the catalytic domain of the enzyme (95).

To investigate subcellular localization of UDG in HeLa cells, fusion proteins between the green fluorescent protein (GFP) and the amino-terminus of either UNG1 or UNG2 were produced *in vivo* (87). The UNG1-GFP and UNG2-GFP fusion proteins were localized to the mitochondria and nuclei, respectively (87). Deletions of the first 20 amino acids of UNG2 abolished nuclear import (87). Transfection of the UNG-GFP constructs into NIH 3T3 cells in the presence of [³²P]orthophosphate revealed that UNG2 is differentially phosphorylated while UNG1 is unphosphorylated (87). The significance of this phosphorylation is currently unknown, but may play a role in mediating protein-protein interactions or regulating uracil-DNA glycosylase activity.

Several investigators have reported that uracil-DNA glycosylase gene expression in human cells is cell cycle-regulated (45, 128). An examination of the promoter region of the *UNG* gene reveals the presence of E2F-, Sp1-, Ap2-, and c-Myc-binding elements which are known to be involved in the regulation of genes differentially expressed during the cell cycle (48). In freely cycling HeLa cells, total cellular UDG in early S phase was approximately doubled relative to levels in early G₁ and increased further during G₂ phase to nearly 3-fold that of early G₁ (89). In synchronized HaCaT cells, the levels of mRNA of both UNG1 and UNG2 increased in late G₁/early S phase with a concomitant 4- to 5-fold increase in UDG activity in S phase relative to early G₁ phase (47). These results suggest that expression of the *UNG* gene prior to DNA replication is important for maintaining the integrity of the genome.

1.2.2.2 Cyclin-Like Uracil-DNA Glycosylase

A third species of mammalian UDG was cloned from a human T cell cDNA (85). This 36,000 molecular weight protein displayed uracil-DNA glycosylase activity on U·A base pairs but showed limited amino acid

homology to the *E. coli* or human uracil-DNA glycosylases described above. Rather, this enzyme was determined to share 23-30% identity (51% similarity considering conservative amino acid substitutions) with the cyclin A protein family (86). The gene encoding this cyclin-like uracil-DNA glycosylase contains 2 exons (86). The promoter region lacks TATA and CAAT boxes but contains an AP2 consensus site (86). Analysis of gene expression during cell cycling revealed that mRNA levels increase 3 to 4-fold in G1 phase (86).

Caradonna *et al.* (15) utilized affinity purification to identify nuclear and mitochondrial species of UDG from HeLa extracts. Ugi-Sepharose affinity chromatography recovered a 30,000 molecular weight protein from mitochondrial fractions and two species corresponding to 36,000 and 30,000 molecular weight from total cell extracts (15). Affinity-purified samples from nuclear extracts did not cross-react with antisera to the conserved UDG, suggesting that nuclear uracil-DNA glycosylase activity was not associated with the highly conserved form of human UDG (15). Rather, antisera generated against the cyclin-like UDG immunoprecipitated a mixture of proteins in the 36,000 molecular weight range from affinity-purified nuclear fractions, indicating that the cyclin-like form of UDG was the major nuclear species (15). Additionally, analysis of mitochondrial fractions indicated that the conserved UDG was targeted to the mitochondria where it underwent proteolytic processing (15). This was in contrast to reports which suggested that both nuclear and mitochondrial forms of UDG arise from differential splicing of transcripts encoded by a single *UNG* gene (125, 126).

More recent work by Caradonna and coworkers demonstrated that all protein recovered by large scale affinity purification of uracil-DNA glycosylase activity from HeLa nuclear extracts corresponded exclusively to the UNG2 gene product originally reported by Nilsen *et al.* (87, 95). The investigators suggest that this discrepancy may result because their original conclusions were based on cross-reactivity of nuclear and mitochondrial fractions with polyclonal antibody to the conserved UDG. This antibody preparation may have recognized epitopes at the N-terminus of the protein, which is variable between mitochondrial and nuclear forms of UDG, and thus was incapable of

detecting the nuclear UNG2. Additionally, the cyclin-like form of UDG was not recovered to appreciable levels in this study (87). It is not clear why the cyclin-like UDG could not be detected in large scale Ugi-affinity purification when it had been previously identified in Ugi-affinity purified fractions, but this provides further evidence that UNG2 is the major source of nuclear uracil-DNA glycosylase activity.

1.2.3 Other Enzymes Exhibiting Uracil-DNA Glycosylase Activity

1.2.3.1 *Thymine-DNA Glycosylase*

Studies of HeLa cell nuclear extracts demonstrated that G·T mispairs were excised from DNA and repaired to G·C base pairs (150). Analysis of the reaction products indicated that free thymine and AP sites were generated, suggesting the presence of a thymine-DNA glycosylase (TDG) in human cells (150, 151). The enzyme was purified to homogeneity from HeLa cells and biochemically characterized (92, 93). The protein migrated with an apparent molecular weight of 55,000 in denaturing polyacrylamide gel electrophoresis (92). In addition to recognizing thymine residues, TDG also functions as a uracil-DNA glycosylase (93). TDG substrate specificity was determined to be G·U > G·T >> C·T > T·T (92, 93). The enzyme was not active on A·T or single-stranded DNA, although it could cleave 5-bromouracil base paired with guanine (93). TDG is also reported to recognize 3,*N*⁴-ethenocytosine (εC) paired to guanine (46, 115) and thymine paired to O⁶-methyl-guanine (122), 2-amino-6-methylpurine (44, 122), and 6-thioguanine (44). TDG activity was not inhibited by the uracil-DNA glycosylase inhibitor protein Ugi (93).

Subsequently, a 1232 bp open reading frame (ORF) encoding the putative human TDG was cloned and expressed *in vitro* and in *E. coli* (91). TDG displayed no homology to any known enzyme (43). The recombinant enzyme had a predicted molecular weight of ~46,000 but migrated anomalously at ~60,000 during denaturing polyacrylamide gel electrophoresis (91). The substrate specificity of the recombinant TDG (rTDG) was identical to

the cellular TDG activity previously identified (91). Polyclonal antisera to the rTDG inhibited both activities, suggesting that TDG is the only enzyme present in HeLa nuclear extracts capable of processing G·T mispairs (91). It is unclear whether the 55,000 molecular weight species represents a degraded or processed form of rTDG. N- and C-terminal deletion mutants of rTDG identified a core region capable of processing G·U but not G·T mispairs, indicating that discrimination of thymine bases is localized to the N-terminal 56 amino acids, while the central 249 residues are involved in catalysis (43).

The extent of G·T incision by TDG was 3-12-fold greater in CpG sequences as compared to TpG, GpG, and ApG sequences, suggesting that sequence context alters TDG activity (122). Kinetic analysis confirmed that the base pair 5' to the G·T mismatch influences the rate of thymine hydrolysis (149). The k_{cat} values for excision of G·T mispairs containing 5' C·G, T·A, G·C and A·T base pairs were 0.91, 0.023, 0.0046, and 0.0013 min⁻¹, respectively (149). Additionally, it was determined that TDG can remove uracil from G·U, C·U, and T·U base pairs more efficiently than from G·T mispairs (149). Uracil was also removed from A·U base pairs by TDG, although the rate was slow, with $k_{\text{cat}} = 0.047$ min⁻¹ (149). In contrast, the k_{cat} value for a G·U mismatch in the same sequence context was 11 min⁻¹ (149).

Interestingly, studies revealed that each TDG molecule was capable of removing only one thymine molecule from DNA containing a G·T mismatch because the enzyme binds tightly to the AP site formed in the reaction (148, 149). Bound TDG interferes with AP site cleavage by human apurinic endonuclease 1 (HAP1) (148). However, HAP1 significantly increases the rate of dissociation of TDG from AP sites (148). Thus the interaction of TDG and HAP1 couples the first two steps of base excision repair in this system.

These observations suggested a role for TDG *in vivo*. In mammalian cells, cytosine methylation in CpG sequences is involved in cell development and transcriptional regulation (35). Deamination of 5meC, which occurs at a faster rate than for cytosine, results in a G·T mispair (36). Unlike uracil, thymine is a normal constituent of DNA. Thus, it was proposed that TDG evolved to address the problem of 5meC deamination by removing

potentially mutagenic thymine bases from G·T mispairs in CpG regions (92, 122, 150). Alternatively, the broad substrate range of TDG suggests that its biological function may be a secondary uracil DNA-glycosylase for the correction of G·U mispairs from GC-rich regions of the genome (43, 93, 149), as these residues are poor substrates for UDG but the preferred substrate of TDG (96, 122, 149).

1.2.3.2 Mismatch-Specific Uracil-DNA Glycosylase

Although TDG displayed no homology to known enzymes, homologs were identified in *E. coli* and *Serratia marcescens* (43). Conservation is limited to the core region of TDG which encodes for G·U mismatch specificity (43). The bacterial enzymes show greater than 30% amino acid sequence identity to this core region (43). The *E. coli* ORF encoding a putative 169 amino acid homolog of TDG was expressed in both rabbit reticulocyte lysates and *E. coli* and as expected, the gene product was active on G·U mispairs but did not recognize G·T mispairs (43). Additionally, the enzyme did not recognize A·U or single-stranded U substrates and the activity was Ugi-insensitive (43). The bacterial enzyme was designated double-strand uracil-DNA glycosylase, and later referred to as mismatch-specific uracil-DNA glycosylase (MUG) (43).

In vivo studies indicated that MUG is a biologically relevant DNA glycosylase. *E. coli* NR8051 (*ung*⁺) hydrolyzed both U and G·U substrates and the hydrolysis was inhibited by Ugi (43). In contrast, *E. coli* NR8052, the isogenic *ung*⁻ strain, cleaved uracil from G·U substrate exclusively and the activity was Ugi-insensitive (43). Additionally, Northern blot analysis demonstrated that a ~700 nucleotide species cross-reacted with a MUG complementary DNA probe, indicating the gene is transcribed *in vivo* (43).

The crystal structure of MUG free and in complex with duplex oligonucleotide containing a G·U mispair has been determined (5). Despite a low level of amino acid sequence homology MUG displays striking structural similarity to uracil-DNA glycosylase (80, 103, 110, 116, 127), which explains the ability of two very divergent proteins to catalyze similar reactions. MUG

is composed of a central 5-stranded β -sheet flanked by α -helices (5). One face of the enzyme displays positive charge and is traversed by a DNA binding channel containing an active site pocket that penetrates the enzyme's core (5). This is very similar to the DNA binding groove and active site pocket of UDG (see "Section 1.2.4") (80, 110, 116, 127). MUG-DNA complex crystallographic data revealed that the uracil-containing DNA strand is bound by the enzyme such that the deoxyuridine is in an extrahelical position, which is a key structural feature of DNA bound to UDG (5, 80, 110, 116, 127). The gap in the DNA duplex formed by the extrahelical uracil is filled by Gly-143 and Leu-144 (5). In addition Arg-146 inserts its side chain between the widowed guanine of the G·U pair and the preceding cytosine (5). These three amino acids form a "wedge" that penetrates the base stack from the DNA minor groove (5). The wedge can be accommodated only if the uracil residue is extrahelical, thus suggesting a "push" mechanism for uracil recognition and binding (5). This is in contrast to UDG, which is predicted to utilize a "push-pull" mechanism for uracil recognition (103). Specificity of MUG for G·U mispairs may arise from interactions of Gly-143 and Ser-145 with the widowed guanine (5). These interactions can only occur in the absence of the base-pairing partner and are absolutely specific for guanine (5). Despite conservation by MUG of several key residues involved in UDG binding to Ugi, a conserved UDG active site glutamine is replaced by isoleucine in MUG (5, 79, 110, 117). This glutamine makes two hydrogen bonds with Ugi Leu-23 that cannot be formed by isoleucine (5, 79, 110, 117). This may explain the inability of Ugi to inhibit MUG activity.

Thus, MUG appears to be a mechanistically and evolutionarily distinct class of uracil-DNA glycosylase. The role MUG plays *in vivo* is unknown at the present time but MUG may serve as a second line of defense against uracil residues in DNA, acting as a secondary uracil-DNA glycosylase activity to *E. coli* Ung.

1.2.3.3 *Single-Strand-Selective Monofunctional Uracil-DNA Glycosylase*

The most recently discovered class of enzymes exhibiting uracil-DNA glycosylase activity was identified by Haushalter *et al.* (49). AP site analog-containing double-stranded oligonucleotides were designed to serve as synthetic inhibitors of DNA glycosylases in a whole-genome screen (49). By a process known as *in vitro* expression cloning, *Xenopus laevis* cDNA library clones were transcribed and translated *in vitro* and the resultant proteins were analyzed in electrophoretic mobility shift assays (EMSA) with the inhibitor oligonucleotides (49). The TD-12 clone was selected as a possible DNA glycosylase based on binding of inhibitor oligonucleotide in EMSA (49). The TD-12 ORF encoded a putative 281 amino acid protein with a predicted molecular weight of ~31,000 (49). Its sequence contained no similarity to known proteins but extensive homology to a human ORF (270 amino acids) (49). The human and *X. laevis* ORFs were 60% identical and 71% similar, considering conservative amino acid substitutions (49).

The *in vitro* transcription/translation reaction mixture containing the TD-12 ORF gene product cleaved uracil with equal efficiency from U·A and U·G base pairs (49). Additionally, single-stranded uracil-DNA was preferred ~20-fold over double-stranded substrate by the *Xenopus* homolog; the human homolog also preferred single-stranded U, although to a lesser extent (49). G·T mismatches were not a substrate for either enzyme (49). Mass spectrometry analysis of the reaction product demonstrated that AP site oligonucleotide was the primary end product, indicating that the enzyme was a true DNA glycosylase with no associated AP lyase activity (49). Thus, the enzyme was designated single-strand-selective monofunctional uracil-DNA glycosylase (SMUG1) (49). Fusion of human SMUG1 to GFP revealed that hSMUG was localized to the nucleus (49). The TD-12-encoded protein was overproduced in *E. coli*, purified, and biochemically characterized (49). Kinetic analysis revealed that the overall catalytic efficiency of xSMUG1 is 10- and 70-fold lower than human UDG on single-stranded and double-stranded

substrate, respectively (49). In comparison, the efficiency of xSMUG1 on U·G mispairs was nearly identical to that of human TDG (49).

PBS1 Ugi protein did not inhibit xSMUG1, which is not surprising based on its lack of similarity to UDG (49). Initially the lack of sequence similarity between SMUG1 and UDG was perplexing, given their functional similarity. However, closer comparison of the crystal structures of herpes simplex virus type-1 (HSV-1) UDG (see “Section 1.2.4”) and *E. coli* MUG (see “Section 1.2.3.2”) revealed that two active site motifs are conserved by all three enzymes, which may explain the ability of structurally divergent enzymes to catalyze very similar reactions (49). Motif I in MUG has the sequence GINPG-N₉-F (5). Crystallographic evidence suggested that the asparagine at position 3 functions in catalysis while the terminal phenylalanine stacks with the uracil base (5). The sequence of Motif I in HSV-1 UDG is GQDPY-N₁₀-F, where the aspartic acid rather than asparagine was implicated in catalysis (116). Furthermore, tyrosine at position 5 sterically excludes thymine from the active site (116). In both *E. coli* and human UDG the Motif I sequence is GQDPY-N₁₀-F, which is identical to that of HSV-1 (110). Motif I in SMUG1 has the sequence GMNPG-N₁₀-F, which more closely resembles MUG (49). SMUG1 discriminates against thymine despite the presence of glycine at position 5 (49). The sequence of the MUG Motif II is NPSGLS (5). Asparagine in position 1 hydrogen bonds with uracil and the glycine residue hydrogen bonds with the guanine of the U·G mismatch (5). The HSV-1, human and *E.coli* UDG Motif II sequence is HPSPLS (110, 116), which is similar to the SMUG1 Motif II sequence of HPSPRN (49). Thus, key structural features are conserved between these three classes of uracil-DNA glycosylases and the difference in these motifs may explain the selectivity of each enzyme for its substrate.

The biological significance of SMUG1 *in vivo* is unclear at the present time. It may serve as a backup glycosylase to the conserved UDG or alternatively the selectivity of SMUG1 for single stranded DNA may indicate its involvement in the repair of transiently single-stranded regions of the genome that occur during transcription, recombination, and replication.

1.2.3.4 Thermostable Uracil-DNA Glycosylases

Because cytosine deamination is enhanced at high temperatures (70), thermophilic organisms are anticipated to face greater threats from cytosine deamination and therefore have greater needs for uracil DNA repair. Koulis *et al.* (59) screened cell extracts of seven hyperthermophilic microorganisms and determined that all possessed uracil-DNA glycosylase activity at 95°C. It was reported that these activities removed uracil from both single- and double-stranded DNA (59), but it is unclear whether the substrate analyzed was double-stranded in nature at 95°C. The addition of PBS1 Ugi in excess to the reaction resulted in only partial inhibition of the detected uracil-DNA glycosylase activity, suggesting that some of the cellular uracil-DNA glycosylase was inaccessible to Ugi or that a Ugi-insensitive uracil-DNA glycosylase exists in thermophilic organisms (59).

Support for the latter hypothesis came with the identification of two enzymes with uracil-DNA glycosylase activity that displayed no significant homology to *E. coli* Ung. The first example was identified in the thermophilic archaeobacteria *Methanobacterium thermoautotrophicum* THF. This organism contains a plasmid which encodes a restriction/modification system that recognizes GGCC sequences (51). Deamination of modified cytosine residues would therefore yield thymine bases. The plasmid also encodes an ORF (*orf10*) with significant sequence homology to *E. coli* MutY and endonuclease III (51). Expression of the *orf10* gene and purification of the expressed protein product yielded a DNA glycosylase with no associated AP lyase activity which removed thymine from a T·G mismatch in the GGTC context at 65°C (51). The substrate specificity of the enzyme was U·G, T·G > G·G >> A·G, T·C, U·C. Single-stranded DNA and the mispairs T·T and T·U were not cleaved (51). The protein is also reported to remove εC residues paired with guanine (46). The enzyme was designated mismatch glycosylase (Mig.Mth) and *orf10* was renamed *mig* (51).

A second class of thermostable uracil-DNA glycosylase lacking homology to *E. coli* Ung was purified from the thermophilic microbe

Thermotoga maritima. An ORF with low homology to *E. coli* MUG was predicted to encode a 185 amino acid protein with a predicted molecular weight of 20,578 Da (113). The ORF was cloned, overexpressed in *ung* *E. coli*, and the expressed protein was purified (113). The gene product released free uracil from U·A, U·G and single-stranded DNA at 75°C (113). T·G mispairs were not excised (113). No associated AP lyase activity was detected (113). The enzyme was designated *T. maritima* UDG (TMUDG). Homologs to TMUDG were identified in several strains of thermophilic eubacteria and archaeobacteria, the human pathogens *Rickettsia prowazekii* and *Treponema palladium*, and the extremely radioresistant *Deinococcus radiodurans* (113). Except for *D. radiodurans*, all strains containing a putative TMUDG homolog lack amino acid sequences homologous to *E. coli* Ung (113), suggesting that this enzyme may be an evolutionarily divergent form of uracil-DNA glycosylase in microorganisms able to withstand extreme environments.

Neither Mig.*Mth* nor TMUDG was analyzed for Ugi binding or inhibition. However based on their lack of sequence homology to Ung, one might not anticipate Ugi to inhibit either Mig.*Mth* or TMUDG.

1.2.4 Structure of Uracil-DNA Glycosylase

The tertiary protein structures have been determined for *E. coli* (110, 111, 153), human (55, 79, 80, 103, 127), and HSV-1 (102, 116) uracil-DNA glycosylases by X-ray crystallography. The enzymes have been crystallized and analyzed in complex with a proteinaceous inhibitor, the PBS1/2 uracil-DNA glycosylase inhibitor protein (Ugi). Comparisons between *E. coli* uracil-DNA glycosylase in complex with Ugi with human UDG•Ugi complex and HSV-1 UDG•Ugi complex reveals that the human and *E. coli* proteins are more similar to each other than to the viral enzyme, although most key structural features are conserved in the HSV-1 enzyme (110, 111, 153). Uracil-DNA glycosylase contains a central, all parallel four-stranded β -sheet flanked by a total of eight α -helices (80, 110). The groove formed by β 1 and β 3 is approximately the width of a DNA double-stranded helix and is lined by

positively charged, highly conserved residues (80, 127). The uracil recognition pocket is located deep within this groove and contains the active site (80). Structural analysis of human UDG indicated that amino acids Gln-144, Asp-145, Tyr-147, and Asn-204 line one side of the uracil binding pocket (80). His-268, Ser-169, and Ser-270 line the other side of the active site, while Phe-158 lies along the bottom of the pocket and stacks with the uracil pyrimidine ring (80). The location of the Tyr-147 side chain allows discrimination against bases substituted at the 5 position, such as thymine or 5-bromouracil (80). Evidence demonstrating the common role of these amino acids recently emerged from the crystallographic structures of *E. coli* Ung resolved to 3.2 Å (111), 2.4 Å (110), and 1.6 Å (153) resolution. An overlay of the polypeptide C α traces of human UDG and *E. coli* Ung showed conservation of both secondary-structural elements and tertiary conformation (110, 111, 153). Thus, these results indicate that *E. coli* Ung closely resembles its human enzyme counterpart and that Ung should be regarded as a prototypical enzyme.

The position of the uracil binding pocket in the floor of the DNA binding groove necessitates that the enzyme bind uracil bases which have become extrahelical or “flipped out” of the DNA double helix (79, 80, 103, 127). Nucleotide flipping is accompanied by the insertion of a conserved leucine (*E. coli*, Leu-190; human, Leu-272) into the DNA minor groove, followed by the rotation of the uracil nucleotide $\sim 180^\circ$ about the phosphodiester backbone into the active site (127).

Human UDG-DNA co-crystal structures suggest that a “Ser-Pro pinch” coupled with a “Leu push-pull” mechanism is utilized for uracil recognition (103). Electrostatic binding orients uracil-DNA glycosylase such that three conserved Ser-Pro loops bind and compress the DNA backbone at successive phosphate moieties (103). The DNA 5' and 3' of the extrahelical uracil is B-form, but the distance between the phosphates on either side of the uracil residue is reduced from ~ 12 to 8 Å and the DNA is compressed at this position (103). Additionally, the conserved Leu loop contacts the minor groove purine N3 atoms through water-mediated interactions (103). Thus, the uracil

nucleotide is extruded from the DNA base stack through the combined forces of enzyme-mediated DNA backbone compression, a concerted push via the leucine side chain, and the attractive pull of the uracil-binding pocket (103). Ung undergoes a “ β -zipper” conformational change during the DNA compression which extends the β -sheet interactions between $\beta 1$ and $\beta 3$ by two additional residues, thus changing from an open conformation to a closed conformation (110).

1.3 Uracil-Initiated Base Excision Repair

The basic steps of uracil-initiated base excision repair are conserved between prokaryotic and eukaryotic cells, underscoring the importance of this pathway in maintaining the integrity of genomic DNA (62, 81). Uracil-initiated base excision repair is a multistep pathway consisting of five steps: uracil removal, phosphodiester bond cleavage, sugar-phosphate removal, DNA synthesis, and phosphodiester bond ligation. The pathway is initiated by uracil-DNA glycosylase with the hydrolysis of the N-glycosyl bond of a uracil base, proceeds through a common DNA damage intermediate, and results primarily in single nucleotide repair patches (21, 38, 58). Repair by this mechanism is referred to as short patch base excision repair; however, repair patches of ≥ 2 nucleotides have also been recognized and referred to as long patch base excision repair (42, 76, 114).

1.3.1 Prokaryotic Uracil-Initiated Base Excision Repair

1.3.1.1 Removal of Uracil from DNA

The first step of uracil-initiated BER in *E. coli* involves hydrolysis of the N-glycosyl bond of a uracil residue by uracil-DNA glycosylase, generating free uracil and an AP site (69). Several lines of evidence have implicated amino acids of *E. coli* Ung that are involved in DNA binding or catalysis. Photochemical cross-linking experiments using Ung and oligonucleotide dT₂₀ revealed four tryptic peptides (T6, T18, T19, T18/19) that adducted to the DNA

(7). These peptides defined two primary sequences (amino acids 58-80 and 185-213) that reside at or near the DNA-binding site. Amino acid sequence conservation between *E. coli* Ung and 9 other uracil-DNA glycosylases led to speculation that Asp-64 and His-187 serve as essential residues for activity (7). Additional insight into the structure and function relationship evolved following the solution of the X-ray crystal structure of HSV-1 and human $\Delta 84$ uracil-DNA glycosylase bound to dT₃ and duplex DNA, respectively (116, 127). $\Delta 84$ UDG is a recombinant protein generated for overexpression in *E. coli* which lacks the N-terminal 77 amino acid pre-sequence as well as the next 7 nonconserved residues encoded by the *UNG* gene (125). Additionally, three amino acid residues encoded by the vector (Met-Glu-Phe) were added to the N-terminus of the enzyme (125). Based on protein structural data, interactions between 13 amino acids and uracil-containing DNA were identified for the human enzyme (127). Table 1 summarizes the human UDG residues that interact with DNA and their homologous amino acids in *E. coli* and HSV-1 uracil-DNA glycosylases. Comparison of the amino acid sequence alignment between *E. coli* and human uracil-DNA glycosylase revealed that *E. coli* Ung possessed 12 (Gln-63, Asp-64, His-67, Phe-77, Ser-88, Asn-123, Ser-166, His-187, Ser-189, Leu-191, Ser-192, Arg-195) of the same 13 residues attributed to DNA interaction (103, 127). Recent protein structural results confirmed a common role for these amino acids in substrate binding (110, 111, 153).

Uracil-DNA glycosylase activity requires enzyme-assisted nucleotide flipping to orient the uracil residue within the recognition pocket and to properly position the N1-C1' bond within the catalytic site (80, 110, 111, 116, 127). Previously, three different catalytic mechanisms for glycosylic bond cleavage were proposed (80, 116). (i) The peptide carbonyl and side-chain carboxyl of Asp-178 (HSV-1) activate a water molecule that attacks a weakened glycosylic bond. Destabilization of the N1-C1' bond is brought about by distortion or protonation of the uracil O2 by His-210 Nε2 (116). (ii) The imidazole group of His-268 (human) catalyzes a direct nucleophilic attack on the N1-C1' glycosylic bond of the uracil residue, and a second nucleophilic

Table 1
*DNA Interactions and Amino Acid Homology
of Human Uracil-DNA Glycosylase*

Human UDG	DNA Interactions ^a		<i>E. coli</i> Ung	HSV-1 UDG
	Site of Contact	Type of Interaction ^b		
Gln-144	Uracil (O ₂)	H-bond (MC)	Gln-63	Gln-177
Asn-145 ^c	Uracil (O ₂)	H-bond (MC)	Asp-64	Asp-178
	AP-sugar (C ₁)	H-bond (SC)		
His-148	(P+1) Phosphate ^d	H-bond (SC)	His-67	His-181
	AP-sugar (O ₄)	H-bond (SC)		
Phe-158	Uracil	Stacking	Phe-77	Phe-191
	Uracil (O ₄)	H-bond (MC)		
Ser-169	(P0) Phosphate	H-bond (MC)	Ser-88	Ser-202
	(P0) Phosphate	H-bond (SC)		
Asn-204	Uracil (O ₄)	H-bond (SC)	Asn-123	Asn-237
	Uracil (N ₃)	H-bond (SC)		
Ser-247	(P-2) Phosphate	H-bond (MC)	Ser-166	Thr-280
	(P-2) Phosphate	H-bond (SC)		
His-268	Uracil (O ₂)	H-bond (SC)	His-187	His-300
	(P-1) Phosphate	H-bond (SC)		
	(P-2) Phosphate	H-bond (MC)		
Ser-270	(P-1) Phosphate	H-bond (SC)	Ser-189	Ser-302
Arg-272 ^c	5' Guanine (N ₇)	H-bond (SC)	Leu-191	Leu-304
	(P+1) Phosphate	H-bond (SC)		
	(P-1) Phosphate	H-bond (SC)		
	Guanine ^e (N ₇)	H-bond (SC)		
Ser-273	3' Deoxyribose (O ₄)	H-bond (SC)	Ser-192	Ser-305
Tyr-275	Deoxyribose ^f (O ₄)	H-bond (SC)	His-194	Lys-306
Arg-276	(P-3) Phosphate	H-bond (SC)	Arg-195	Val-307

^a The locations and types of interactions by human UDG with DNA were summarized from (127).

^b Hydrogen bond interactions with amino acid main chain (MC) or side chain (SC) atoms are indicated.

^c UDG-DNA co-crystal structure was determined by using a human Δ84UDG Asp145Asn/Leu272Arg double mutant (127).

^d Phosphate groups are numbered from P0 at the uncleaved dUMP residue with phosphates of nucleotides 5' to the uracil base designated P+n and those 3' as P-n where n equals the number of phosphate groups removed from the dUMP site.

^e This residue corresponds to the widowed guanine on the non-uracil containing DNA strand (127).

^f This deoxyribose moiety is located on the non-uracil containing DNA strand two nucleotides 3' of the widowed guanine residue (127).

attack of a water molecule provides H- and OH-group addition to the N1 and C1' atoms, respectively (80). (iii) A single nucleophilic attack by His-268 (human) on a water molecule abstracts a proton and creates an OH nucleophile that acts on the glycosylic bond (80). In each case, an absolutely conserved histidine residue (human, His-268; HSV-1, His-210) corresponding to *E. coli* Ung His-187 was proposed to play an essential role in catalysis. Recent kinetic studies examined the role of the conserved Asp-64 and His-187 residues of *E. coli* Ung by generating D64N and H187Q mutants (153). The results implicated Asp-64 as a general base catalyst, while providing no evidence that His-187 is involved in general acid catalysis (153). However, common agreement on the reactive mechanism and the function of Ung His-187 remained to be fully elucidated.

1.3.1.2 *AP-Site Incision and Removal of 5'-Deoxyribose Phosphate*

DNA glycosylases hydrolyze the N-glycosylic bond linking damaged or inappropriate bases to the deoxyribose-phosphate backbone (29, 67). The resultant abasic sugar-phosphate is called an apurinic or apyrimidinic (AP) site. Removal of AP sites is initiated by the action of an AP endonuclease or AP lyase (25, 82, 146). AP lyases, formerly referred to as Class I AP endonucleases, catalyze a β -elimination reaction to incise the phosphodiester bond 3' to the AP site (4, 57, 82). Alternatively, the DNA backbone is nicked when a Class II AP endonuclease cleaves the phosphodiester bond to the 5' side of an AP site, generating a 3'-terminal hydroxyl moiety and a 5'-deoxyribose-phosphate residue (82). The 3'-OH group generated by the action of an AP endonuclease provides a substrate for DNA synthesis; however, the 5'-deoxyribose phosphate (dRp) group must be removed in order to complete the repair process (83). Some DNA glycosylases have an associated AP lyase activity, catalyzing sequential steps of the base excision repair pathway (2, 97, 135). Uracil-DNA glycosylase produces apyrimidinic sites and does not have an associated AP lyase activity (69).

Although some studies suggest that in *E. coli* the 5'→3' exonuclease activity of DNA polymerase I may liberate the 5'-dRp moiety as a small oligonucleotide (3), a DNA deoxyribophosphodiesterase (dRpase) has been identified which acts on termini formed as the result of AP endonuclease activity (39). This 50,000 molecular weight protein does not display exonuclease, AP endonuclease, or DNA phosphatase activities (39). Rather, it generates a free sugar-phosphate and a single-nucleotide gap in the DNA backbone at a 5'-incised AP site (39). The identity of dRpase activity in *E. coli* was elucidated upon characterization of the *recJ* gene product. Purified RecJ protein displayed dRpase activity (22) and the combined activities of Ung, AP endonuclease and RecJ/dRpase were capable of generating a BER intermediate containing a one-nucleotide gap with 3'-OH and 5'-phosphate termini (20). This reaction intermediate supported DNA synthesis and ligation (20). Together these results implicated RecJ in the elimination of 5'-dRp residues during BER.

In contrast, studies of the post-incision steps of bacterial BER using a closed circular DNA substrate containing a U-G mispair demonstrated that cell extracts derived from *E. coli* strains deficient in *recJ* were proficient in uracil-DNA repair (114). Repair occurred with a patch size of ~15 nucleotides, which was similar to the results observed with cell extracts of wild type *E. coli* (114). This suggests that other activities, for example the 5'→3' exonuclease of DNA polymerase I, may substitute for the dRpase activity of RecJ in BER *in vivo*.

1.3.1.3 DNA Synthesis and Ligation

Ung, DNA polymerase I, and DNA ligase were implicated in BER by studies of *E. coli* strains defective in dUTPase (138). *E. coli dut* strains have increased intracellular dUTP concentrations (147), which leads to increased incorporation of uracil during DNA synthesis (136). Mutants in dUTPase accumulate DNA fragments that resemble Okazaki fragments (138). These short Okazaki-like fragments appear transiently and are readily incorporated into higher molecular weight DNA (137, 138). The accumulation of short

Okazaki-like fragments was suppressed in *dut ung* double mutants (137). Furthermore, *dut polA* and *dut lig* double mutations resulted in a decreased rate in rejoining of the fragments (137). Thus uracil-DNA glycosylase, DNA polymerase I and DNA ligase appeared to be necessary for uracil-initiated BER.

The 3'-OH terminus generated by AP endonuclease is a substrate for DNA polymerase I (83, 146). Uracil-initiated BER of a double-stranded oligonucleotide substrate containing a single dUMP residue was examined *in vitro* using *E. coli* cell extracts. The primary product was a one-nucleotide repair patch and no significant DNA repair synthesis occurred 5' to the uracil residue (21). This suggested that the 5'→3' exonuclease activity of DNA polymerase I was not involved in the hydrolysis of the 5'-dRp to a significant extent, although this process may be an alternative pathway which explains the low occurrence of larger repair patches (21). Additionally, the uracil-initiated BER pathway was reconstituted using purified Ung, AP endonuclease, RecJ, DNA polymerase I, and DNA ligase III (20). The results were similar to those obtained using crude cell extracts, indicating that these species are sufficient to support repair (20). In contrast, when a closed circular DNA substrate containing a U·G mismatch was incubated with *E. coli* crude extracts, the predominant reaction product was not single-nucleotide repair patches (114). Rather, the results indicated that repair synthesis involved the incorporation of 11-19 nucleotides (~15 nt) 3' to the uracil residue (114). This suggests that repair patch size may be dependent on DNA substrate conformation. DNA synthesis was not detected in *ung E. coli*; thus, repair was absolutely dependent on hydrolysis of the uracil base by Ung (114). Additionally, similar repair patch sizes were observed with *recJ* and *xon E. coli* cell extracts, indicating that other cellular dRpase activities may function in BER in addition to RecJ (114).

1.3.2 Eukaryotic Uracil-Initiated Base Excision Repair

The overall process of uracil-initiated BER in eukaryotic cells is similar to that described for *E. coli* (62, 81). Repair involves hydrolysis of the N-glycosyl bond to release uracil, phosphodiester bond cleavage at the resultant apyrimidinic site, deoxyribose phosphate removal, DNA synthesis and ligation. However, recent reports indicate that following removal of the uracil base by uracil-DNA glycosylase and AP site cleavage by a Class II AP endonuclease, the repair process may be completed by two alternative pathways (42, 77). Short patch BER involves the formation of a one-nucleotide repair patch, while long patch BER results from the incorporation of 2-7 nucleotides during repair synthesis (20, 21, 42, 77, 123). The predominant mechanism observed in human cell extracts is short patch BER (21, 38, 58).

Short patch BER has been reconstituted *in vitro* using purified human proteins. UDG, AP endonuclease (HAP1), DNA polymerase β (pol β), and DNA ligase I have been implicated (94, 107). Similar reconstitution experiments indicated that pol β , DNA ligase III and XRCC1 are involved in short patch BER, with XRCC1 acting to suppress the strand displacement activity of pol β (63). Long patch BER has also been reconstituted *in vitro* with AP endonuclease, pol β , DNase IV, and DNA ligase I or III (58). The longer patch formation was due to the 5'→3' exonuclease activity associated with DNase IV, which was stimulated by the proliferating cell nuclear antigen (PCNA) (58).

DNA pol β appears to be the primary DNA polymerase involved in uracil-initiated BER in eukaryotic cells (21, 63, 90, 123, 129). Although the preferred substrate of pol β is a one-nucleotide gap, the enzyme is also capable of filling gaps consisting of 2-6 nucleotides (84, 124), suggesting it could function in both short and long patch BER. DNA pol β also has an intrinsic dRpase activity, which suggests that the enzyme may participate in sequential steps of the repair process (76, 104). The addition of purified pol β to human nuclear extracts increased uracil-initiated BER ~10-fold, while DNA

polymerases α , δ , and ϵ had no significant effect (123). A multiprotein complex purified from bovine cell extracts which was capable of short patch BER *in vitro* consisted of UDG, AP endonuclease, pol β , and DNA ligase I (123). Embryonic fibroblast M β 19tsA cells homozygous for a deletion mutation in the gene for pol β were unable to perform BER on a uracil-containing linear substrate and the pathway was restored upon transfection of the cell line with a minigene expressing pol β , providing evidence for the role of this polymerase in BER *in vivo* (129).

However, pol β activity does not completely account for all BER DNA synthesis detected in eukaryotic cells. Studies with nuclear extracts demonstrated that the addition of ddNTPs, inhibitors of pol β , to the base excision repair reaction resulted in only partial inhibition of DNA repair synthesis (21, 90). Similarly, the addition of aphidicolin in these reactions resulted in partial inhibition of DNA repair synthesis, suggesting the involvement of DNA polymerase δ (pol δ) or ϵ (pol ϵ) (21). Similarly, a circular AP site-containing DNA substrate was repaired by extracts of the pol β -deficient M β 19tsA fibroblast cell line previously described, indicating that other cellular DNA polymerases could replace pol β in the repair of a circular DNA (38). In this case both short and long patch repair were observed, although short patch repair was significantly slower than pol β -containing extracts (38). Long patch repair was proliferating cell nuclear antigen (PCNA)-dependent, further implicating pol δ or ϵ in BER (38).

Biade *et al.* (13) examined the effect of DNA substrate conformation on PCNA-dependent BER more carefully. They compared repair of covalently closed circular and linear DNA substrates containing a single AP site in pol β -proficient and pol β -deficient cell extracts. Both linear and circular DNA substrates were repaired in wild type cell extracts (13). In the pol β mutant cell extracts, linear DNA was not efficiently repaired, but circular DNA was repaired in a PCNA-dependent fashion (13). DNA binding by PCNA is facilitated by replication factor C (RF-C), forming a PCNA/RF-C complex required for efficient DNA synthesis by pol δ or pol ϵ (56). Podust *et al.* (106)

demonstrated that PCNA/RF-C complex pre-assembled on gapped circular DNA quickly dissociated when the DNA was linearized. Thus, the use of linear DNA substrate in BER assays may bias the reaction against pol δ , pol ϵ , or other PCNA-dependent enzymes such as DNase IV.

Dianov *et al.* (23) analyzed the products of long patch excision repair of circular DNA substrate in mammalian extracts, and the predominant product was a dRp-oligonucleotide which co-migrated with a trinucleotide marker during 20% polyacrylamide gel electrophoresis. Production of this product was reduced in pol β -deficient cell extract and the size distribution of excision products was altered (23). The addition of purified pol β to the extract restored dRp-oligonucleotide release (23). The investigators concluded that pol β performs both the excision and repair synthesis steps in long patch BER. Alternatively, Stucki *et al.* (130) utilized fractionated cell extracts of pol β -deficient mouse fibroblast cells to examine the contributions of pol δ and pol ϵ to long and short patch BER. The substrate was a circular DNA template containing a single abasic site (130). Surprisingly, fractions containing pol δ or pol ϵ were capable of producing a one-nucleotide repair patch in the absence of PCNA (130). Completion of the repair process was slowed due to a reduced rate of 5'-dRp processing, which inhibited ligation (130). Additionally, both pol δ and pol ϵ were functional in long patch DNA repair synthesis, requiring PCNA and RF-C for nucleotide incorporation (130). Thus, it appears that DNA polymerases β , δ , and ϵ are each capable of functioning in the two alternative pathways utilized by mammalian cells to complete uracil-initiated BER. At the present time it is unclear which polymerase has a primary role in BER *in vivo*; however, it appears that pol β may catalyze repair synthesis in both long patch and short patch BER with pol δ and/or ϵ serving as a back-up system for repair synthesis.

The fidelity of DNA synthesis associated with uracil-initiated BER in human glioblastoma cell extracts was examined recently by using a M13mp2 *lacZ* α DNA-based reversion assay (112). The assay was designed to detect misincorporations at a uracil target; thus, the study analyzed the error rates of

short patch BER and the first nucleotide incorporation of long patch BER, but no attempt to determine patch size was made (112). The fidelity of DNA repair synthesis at a U·T mispair was estimated to be ~1 misincorporated nucleotide per 1900 repaired uracil residues (112). The majority (94%) of the base substitutions at the uracil lesion resulted in transversion mutations, which were approximately equally distributed between T→G and T→A transversions (112).

Repair of abasic sites located in covalently closed circular DNA has also been studied by using purified mitochondrial enzymes from *Xenopus laevis* (105). Reconstitution of the reaction required a mitochondrial Class II AP endonuclease, DNA polymerase γ (pol γ), and mitochondrial DNA ligase (105). Repair was optimized when reaction conditions included high concentrations of MgCl_2 to minimize strand displacement synthesis, resulting primarily in a filled gap size of one nucleotide (105). In these studies, both DNA pol γ and mtDNA ligase were shown to have AP lyase activity, which may fulfill the role of dRpase in the mitochondrial system (105). Longley *et al.* (73) purified and characterized recombinant and native forms of the catalytic subunit of human pol γ . Both forms exhibited DNA polymerase and 3'→5' exonuclease activities (73). Mutations in the exonuclease motif of the catalytic subunit abolished the 3'→5' exonucleolytic activity (73). Reconstitution of uracil-initiated BER with purified proteins revealed that the human pol γ catalytic subunit was capable of filling a single nucleotide gap in the presence of a 5'-terminal dRp moiety (72). In addition, this peptide catalyzed the release of a dRp residue from incised AP sites, indicating that pol γ contains an intrinsic dRpase activity (72). The mtDNA ligase cross-reacted with polyclonal antibody raised to a peptide fragment of DNA ligase III, suggesting that the mitochondrial ligase is related to nuclear DNA ligase III (105).

1.4 Bacteriophage PBS2 Uracil-DNA Glycosylase Inhibitor Protein

1.4.1 Bacteriophage PBS2

The *Bacillus subtilis* bacteriophages PBS1 and PBS2 are unique because their double-stranded DNA genomes contain uracil in place of thymine (131). In addition, the overall base composition of their genomes is unusual in having a 72% A-U content (52, 131). In order for this AU-rich genome to be successfully replicated in a bacterial host which contains mechanisms for eliminating uracil-containing DNA, these bacteriophages have evolved strategies to increase the intracellular pool of dUTP for DNA replication and to inactivate uracil-DNA repair. Virally encoded dTMP 5'-phosphatase (108), dCTP deaminase (134), dUMP kinase (53), and dUTPase inhibitor (109) act to increase dUTP levels while depleting the dTTP pool. Similarly, production of uracil-DNA glycosylase inhibitor protein (Ugi) is induced upon infection to inactivate *B. subtilis* Ung, thus protecting the uracil-substituted genome from degradation by the host uracil-initiated BER enzymes (41).

1.4.2 PBS2 Uracil-DNA Glycosylase Inhibitor

The PBS2 uracil-DNA glycosylase inhibitor protein is a heat-stable, monomeric, 9,474 Dalton polypeptide (8). The deduced amino acid sequences of PBS1 and PBS2 Ugi are identical (74, 117, 143). Ugi is unusually acidic, with 21% of its 84 amino acid residues being Glu or Asp (143). As a result, the protein has a pI of 4.2 and migrates anomalously during sodium dodecyl sulfate-polyacrylamide gel electrophoresis (8). Ugi is highly specific, inactivating uracil-DNA glycosylase from diverse biological sources but having no detectable effect on other classes of DNA glycosylases or other DNA repair enzymes that have been examined (54, 143, 152).

Ugi inactivates uracil-DNA glycosylase by forming a noncovalent complex with 1:1 stoichiometry that is essentially irreversible under physiological conditions (8). Stopped-flow kinetic analysis indicated that the formation of Ung•Ugi complex occurs via a two-step mechanism (10). The

first step involves the formation of a reversible association between Ung and Ugi with a dissociation constant of $1.3 \mu\text{M}$ (10). The second step produces the Ung•Ugi complex and is characterized by a rate constant of $k=195 \text{ sec}^{-1}$ (10). Thus complex formation proceeds through a “docking” and “locking” mechanism where the proteins become properly aligned and tightly bound (10).

Several observations suggest that Ugi inhibits Ung by binding at the enzyme’s DNA binding site: (i) formation of Ung•Ugi complex prevented enzyme binding to DNA (8); (ii) Ugi was capable of dissociating an Ung•DNA complex (8); (iii) UV cross-linking of oligonucleotide dT₂₀ to Ung prevented association between Ung and Ugi (7); (iv) the addition of Ugi to UV cross-linking reactions prevented the formation of cross-linked Ung x dT₂₀ (7); and (v) X-ray crystallographic analysis of Ugi in complex with uracil-DNA glycosylase from human (79, 80), herpes simplex virus type-1 (117), and *E. coli* (110, 111) uracil-DNA glycosylases revealed that Ugi complexes with uracil-DNA glycosylase at the DNA binding domain by mimicking the structure of DNA.

1.4.3 Structure of Uracil-DNA Glycosylase Inhibitor Protein

The crystal structure of the PBS2 uracil-DNA glycosylase inhibitor protein has been reported in free form (110) and in complex with human [Mol, 1995 #169], HSV-1 [Savva, 1995 #243], and *E. coli* [Ravishankar, 1998 #226; Putnam, 1999 #338] uracil-DNA glycosylases. The inhibitor displays charge, shape, and hydrophobic complementarity to the enzyme (79, 110). Crystal structures of free inhibitor indicated that Ugi complementarity with uracil-DNA glycosylase is pre-existing, although localized conformational changes around Ugi Glu-20 are observed following Ung•Ugi complex formation (110). Ugi consists of a five-stranded antiparallel β -sheet and two α -helices, which lie on opposite sides of the β -strands (110). The protein has a compact, globular fold and displays extensive hydrophobic packing, observations which are consistent with its thermostability (110).

Ugi forms a complex with the enzyme through two major interactions: (i) a hydrophobic cavity in Ugi between $\alpha 2$ and the β -sheet envelops the leucine side chain in the conserved leucine loop (human Leu-272, *E. coli* Leu-191) (110) and (ii) the Ugi $\beta 1$ edge sequesters the DNA binding groove of the enzyme without contacting the uracil binding pocket (110). Upon binding Ung, Ugi undergoes a “ β -zipper” conformational change which extends the intramolecular interactions between the $\beta 1$ - and $\beta 2$ -strands (110). Rotation of the Gln-19 carbonyl by $\sim 180^\circ$ positions Glu-20 to make important DNA-phosphate-mimicking interactions with Ung (110). Alignment of *E. coli* Ung-bound Ugi and human UDG-bound DNA reveals striking structural similarities between Ugi and DNA (110). Most carboxylate side chains in Ugi superimpose with the DNA phosphate backbone, including the DNA strand that is not contacted by UDG (110). Thus, irreversible inhibition of uracil-DNA glycosylase by Ugi is a result of Ugi’s mimicry of bound DNA.

1.5 Research Objectives

Several amino acid residues of *E. coli* Ung have been implicated in DNA binding or catalysis based on biochemical and structural data and amino acid sequence conservation between biologically distant species (7, 103, 116, 127). Several investigators have proposed catalytic mechanisms for uracil-DNA glycosylase and in each an absolutely conserved histidine residue corresponding to *E. coli* Ung His-187 was proposed to play an essential role in catalysis (80, 116); however, the function of Ung His-187 remains to be fully elucidated. Previously, an *E. coli* Ung H187D mutation was generated to examine the role of this absolutely conserved amino acid in substrate recognition, binding, and catalysis (6). As part of the research for this thesis the mutant protein was overproduced, purified to apparent homogeneity, and biochemically characterized. The mutation was anticipated to disrupt DNA binding or hydrolysis of the uracil N-glycosyl bond; thus, a comparison between wild type and H187D mutant proteins was expected to provide insight into the mechanism of uracil-DNA glycosylase catalysis.

Additionally, techniques were developed to identify and purify uracil-DNA glycosylases from biological samples by exploiting the high degree of homology displayed by this enzyme and the ability of the Ugi inhibitor protein to bind uracil-DNA glycosylase from sources other than *B. subtilis*. A Ugi-affinity resin and polyclonal antibody to *E. coli* Ung were used as probes to purify mitochondrial uracil-DNA glycosylases from partially purified extracts. The tools developed provide a rapid means for identifying and recovering uracil-DNA glycosylases from crude samples.

2. MATERIALS AND EXPERIMENTAL PROCEDURES

2.1 Materials

2.1.1 Chemicals

Trizma (Tris base), ethylenediaminetetraacetic acid (EDTA), MgSO_4 , HEPES, CAPS, MOPS, MES, β -mercaptoethanol for buffers, bovine serum albumin, ATP, calf thymus DNA (type I), thiamine, tetracycline, ampicillin, streptomycin sulfate, alumina, phenylmethylsulfonyl fluoride (PMSF), tetrasodium pyrophosphate, uracil, 6-amino uracil, 5-fluorouracil, Freund's complete and incomplete adjuvants, Tween-80, and SDS-7L protein molecular weight markers were purchased from Sigma. Agarose, glycine, sodium dodecyl sulfate (SDS), isopropyl- β -D-thiogalactopyranoside (IPTG), dithiothreitol (DTT), ammonium sulfate, sucrose, urea, formamide, and 1 kb and 100 bp DNA ladders were obtained from Life Technologies. J.T. Baker was the source of triethylamine, glycerol, NaOH, NaHCO_3 , glucose, isoamyl alcohol, perchloric acid, boric acid, mono- and dibasic potassium phosphate, dimethyl formamide (DMF), and lithium chloride. Potassium acetate, KCl, MgCl_2 , methanol, ammonium hydroxide (50%), hydrochloric acid, acetic acid, trichloroacetic acid, and phenol were purchased from Fisher. β -mercaptoethanol for gel electrophoresis, protein assay (Bradford) dye reagent, bovine gamma globulin, bromophenol blue, xylene cyanol, prestained SDS-PAGE protein standards (Low Range), acrylamide, bis N,N'-methylene-bis-acrylamide, ammonium persulfate, TEMED, Coomassie Brilliant Blue G250, bromochloroindolyl phosphate (BCIP) and nitro blue tetrazolium (NBT) were obtained from Bio-Rad. The source of horseradish peroxidase- and alkaline phosphatase-conjugated goat anti-rabbit antibodies, 2,2'-azino-di-[3-ethylbenzthiazoline sulfonate] (ABTS) and ABTS buffer was Boehringer Mannheim. Hydrogen peroxide and chloroform were purchased from Mallinckrodt. Pharmacia Biotech was the source of dATP, dCTP, dGTP, and dTTP. Formic acid was from EM Science.

2.1.2 Radionucleotides

[³⁵S]methionine, [γ -³²P]ATP, [³H]uracil, and [³H]leucine were purchased from DuPont-New England Nuclear. [³H]dUTP was obtained from Amersham Corp.

2.1.3 Bacterial Growth Media

2xYT medium was composed of 1% yeast extract (Difco), 2% tryptone (Difco). TYEN medium contained 1% tryptone, 1% yeast extract, and 0.5% NaCl, adjusted to pH 7.5 with 10 M NaOH. LB medium was comprised of 1% tryptone, 0.5% yeast extract, 1% NaCl, adjusted to pH 7.5 with 10 M NaOH. SOC medium contained 2% tryptone, 0.5% yeast extract, 0.05 % NaCl, 2.5 mM KCl, 10 mM MgCl₂, and 20 mM glucose, adjusted to pH 7.0 with 5 M NaOH. M9 medium contained 1.28% Na₂HPO₄•7H₂O, 0.3% KH₂PO₄, 0.05% NaCl, and 0.1% NH₄Cl. Following sterilization, M9 medium was supplemented with 2 mM MgSO₄, 0.1 mM CaCl₂, 0.4% glucose, and 10 µg/ml thiamine from individual sterile stock solutions.

Solid plates were prepared by the addition of 1.5% (w/v) bacto-agar (Difco) to liquid media. Where appropriate, liquid media or media plates were supplemented with 100 µg/ml ampicillin from a filter-sterilized stock solution (100 mg/ml) or with 15 µg/ml tetracycline from a 15 mg/ml stock (in ethanol).

2.1.4 Bacterial Strains and Bacteriophage

The genotypes of *E. coli* strains used in this research are listed in Table 2. *E. coli* strains JM105 and JC10289 and the P1*vir* lysate of JC10289 were provided by W. Ream (Oregon State University).

Table 2

E. coli Strains and Genotypes

<i>E. coli</i> Strain	Genotype	Reference
BD2314	<i>thi-1 his-68 tyrA2 purC50 trp-45</i> <i>lacY1 gal-6 xyl-7 mtl-2 malA1</i> <i>rpsL125 tonA2 tsx-70 supE</i> <i>ung-152::Tn10</i>	(30)
BW310	<i>relA1 spoT1 thi-1 ung-1</i>	(34)
JC10289	<i>thr-1 leuB6 proA2 his-4 argE3 thi-1</i> <i>mtl-1 gatC? ara-14 lacY1 galK2</i> <i>xyl-5 rpsL31tsx-33 supE44</i> <i>srlR301::Tn10-84 Δ(recA-srl)306</i>	(19)
JM105	F' <i>traD36 lacI^q Δ(lacZ)M15</i> <i>proA⁺B⁺/thi rpsL endA sbcB15</i> <i>sbcC? hsdR4 (r_k⁻m_k⁺)Δ(lac-proAB)</i>	(154)
MJ100 ^a	BW310 <i>srlR301::Tn10-84 Δ(recA-srl)306</i>	

^aStrain constructed as described under "Experimental Procedures".

2.1.5 Plasmids

The overexpression vectors for producing Ung (pSB1051) (10), Ung H187D (pUngH187D) (6), and Ugi (pZWtac1) (144) were constructed as previously described. The plasmid pKK223-3 was purchased from Pharmacia Biotech.

2.1.6 Chromatographic Resins

DEAE-cellulose (DE52) anion exchange resin was obtained from Whatman. Sephadex G-25 and G-75, poly(U)-Sephadex, and activated Sephadex 4B were purchased from Pharmacia Biotech. Bio-Rad was the source of hydroxyapatite Bio-Gel HTP, Bio-Gel P-4, and Dowex 1-X8 ion exchange resins.

2.1.7 Oligonucleotides

The nucleotide sequences of the oligonucleotides used in the assays described in this thesis are listed below, where "B" indicates an abasic sugar and "P" indicates a 2-aminopurine residue. The dT₂₀, U-25-mer, A-25-mer, and G-25-mer oligonucleotides were synthesized by the Center for Gene Research and Biotechnology (Oregon State University) on an Applied Biosystems Model 380B DNA synthesizer. dT₁₉-U, 2AP-27-mer and U-27-mer oligonucleotides were supplied by Midland Certified Reagent Company. The dT₁₉-AP oligonucleotide was produced as described in this thesis. The following oligonucleotides were used in this research:

1. Substrate Specificity Assays ("Section 2.2.22.5"):

U-25-mer: 5'-GGG GCT CGT AUA AGG AAT TCG TAC C-3'

A-25-mer: 5'-CCC CGG TAC GAA TTC CTT ATA CGA G-3'

G-25-mer: 5'-CCC CGG TAC GAA TTC CTT GTA CGA G-3'

2. UV-Crosslinking Assays ("Section 2.2.22.7"):

dT₂₀: 5'-TTT TTT TTT TTT TTT TTT TT-3'

dT₁₉-U: 5'-TTT TTT TTT TTU TTT TTT TT-3'

dT₁₉-AP: 5'-TTT TTT TTT TTB TTT TTT TT-3'

3. Steady-State Fluorescence Assays ("Section 2.2.23"):

2AP-27-mer: 5'-CCC CGG TAG ACG APT TCC TTG TAC GAG-3'

U-27-mer: 5'-GGG GCT CGT ACA AGG AAU TCG TCT ACC-3'

2.1.8 Enzymes

*Bam*HI, *Pvu* II, T4 polynucleotide kinase, and DNA polymerase I were obtained from New England Biolabs. The source of RNase H was GibcoBRL.

2.2 Experimental Procedures

2.2.1 Preparation of Chromatographic Resins

2.2.1.1 *Preparation of DEAE-Cellulose, Sephadex G-25 and G-75, Bio-Gel P-4, and Poly(U) Sepharose*

DEAE-cellulose was prepared by using pre-swollen DE52 diethylaminoethyl cellulose resin suspended at a 1:5 ratio (v/v) in TED buffer (10 mM Tris-HCl (pH 8.0), 1 mM EDTA, 1 mM DTT). The resin was allowed to settle at room temperature, the buffer decanted to remove the fines, and fresh TED added with gentle agitation. The resin was defined 4-5 times in this manner and stored as a 50% (v/v) slurry in TED buffer containing 1 M NaCl at 4°C.

Sephadex G-25 and G-75, Bio-Gel P-4, and poly(U) Sepharose resins were prepared as described above with various buffer conditions for hydration and storage. Sephadex G-25 was prepared in TEAB buffer (10 mM triethylammonium bicarbonate, pH 7.0). Sephadex G-75 was prepared in Ung Equilibration Buffer (UEB) (10 mM HEPES-KOH (pH 7.4), 10 mM

β -mercaptoethanol, 1 mM EDTA, 5% (w/v) glycerol, 1 M NaCl) or Ugi Equilibration Buffer (IEB) (50 mM Tris-HCl (pH 8.0), 1 mM EDTA, 1 mM DTT, 100 mM NaCl, 10% (w/v) glycerol) for the purification of Ung and Ugi, respectively. Bio-Gel P-4 was prepared in TE (10 mM Tris-HCl (pH 7.5), 1 mM EDTA) or DAB (30 mM Tris-HCl (pH 7.4), 1 mM EDTA, 1 mM DTT, 5% (w/v) glycerol) buffers. Poly(U) Sepharose was hydrated in TMEG buffer (50 mM Tris-HCl (pH 7.5), 10 mM β -mercaptoethanol, 1 mM EDTA, 10% (w/v) glycerol) and stored in TMEG buffer containing 1 M NaCl.

2.2.1.2 *Preparation of Hydroxylapatite*

Hydroxylapatite powder was suspended in 10 volumes of 0.5 M potassium phosphate (pH 7.5). After settling, the buffer was decanted and the resin suspended in 10 volumes of 20 mM potassium phosphate (pH 7.5). The resin was defined at least 5 times before storing as a 50% (v/v) slurry in 20 mM potassium phosphate (pH 7.5) at 4°C.

2.2.1.3 *Preparation of Single-Stranded DNA-Agarose*

Calf thymus DNA (Type I, Sigma) was solubilized at 15 mg/ml in 250 ml of 20 mM NaOH by gently stirring overnight at room temperature. The DNA solution was incubated at 95°C for 15 min and mixed with an equal volume of molten 4% agarose equilibrated at 70°C. The mixture was poured into an ice cold Pyrex dish resting in an ice bath and allowed to solidify. The solid DNA/agarose mixture was passed twice through a stainless steel sieve (60 mesh) and the resultant gel particles were suspended in 150 ml of resuspension buffer (10 mM Tris-HCl (pH 7.4), 1 mM EDTA, 100 mM NaCl). The gel was placed in a Buchner funnel (200 ml, 40-60 C) and washed with approximately 10 L of resuspension buffer until the $A_{260\text{ nm}}$ of the wash was below 0.02 absorbance units. The resin was stored at 4°C as a 50% (v/v) slurry in resuspension buffer.

2.2.1.4 Preparation of Dowex 1-X8

Dowex resin was converted from the chloride to the formate form for use in Ung and Ugi assays. A 1000 ml cylinder was filled with 800 ml of 1 M NaOH, and Dowex resin was added to bring the volume to 1000 ml. The mixture was inverted several times and allowed to settle 20 min at room temperature. The NaOH was removed by aspiration and the cylinder refilled with 1 M NaOH to 1000 ml. This procedure was repeated until 4 L of 1 M NaOH was used. The resin was equally divided between three 200 ml glass filter funnels (40-60 C) and the residual NaOH allowed to drain by gravity. Each funnel was washed with 200 ml of 1 M ammonium formate buffer (1 M formic acid adjusted to pH 4.2 with concentrated ammonium hydroxide), followed by ~667 ml of 10 mM ammonium formate buffer (pH 4.2). Dowex resin was stored as a 50% (v/v) slurry in 10 mM ammonium formate buffer at 4°C.

2.2.1.5 Preparation of Ung- and Ugi-Sepharose

Ung- and Ugi-Sepharose were prepared by coupling purified Ung or Ugi to CNBr-activated Sepharose 4B. Activated Sepharose (6 g) was suspended in 40 ml of 1 mM HCl at room temperature. The gel was washed with 1160 ml of 1 mM HCl over 15 min using a sintered glass filter (40-50 M), followed by a 50 ml wash with coupling buffer (0.1 M NaHCO₃ (pH 8.3), 0.5 M NaCl). The gel was resuspended in 7 ml of coupling buffer and divided into two equal fractions based on settled gel volume. One portion was coupled to purified Ung or Ugi and the second was treated in a mock coupling reaction to produce control resin. In the mock reaction, an equal volume of coupling buffer (15 ml) was added to the gel. Purified Ung or Ugi (30 mg protein/g of dry Sepharose), diafiltered in coupling buffer, was diluted in coupling buffer such that the total volume addition of protein would equal the volume of gel. The coupling reaction was allowed to proceed for 2 h at room temperature with gentle rocking. The buffer was removed by filtration and the gel was washed with 5 volumes of coupling buffer.

The unreacted active sites on the resin were blocked by incubating the gel with 35 ml of 0.1 M Tris-HCl (pH 8.0) for 16 h at 4°C without agitation. The Tris buffer was decanted and fresh 0.1 M Tris-HCl was added for an additional 1 h incubation at 4°C. The buffer was then removed by filtration. Uncoupled ligand was removed by washing the resin with three alternating cycles of low and high pH. For Ugi- and mock-treated Sepharose, washes consisted of 5 gel volumes of 100 mM glycine (pH 2.5) containing 1 M NaCl and 100 mM Tris-HCl (pH 8.0) containing 1 M NaCl. For Ung-Sepharose, 100 mM acetate (pH 4.0) containing 0.5 M NaCl and 100 mM Tris-HCl (pH 8.0) containing 0.5 M NaCl were used. The amount of ligand coupled was estimated by monitoring the coupling, blocking, and wash buffers for absorbance at 280 nm, determining their protein concentrations using the known extinction coefficient for each protein, and subtracting the total amount of recovered protein from the initial starting amount.

The resin was washed with 5 gel volumes of 50 mM Tris-HCl (pH 8.0), 1 mM EDTA, 1 mM DTT, 100 mM NaCl and stored as a 25% (v/v) slurry at 4°C in the same buffer. When used for affinity purification of antibody, DTT was omitted from the storage buffer.

2.2.2 Preparation of Dialysis Tubing

Dialysis tubing was cut into 25-30 cm lengths and soaked for 1 h in 1% acetic acid. The tubing was rinsed in distilled water then boiled in 1% (w/v) NaHCO_3 , 0.1% (w/v) EDTA with intermittent stirring. The solution was discarded upon turning a yellow color and replaced with fresh NaHCO_3 /EDTA buffer. This procedure was repeated at least 3 times or until the solution no longer changed color with boiling. The tubing was rinsed with distilled water and boiled in fresh distilled water with one exchange. The prepared dialysis tubing was then stored in 10 mM EDTA at 4°C.

2.2.3 Protein Concentration Measurements

2.2.3.1 Concentration Determination by Bradford Assay

The protein concentrations of crude extracts and sera were determined by the modified Bradford method (14) using the Bio-Rad Protein assay. For the standard procedure (20-140 μg protein, 200-1400 $\mu\text{g}/\text{ml}$), Bradford dye reagent was diluted 1:5 in distilled water and filtered through Whatman No. 1 filter paper. Standards and diluted samples (100 μl) were gently mixed with 5 ml of dye diluted reagent. For the microscale procedure (1-20 μg protein, ≤ 25 $\mu\text{g}/\text{ml}$), 0.8 ml of standards or diluted samples was mixed with 0.2 ml of Bradford dye reagent concentrate. After incubation at room temperature for 5-60 min, absorbance at 595 nm was measured. BSA was used as a standard for crude extracts and bovine gamma globulin was used as a standard for sera.

2.2.3.2 Concentration Determination by Spectrophotometric Measurements

The concentrations of purified *E. coli* Ung and Ugi were determined by absorbance spectroscopy using the molar extinction coefficients $\epsilon_{280\text{ nm}} = 4.2 \times 10^4$ liters/mol \cdot cm and $\epsilon_{280\text{ nm}} = 1.2 \times 10^4$ liters/mol \cdot cm for Ung and Ugi, respectively (8).

2.2.4 Small-Scale Preparation of Plasmid DNA

Minipreparation of plasmid DNA was performed by a modified alkaline lysis method (75). A single bacterial colony was transferred to 2 ml of 2x YT medium (2% tryptone, 1% yeast extract) containing the appropriate antibiotic and the culture was incubated overnight at 37°C with shaking. The culture (1.5 ml) was transferred to a microfuge tube and centrifuged for 5 min at maximum speed in a microcentrifuge to pellet the bacteria. The medium was removed by using aspiration, leaving the pellet as dry as possible. The bacterial pellet was resuspended by vigorous vortexing in 100 μl of ice-cold

buffer containing 50 mM glucose, 25 mM Tris-HCl (pH 8.0), and 10 mM EDTA. A freshly prepared solution of 0.2 M NaOH containing 1% SDS (200 μ l) was added, the tube was gently inverted several times, and the mixture placed on ice for 5 min. Ice-cold potassium acetate buffer (150 μ l; 3 M with respect to potassium, 5 M with respect to acetate) was added and the tube was gently vortexed in an inverted position. The mixture was stored on ice for 5 min then centrifuged at 12,000xg for 5 min at 4°C. The supernatant was transferred to a fresh tube.

The DNA was extracted with an equal volume of phenol equilibrated in TE buffer by briefly vortexing, and centrifugation was conducted for 2 min in a microcentrifuge. The aqueous layer was transferred to a fresh tube and extracted with an equal volume of chloroform:isoamyl alcohol (24:1). After centrifugation as before, the aqueous layer was transferred to a fresh tube and the DNA was precipitated with the addition of 2.5 volumes of ice-cold absolute ethanol. After incubating 2 min at room temperature, the DNA was recovered by centrifugation in a microcentrifuge for 5 min at maximum speed. The supernatant was removed by aspiration, the pellet washed with ice-cold 70% ethanol, and the tube centrifuged as described previously.

After removing the ethanol by aspiration, the pellet was dried under vacuum, then resuspended in 20 μ l of TE buffer. The DNA was stored at -20°C and used for restriction enzyme digestion or electroporation.

2.2.5 Restriction Enzyme Digestion of Plasmid DNA

Plasmid DNA from minipreps (1-2 μ g) was incubated in a 20 μ l reaction mixture for 1 h at 37°C with 10 units of *Bam*HI or *Pvu*II restriction endonuclease in reaction buffer containing 10 mM Tris-HCl (pH 7.9), 150 mM NaCl, 10 mM MgCl₂, 1 mM DTT. *Bam*H I digestion mixtures were supplemented with 100 μ g/ml BSA. Loading dye (10 mM EDTA, 0.1% SDS, 0.001% bromophenol blue, 5% (w/v) glycerol) was added to each sample for analysis by 2% agarose gel electrophoresis.

2.2.6 Oligonucleotide Purification

Synthetic oligonucleotides were supplied from either the Center for Gene Research and Biotechnology or Midland Certified Reagent Company as a lyophilized powder. The powder was resuspended in 1 ml of TEAB buffer (10 mM triethylamine-bicarbonate adjusted to pH 7.0 by bubbling CO₂ gas through the solution). The sample was loaded onto a Sephadex G-25 column (1.5 cm² x 7 cm) equilibrated in TEAB at room temperature and eluted with equilibration buffer. Fractions (1 ml) were collected at a flow rate of ~15 ml/h and oligonucleotide-containing fractions were identified by absorbance at 260 nm. Peak fractions were pooled and evaporated to dryness by using a Speed-Vac Concentrator. When ready for use, each oligonucleotide preparation was resuspended in a total of 100-150 µl of distilled H₂O. The concentration of resuspended oligonucleotide was determined by absorbance spectroscopy (1 A_{260 nm} = 20 µg/ml) and the purity was determined by the OD_{280 nm}/OD_{260 nm} ratio. The expected OD_{280 nm}/OD_{260 nm} value for pure preparations of DNA is 1.8.

2.2.7 5'-end ³²P-Phosphorylation of Oligonucleotides

For oligonucleotides used in substrate specificity assays, phosphorylation reactions (138 µl) consisting of 4 nmol of U-25-mer, 50 units of T4 polynucleotide kinase, and 0.3 µM of [³²P]ATP in kinase reaction buffer (50 mM Tris-HCl (pH 7.6), 10 mM MgCl₂, 5 mM DTT, 0.1 mM EDTA) were incubated for 15 min at 37°C then supplemented with 200 µM of ATP. The reaction was continued for 45 min at 37°C and terminated by the addition of EDTA to a final concentration of 10.7 mM plus heating at 70°C for 10 min. Complementary oligonucleotides were phosphorylated in a similar fashion using nonradioactive ATP in place of [³²P]ATP.

To radiolabel oligonucleotide for UV crosslinking experiments, reaction mixtures (200 µl) typically contained ~300 nmol of oligonucleotide, 100 units of T4 polynucleotide kinase, 0.2 µM of [³²P]ATP, and a 2-fold molar excess of nonradioactive ATP relative to oligonucleotide in kinase reaction buffer. The

samples were incubated for 60 min at 37°C and reactions were terminated by the addition of EDTA to a final concentration of 10.7 mM and heating at 70°C for 5 min

Phosphorylated oligonucleotide was purified from free ATP by using P-4 spun columns equilibrated in TE or DAB buffer for specificity or crosslinking studies, respectively. The sample was typically split into two equal volumes and each diluted to 250 µl with the appropriate equilibration buffer. The samples were applied to two consecutive P-4 columns (1.5 ml resin, each) and centrifuged for 2.5 min in an IEC clinical centrifuge (setting #4) at room temperature.

2.2.8 Generation of Abasic Site-Containing Oligonucleotide

Oligonucleotide dT₁₉-U (5'-TTT TTT TTT TTU TTT TTT TT-3') was treated with *E. coli* Ung (Fraction IV) to generate an apyrimidinic site containing DNA substrate. After 5'-end ³²P-labeling of dT₁₉-U as described above, 110 nmol of [³²P]dT₁₉-U (4600 cpm/pmol) was incubated with ~7.5 x 10⁵ units of Ung for 30 min at 37°C in a total reaction volume of 315 µl. The DNA-enzyme mixture was then incubated with 575 µl of Ugi-Sepharose resin for 45 min at 4°C, with inversion of the reaction tube several times during the incubation period. The reaction tube was centrifuged for 2.5 min in an IEC clinical tabletop centrifuge (setting #4) to separate the resin from the DNA-containing supernatant. The resin was washed once with 250 µl of distilled water to recover any residual DNA, and the wash was pooled with the supernatant buffer. The recovered oligonucleotide was concentrated to 100 µl in a Centricon-3 (Amicon) concentrator. The substrate was verified by subjecting the abasic site to alkaline lysis and analyzing the cleavage product by 12% polyacrylamide gel electrophoresis.

2.2.9 Hybridization of Oligonucleotides

Double-stranded DNA was formed by annealing 750 pmol of [³²P]U-25-mer to 1,500 pmol of A-25-mer or G-25-mer to construct duplex [³²P]U/A- and

[³²P]U/G-25-mer DNA substrates. Annealing reaction mixtures (186 μ l) contained SSC buffer (20 mM Tris-HCl (pH 7.4), 2 mM MgCl₂, and 50 mM NaCl). Reaction mixtures were placed in a 500 ml beaker containing 70°C distilled H₂O and allowed to cool to room temperature (~4 h).

Uracil-containing 27-mer was annealed in excess of complementary 2-aminopurine-containing 27-mer oligonucleotide to generate substrate for steady-state fluorescence experiments. U-27-mer (74 nmol) and (2AP)-27-mer (59.2 nmol) were combined in an annealing reaction mixture (470 μ l) containing SSC buffer and treated as described above.

2.2.10 Electroporation of *E. coli* with Plasmid DNA

E. coli strains were transformed by electroporation. Cells were prepared for electroporation by growing in 1 L of TYEN broth (1% tryptone, 1% yeast extract, 0.5% NaCl, adjusted to pH 7.5 with 10 M NaOH) at 37°C to mid-log phase (0.5-1.0 OD_{600 nm}). The culture was chilled on ice for 5 min before centrifugation at 4,000xg for 15 min at 4°C. All subsequent centrifugations were performed in an identical manner. The bacterial pellets were resuspended in an equal volume of ice-cold distilled water, centrifuged, resuspended in 0.5 volume of ice-cold distilled water, centrifuged, resuspended in 0.02 volume of ice-cold 10% glycerol (w/v), centrifuged, and finally resuspended in 2-3 ml of ice-cold 10% glycerol (w/v). Cells were frozen at -80°C in 50 μ l aliquots until ready for use.

For electroporation, 4-8 ng of plasmid DNA was mixed with 50 μ l of prepared cells. The cell/DNA mixture was transferred to a cold electroporation cuvette (0.2 cm electrode gap) and incubated on ice for 1 min. The cells were exposed to a pulse of 2.5 kV, 25 μ F, and 200 Ω with a time constant of ~5-7 msec (Gene Pulser II, BioRad). Immediately after the pulse, 1 ml of SOC medium was added to the cuvette, then the culture was transferred to a culture tube and incubated for 1 h at 37°C with shaking. Aliquots of cells were then plated on the appropriate selective media.

2.2.11 Transduction of *E. coli* BW310 by P1_{vir}

A saturated culture of *E. coli* BW310 was diluted (1:100) with 10 ml of fresh TYEN broth and grown to early mid-log stage ($OD_{600\text{ nm}}$ 0.4-0.5) at 37°C with shaking. The cells were pelleted at room temperature in an IEC clinical centrifuge (setting #5) for 20 min and then resuspended in 1 ml of LB broth (1% tryptone, 0.5% yeast extract, 1% NaCl, adjusted to pH 7.5 with 10 M NaOH). The bacterial suspension (0.5 ml; $\sim 1 \times 10^9$ cells/ml) was mixed with an equal volume of 15 mM CaCl_2 containing 30 mM MgSO_4 and one half volume of a P1 lysate ($\sim 1 \times 10^8$ pfu/ml in LB). The multiplicity of infection was ~ 0.05 . The mixture was incubated for 20 min at 37°C, centrifugation was conducted as described, and the cell pellet was washed with an equal volume (1.25 ml) of TYEN broth. The cells were pelleted again and resuspended in 0.1 ml of LB. The entire volume was plated on LB agar containing 15 $\mu\text{g}/\text{ml}$ tetracycline and incubated overnight at 37°C. Approximately 300 tetracycline resistant colonies appeared. Sixteen colonies were purified on LB-tet plates and one was screened for sensitivity to UV-irradiation.

Overnight cultures (5 ml) of the transductant, *E. coli* BW310, and JC10289 were grown in the appropriate media. The cultures were streaked across LB agar in parallel lines. While working in the dark, the lids of the Petri plates were removed and the plates were placed ~ 75 cm from a UV source ($\lambda_{\text{max}} = 254\text{ nm}$) with a dose rate of $2.4\text{ J}/\text{m}^2/\text{sec}$. Sections of the plates were UV-irradiated for increasing intervals of time, resulting in exposures of 4.8-57.6 J/m^2 . The lids were replaced and the plates were wrapped in aluminum foil before incubating overnight at 37°C.

2.2.12 Preparation of Crude Cell Extracts

E. coli JM105 containing pUngH187D, pSB1051, or pKK223-3 was streaked onto fresh LB agar plates containing 100 $\mu\text{g}/\text{ml}$ ampicillin (Amp) and grown at 37°C overnight. An isolated colony was used to inoculate TYEN-Amp broth and the culture was incubated overnight with shaking at 37°C. The overnight culture was diluted (1:100) into 10 ml of fresh TYEN-Amp and

grown with shaking at 37°C to an optical density of 0.6-0.8 at 600 nm. Gene expression was induced with 1 mM IPTG and the culture incubated an additional 3 h. Uninduced cultures were grown to 0.6-0.8 OD_{600 nm} and allowed to grow an additional 3 h without addition of IPTG. The cultures were then chilled and the cells harvested by centrifugation at 3500xg at 4°C for 15 min. Cell pellets were stored at -80°C until ready to use.

Thawed pellets were resuspended in 4 ml of 10 mM Tris-HCl (pH 8) and lysed by sonication using 8-12 pulses (30 s on/30 s off). Intact cells and cellular debris were removed from the suspension by centrifugation at 7500 rpm (SA600) for 20 min at 4°C. The supernatant was designated cell-free extract (CFE). CFE (25 µg) was mixed with cracking buffer (50 mM Tris-HCl (pH 6.8), 1% SDS, 143 mM β-mercaptoethanol, 10% (w/v) glycerol, 0.04% bromophenol blue), placed in a boiling water bath for 10 min, and then analyzed by 12.5% SDS-PAGE.

2.2.13 Purification of *E. coli* Uracil DNA Glycosylase

2.2.13.1 Large Scale Purification of Ung

A saturated culture (25 ml) of *E. coli* JM105 containing pSB1051 was diluted (1:100) into 2 L of LB broth supplemented with 0.01% ampicillin. The culture was grown at 37°C until the OD_{600 nm} reached ~0.8. IPTG was added to a final concentration of 1 mM and the culture incubated an additional 3 h to induce expression of the *ung* gene. The culture was then chilled on ice and centrifuged at 3,500xg for 15 min at 4°C. The supernatant was discarded and the pellets were stored at -80°C until ready for use.

Cell pellets were thawed and resuspended in TED buffer (40 ml/L culture) using a Dounce homogenizer to disrupt aggregates. The cells were lysed either in 40 ml aliquots by using a French pressure cell at 15,000 psi or by sonication using 10-12 pulses of 30 sec each. All subsequent procedures were performed at 4°C. Cellular debris was removed by centrifugation at 6,500xg for 20 min. An equal volume of 1.6% (w/v) streptomycin sulfate in TED

buffer was added to the supernatant (Fraction I) dropwise with stirring. After the entire volume of streptomycin sulfate had been added, the solution was stirred for an additional 30 min then centrifuged for 20 min at $6,500 \times g$. Finely ground ammonium sulfate was slowly added to the supernatant with stirring to a final concentration of 70% (saturation). After stirring for 30 min, the precipitate was collected by centrifugation at $10,000 \times g$ for 15 min. The pellet was resuspended in 5 ml of UEB buffer (10 mM HEPES-KOH (pH 7.4), 10 mM β -mercaptoethanol, 1 mM EDTA, 5% (w/v) glycerol, 1 M NaCl). The solution was dialyzed in 12-14,000 MWCO tubing overnight against UEB (2 L) with 2-3 changes of buffer. The solution (Fraction II) expanded to ~25 ml during dialysis.

The sample was applied to a Sephadex G-75 column ($6 \text{ cm}^2 \times 88 \text{ cm}$) equilibrated in UEB buffer and eluted at a rate of 20 ml/h with the equilibration buffer. Fractions (5 ml) containing Ung activity were pooled and concentrated 2-fold using an Amicon stirred cell (YM10 membrane) under N_2 gas (55 psi). After diafiltration against HAB buffer (10 mM potassium phosphate (pH 7.4), 1 mM DTT, 200 mM KCl), the sample (Fraction III) was loaded onto a hydroxylapatite column ($2 \text{ cm}^2 \times 10 \text{ cm}$) equilibrated in the same buffer. Fractions (5 ml) were collected and Ung activity was recovered in the flow through. The peak fractions were pooled (Fraction IV) and dialyzed against DAB buffer (30 mM Tris-HCl (pH 7.4), 1 mM EDTA, 1 mM DTT, 5% (w/v) glycerol). The sample was applied to a DNA agarose column ($19.6 \text{ cm}^2 \times 42 \text{ cm}$) equilibrated in DAB and fractions (6.5 ml) were collected. The column was washed with ~750 ml of equilibration buffer before performing a step-wise elution with DAB containing 150 mM NaCl. Fractions containing Ung activity were pooled, concentrated 40-fold, and diafiltered into DAB by using an Amicon stirred cell (YM10 membrane) as described above. The purified protein (Fraction V) was stored in aliquots at -80°C .

2.2.13.2 Purification of [^3H -Leu]Ung

Radioactively labeled Ung was purified as described above with the following modifications: Cells were grown in M9 minimal salts medium supplemented with 10 $\mu\text{g}/\text{ml}$ thiamine and 0.01% ampicillin. A 1 L culture was grown to 0.625 $\text{OD}_{600\text{ nm}}$ (5×10^8 cells/ml) before adding 1.0 mCi (180 Ci/mmol) [3,4,5- $^3\text{H}(\text{N})$]-leucine. The cells were grown for 35 min before inducing with IPTG. Cells were lysed by sonication as described previously.

2.2.13.3 Purification of Ung H187D

Ung H187D was purified from *E. coli* JM105 harboring pUngH187D by essentially the same protocol as the wild-type enzyme through Fraction IV. Subsequently, Fraction IV (26 ml) was dialyzed against DAB buffer and one half the preparation was applied to a single-stranded DNA agarose column ($5.3\text{ cm}^2 \times 28\text{ cm}$) equilibrated in DAB. The column was washed with 150 ml of equilibration buffer and then eluted with a 400 ml linear gradient from 0 to 150 mM NaCl in DAB. Fractions (2.5 ml) were analyzed for Ung activity, the absorbance at 280 nm was measured, and the salt concentration was determined by measuring the conductivity of the fractions. The flow through fractions containing Ung H187D were pooled, dialyzed into TMEG buffer (50 mM Tris-HCl (pH 7.5), 10 mM β -mercaptoethanol, 1 mM EDTA, 10% (w/v) glycerol) and designated Fraction V. Ung H187D (~8 mg) was applied to a poly(U) Sepharose column ($2\text{ cm}^2 \times 12\text{ cm}$) equilibrated in TMEG. The column was washed with 24 ml of equilibration buffer and eluted with 30 ml of TMEG containing 500 mM NaCl. Fractions containing Ung H187D were pooled, concentrated, dialyzed into DAB buffer and designated Fraction VI.

2.2.13.4 Rechromatography of Ung and Ung H187D

Purified Ung H187D (4.53 mg, 167 units) or a mixture of Ung H187D (4.53 mg, 167 units) and purified wild-type *E. coli* Ung (8.35×10^{-5} mg, 167 units) were applied to separate single-stranded DNA agarose columns ($1.8\text{ cm}^2 \times 5.6\text{ cm}$), washed, and step eluted with DAB buffer containing 150 mM NaCl.

Fractions (1ml) were assayed for Ung activity and protein concentration was determined by absorbance at 280 nm.

2.2.14 Purification of PBS2 Uracil-DNA Glycosylase Inhibitor Protein

2.2.14.1 Large Scale Purification of Ugi

A saturated culture (25 ml) of *E. coli* JM105/pZWtac1 was diluted (1:100) into 2 L of TYEN medium containing 0.01% ampicillin. Cells were grown to 0.6-0.8 OD_{600 nm} and IPTG added to 1 mM to induce expression of the *ugi* gene. Growth was continued for an additional 3 h then the culture was chilled and the cells harvested by centrifugation at 3,500xg for 15 min at 4°C. The supernatant was decanted and the pellets stored at -80°C. Pellets were thawed and resuspended in 80 ml of 10 mM Tris-HCl (pH 8.0) with a Dounce homogenizer. Cells were disrupted by sonication using 10-12 pulses of 30 sec each. The sonicated solution was centrifuged at 11,500xg for 15 min at 4°C. The cell extract (Fraction I) was heated at 100°C for 10 min then allowed to cool to room temperature. The precipitates were removed by centrifugation at 11,500xg for 20 min at 4°C. The supernatant was dialyzed against TED buffer (10 mM Tris-HCl (pH 8.0), 1 mM EDTA, 1 mM DTT) using 6-8,000 MWCO tubing.

After dialysis, the sample was centrifuged at 11,500xg for 20 min at 4°C to remove remaining precipitates and the supernatant was designated Fraction II. Fraction II (48 ml) was loaded onto a DEAE-cellulose column (4.9 cm² x 10 cm) equilibrated in TED buffer. Fractions (4.5 ml) were collected as the column was washed with 112 ml of equilibration buffer at a flow rate of 40 ml/h. Ugi was eluted with a 200 ml linear gradient from 0 to 650 mM NaCl in TED buffer. Fractions were assayed for NaCl concentration, inhibitor activity, and protein concentration by absorbance spectroscopy. Peak fractions were pooled and designated Fraction III. Fraction III was concentrated with a Centriprep 10 concentrator to approximately one half the initial volume. The concentrated sample was loaded onto a Sephadex G-75 column (5.3 cm² x 70

cm) equilibrated in IEB buffer (50 mM Tris-HCl (pH 8.0), 1 mM EDTA, 1 mM DTT, 100 mM NaCl, 10% (w/v) glycerol). The protein was eluted from the column with equilibration buffer at a rate of ~15 ml/h. Fractions (4.2 ml) containing inhibitor activity were analyzed for purity by using 20% SDS-polyacrylamide gel electrophoresis and peak fractions were pooled. The purified protein was designated Fraction IV, concentrated under N₂ gas (55 psi) by using an Amicon stirred cell (YM3 membrane) to obtain a concentration of 2-5 mg/ml, and stored in aliquots at -80°C.

2.2.14.2 Purification of [³⁵S-Met]Ugi

Radioactively labeled Ugi was purified as described above with the following modifications: Cells were grown in M9 minimal salts medium supplemented with 10 µg/ml thiamine and 0.01% ampicillin. A 1.5 L culture was grown to 0.625 OD_{600 nm} (5 × 10⁸ cells/ml) before addition of 5.0 mCi (1175 Ci/mmol) [³⁵S]-methionine. The cells were grown for 35 min before inducing with IPTG.

2.2.15 Ung- and Ugi- Sepharose Chromatography

Ung- or Ugi-Sepharose affinity chromatography was performed by incubating samples (100 µl) with an equal volume of the resin slurry in DAB buffer for 10 min at 25°C. Micro-purification columns were designed by plugging gel-loading micropipet tips with Sigma-coat-treated glass wool. The plugged tips were incubated 10 min at 25°C with 100 µl of 10 mM potassium phosphate buffer containing 100 µg/ml BSA to block nonspecific protein binding. The buffer was removed by brief centrifugation in an IEC clinical centrifuge (setting #4) at room temperature and the resin-enzyme slurry was transferred to the micro-columns. The buffer was removed from the resin by centrifugation as described. The resin was washed three times with 200 µl of DAB buffer applied in two equal aliquots, while centrifuging between buffer additions. The columns were sealed by heating and 100 µl of SDS gel loading dye (50 mM Tris-HCl (pH 6.8), 1% SDS, 143 mM β-mercaptoethanol, 10%

(w/v) glycerol, and 0.04% bromophenol blue) was added to the resin. The columns were incubated at 100°C for 10 min to remove bound protein. The columns were then unsealed and centrifuged to dryness. Aliquots (25 µl) of flow through and wash fractions and 50 µl of each SDS elution fraction were analyzed by 12.5% SDS polyacrylimide gel electrophoresis. When applicable, aliquots of flow through (100 µl), wash (100 µl), and SDS elution (25 µl) fractions and the resin were quantitated for radioactivity by liquid scintillation counting in 0.5 ml of water by using 5 ml of Formula 989 fluor.

2.2.16 Isolation of Liver Mitochondria

A fresh pig liver (Clark Meat Laboratory, Oregon State University) was obtained and the gall bladder removed. The tissue was lacerated several times and placed in 500 ml of 0.25 M sucrose on ice. The liver was sliced into ~2 cm³ pieces and soaked in 0.25 M sucrose. The tissue slices were pulverized with a meat grinder and 1200 g of ground liver was mixed with 2.5 L of 0.25 M sucrose. The tissue was homogenized two times through a Zeigler homogenizer, 200 ml of 1 M potassium phosphate (pH 7.5) was added, and the total volume was brought to 4 L with 0.25 M sucrose. The liver homogenate was centrifuged at 2,750 rpm for 10 min in a GSA rotor at 4°C to remove whole cells and nuclei. The supernatant was filtered through two layers of cheesecloth and the filtrate centrifuged at 9,000 rpm in an SA-600 rotor for 30 min at 4°C to remove lysosomes. The mitochondrial pellets were resuspended in 800 ml of homogenization buffer (0.25 M sucrose, 50 mM Tris-HCl (pH 8.0), 25 mM KCl, 5 mM β-mercaptoethanol, 1 mM EDTA, 5 mM MgCl₂) with a Dounce homogenizer. The resuspended mitochondria were further centrifuged at 2,750 rpm for 10 min at 4°C in a GSA rotor. The supernatant fraction was centrifuged in an SA-600 rotor at 9,000 rpm for 10 min at 4°C. The mitochondrial pellet was resuspended in an equal volume of homogenization buffer then centrifuged as described above. This process was repeated 3 times, reducing the volume of homogenization buffer by 50% with

each resuspension. The final mitochondrial pellets were pooled, frozen in liquid nitrogen, and stored at -80°C.

Rat liver mitochondria were prepared by Dr. John Domena by the previously described procedure (27).

2.2.17 Purification of Mitochondrial Ung

Approximately 200 g of frozen rat or pig liver mitochondrial pellets was ground to a paste with 125 g alumina powder in a chilled mortar, 500 ml of extraction buffer (50 mM Tris-HCl (pH 8.0), 5 mM β -mercaptoethanol, 1 mM EDTA, 1 M NaCl, 1 mM PMSF) was slowly added, and the slurry was further ground until smooth. The slurry was centrifuged at 470 \times g for 10 min at 4°C. The supernatant was centrifuged at 10,000 \times g for 10 min at 4°C. The final supernatant was subjected to ultracentrifugation at 100,000 \times g for 1 h at 4°C. The supernatant was recovered (the pellets and lipids being discarded), and dialyzed into TMEG buffer (20 mM Tris-HCl (pH 8.0), 5 mM β -mercaptoethanol, 1 mM EDTA, 10% (w/v) glycerol) containing 150 mM NaCl, and designated Fraction I. Ammonium sulfate precipitations at 0-35% and 35-65% of saturation were performed on the sample and the resultant pellet was resuspended in 30 ml of TEDG buffer (20 mM Tris-HCl (pH 8.0), 1 mM DTT, 1 mM EDTA, 10% (w/v) glycerol). The solution was dialyzed extensively against TEDG then centrifuged in an SA-600 rotor at 10,000 rpm for 15 min at 4°C to remove precipitates. The supernatant, designated Fraction II, was allowed to flow over a Ugi-Sepharose column (100 μ l). The column was washed with 100 μ l of 10 mM potassium phosphate (pH 7.2). Nonspecifically bound proteins were removed with three 100 μ l washes of 0.5 M NaCl followed by 100 μ l of 10 mM potassium phosphate (pH 7.2). The bound Ung was eluted with three 50 μ l washes of 10 mM potassium phosphate (pH 7.2) containing 5 M MgCl_2 .

2.2.18 Polyacrylamide Gel Electrophoresis

2.2.18.1 *Sodium Dodecyl Sulfate Polyacrylamide Gel Electrophoresis*

Denaturing polyacrylamide gel electrophoresis was performed essentially as described by Laemmli (64). The stacking gel (1 cm) contained 3% acrylamide, 0.08% N,N'-methylenebis(acrylamide), 0.125 M Tris-HCl (pH 6.8), and 0.1% SDS. The resolving gel (13 cm) contained 12.5% acrylamide, 0.33% N,N'-methylenebis(acrylamide), 0.375 M Tris-HCl (pH 8.8), and 0.1% SDS. Protein samples were mixed with an equal volume of loading dye containing 50 mM Tris-HCl (pH 6.8), 1% SDS, 143 mM β -mercaptoethanol, 10% (w/v) glycerol, and 0.04% bromophenol blue and heated for 10 min at 90°C. Electrophoresis was performed for 1 h at 100 V, at which time the voltage was increased to 200 V until the tracking dye had migrated approximately 2 cm from the bottom of the gel. The running buffer contained 25 mM Trizma base, 192 mM glycine, and 0.1% SDS.

Protein bands were detected by staining overnight with 0.05% Coomassie Brilliant Blue G-250 in 50% methanol and 10% acetic acid. The gels were washed with destain solution (7% acetic acid and 5% methanol) to reduce background staining. When more sensitive detection was required, protein bands were visualized by silver staining using the ICN Rapid Ag-Stain kit with minor modifications to the manufacturer's directions. The gels were first fixed for 12-24 h in a solution of 40% methanol and 10% acetic acid, followed by a 30 min wash with 10% ethanol and 5% acetic acid. The gel was then soaked in distilled water for 30 min before proceeding with the kit instructions. In addition, following incubation with the silver staining solution, the gel was washed extensively with distilled water to reduce background staining. The staining reaction was stopped by washing the gel with 5% acetic acid.

2.2.18.2 *Nondenaturing Polyacrylamide Gel Electrophoresis*

Nondenaturing polyacrylamide gel electrophoresis was performed with slab gels containing a stacking gel (1 cm) composed as described above but without the 0.1% SDS. The resolving gel (13 cm) contained 18% acrylamide, 0.48% N,N'-methylenebis(acrylamide), and 0.375 M Tris-HCl (pH 8.8). Protein samples (115 μ l) were combined with 23 μ l of loading dye containing 300 mM Tris-HCl (pH 6.8), 60% (w/v) glycerol, and 0.12% bromophenol blue before loading samples onto the gel. The running buffer consisted of 90 mM Trizma base, 90 mM boric acid, and 2 mM EDTA. Electrophoresis was performed as described but at 4°C.

Proteins were visualized by rapid staining with a solution of 0.04% Coomassie Brilliant Blue G-250 in 3.5% perchloric acid. The gel was destained as described above to eliminate background.

2.2.18.3 *Polyacrylamide Sequencing-Gel Electrophoresis*

Analysis of uracil-DNA glycosylase reaction products produced from 5'-end 32 P-labeled oligonucleotide substrates was performed using denaturing polyacrylamide gels composed of 12% acrylamide, 0.41% N,N'-methylenebis(acrylamide), 8.3 M urea, and TBE buffer (90 mM Tris base, 90 mM boric acid, 2 mM EDTA). Samples were mixed with an equal volume of dye buffer (95% formamide, 10 mM EDTA, 0.1% (w/v) bromophenol blue, and 0.1% xylene cyanol) and heated for 3 min at 95°C before loading on the gel. Electrophoresis was performed in TBE buffer at 1200 V until the bromophenol blue had migrated approximately 20 cm. Gels were soaked briefly in water to remove urea and dried for 2 h at 80°C, followed by autoradiography.

2.2.19 Agarose Gel Electrophoresis

Plasmid DNA and restriction digest products were analyzed on 2% (w/v) agarose gels. Mini-gels (7 cm x 8 cm x 1 cm) and standard gels (13 cm x 14 cm x 1 cm) were prepared by melting agarose (electrophoresis grade) in

TAE buffer (40 mM Trizma-acetate, 1 mM EDTA). After the mixture had cooled to ~60 °C, ethidium bromide was added to 0.5 µg/ml. The mixture was poured into a gel-casting tray and allowed to polymerize for ~30 min. DNA samples were combined with dye buffer (10 mM EDTA, 0.1% SDS, 0.01% bromophenol blue, 5% (w/v) glycerol) and loaded into the sample wells. Electrophoresis was performed in TAE buffer at 70 V until the tracking dye had migrated approximately 75% of the length of the gel. DNA bands were visualized by 300 nm UV-light.

2.2.20 Quantitation of Radiolabeled Proteins and DNA from Polyacrylamide Gels

Radioactive products resolved by polyacrylamide gel electrophoresis were quantitated using a “cutting and counting” method. Native or denaturing polyacrylamide gels were dried under vacuum for 2 h at 80°C then exposed to Kodak X-OMAT AR X-ray film for autoradiography. The gels were overlaid with the films to visualize the location of the radioactive bands, and the positions of the products of interest were marked on the gel. The areas containing the radioactivity were excised as dried gel slices. A gel slice was placed in a liquid scintillation vial (7 ml) and 30% hydrogen peroxide (500 µl) was added. The vials were tightly capped and incubated at 55°C for 24 h to solubilize the gel slice. After cooling to room temperature, 10 ml of scintillation fluor (Formula 989, DuPont NEN) was added to each vial and the samples were mixed by shaking. The vials were then counted for radioactivity to detect the appropriate isotope (³⁵S or ³²P) in a liquid scintillation counter.

2.2.21 Synthesis of [*uracil*-³H] DNA

Activated calf thymus DNA was incubated with *E. coli* DNA polymerase I and [³H]dUTP in a nick translation DNA synthesis reaction to produce substrate for uracil-DNA glycosylase and uracil-DNA glycosylase inhibitor assays. The reaction mixture (50 ml) consisted of 70 mM potassium phosphate

(pH 7.5), 1 mM β -mercaptoethanol, 10 mM MgCl_2 , 90 μM each of dATP, dGTP, dCTP and dUTP, 450 $\mu\text{g}/\text{ml}$ of activated calf-thymus DNA, 2.0 units/ml, *E. coli* DNA polymerase I, and 1 mCi of [^3H]dUTP (specific activity = 15 Ci/mmol). The buffer components and DNA were pre-warmed at 37°C before initiating the reaction with the addition of DNA polymerase and radioisotope. Incorporation of [^3H]dUTP was monitored by removing 50 μl aliquots at 30 min intervals; these were mixed with 100 μl of 1 mg/ml bovine serum albumin containing 0.1 M sodium pyrophosphate followed by 500 μl of cold 10% (saturation) trichloroacetic acid. The mixtures were then applied to #30 glass fiber filters and washed 6 times with 3 ml each of 1 M HCl containing 0.1 M sodium pyrophosphate to recover acid-insoluble precipitates. The filters were washed with 95% ethanol and dried under a heat lamp for 5 min. The amount of radioactivity incorporated into the activated DNA was determined by analyzing the dried filters in 10 ml of 0.4 % 2,5-bis-2-(5-tertbutylbenzoxazolyl)-thiophene in a liquid scintillation counter.

When incorporation of [^3H]dUMP had plateaued, typically after 2 h, the reaction was terminated by the addition of NaCl to a final concentration of 500 mM and heating for 5 min at 70°C. The DNA was then extracted with an equal volume of phenol equilibrated in 10 mM Tris-HCl (pH 7.5), 1 mM EDTA, and 500 mM NaCl. The aqueous phase was sequentially dialyzed against: (i) 3.0 L of 10 mM Tris-HCl (pH 7.5), 1 mM EDTA, 500 mM NaCl, (ii) 2.0 L of 10 mM Tris-HCl (pH 7.5), 1 mM EDTA, and (iii) 2.0 L of 10 mM Tris-HCl (pH 7.5). The specific radioactivity of the resultant substrate was typically 180-190 cpm/pmol [^3H]dUMP.

2.2.22 Enzyme Assays

2.2.22.1 *Ugi Assay*

Uracil-DNA glycosylase inhibitor activity was measured in reaction mixtures (100 μl) containing 70 mM HEPES-KOH (pH 8.0), 1 mM EDTA, 1 mM DTT, 1.5 μg of [*uracil*- ^3H]DNA (180 cpm/pmol, 435 pmol [^3H]uracil/assay),

0.03-0.13 units of *E. coli* uracil-DNA glycosylase (fraction V) and serial dilutions of uracil-DNA glycosylase inhibitor protein in Ugi dilution buffer (50 mM Tris-HCl (pH 8.0), 1 mM EDTA, 1 mM DTT, 100 mM NaCl) introduced as 25 μ l additions. Reactions were allowed to proceed for 30 min at 37°C then terminated with the addition of 250 μ l of formate buffer (10 mM ammonium formate (pH 4.2)). To resolve free [3 H]uracil from [uracil- 3 H]DNA, 300 μ l of the terminated reaction mixture was applied to a 1 ml Dowex 1X-8 column. The column was washed with 700 μ l of formate buffer. The flow through and wash were collected in a 7 ml liquid scintillation vial. In a second vial, an additional 1 ml of wash buffer was collected. Formula 989 fluor (5 ml) was added to each vial and radioactivity was measured by liquid scintillation counting. One unit of uracil-DNA glycosylase inhibitor is defined as the amount that inactivates 1 unit of uracil-DNA glycosylase under standard reaction conditions.

2.2.22.2 Ung Assay

E. coli uracil-DNA glycosylase (fraction V), uracil-DNA glycosylase H187D (fraction VI), and *E. coli* and mitochondrial crude extracts were assayed for Ung activity in reactions (100 μ l) containing 70 mM HEPES-KOH (pH 8.0), 1 mM EDTA, 1 mM DTT and 1.5 μ g of [uracil- 3 H]DNA (180 cpm/pmol, 435 pmol [3 H]uracil/assay). Samples of interest were serially diluted in UDB (Ung dilution buffer: 50 mM HEPES-KOH (pH 7.4), 1 mM EDTA, 1 mM DTT, 100 μ g/ml BSA) and introduced into the assay as 25 μ l additions. Reactions were conducted for 30 min at 37°C, then terminated and processed using Dowex 1-X8 columns as described for Ugi assays above. One unit of uracil-DNA glycosylase is defined as the amount that releases 1 nmol of uracil/h under standard conditions.

2.2.22.3 Assay for pH Optima

To determine pH optima of uracil-DNA glycosylase, standard Ung assays were performed with modifications. The following buffers were

substituted for HEPES-KOH (pH 8.0) in the reaction mixture: HEPES-KOH (pH 6.5-8.5), Tris-HCl (pH 7.0-9.5), CAPS-KOH (pH 9.6-11.5), MES-KOH (pH 5.0-7.0), MOPS-KOH (pH 6.0-8.0). Ung or Ung H187D were diluted to 0.03-0.13 units in UDB made with the same buffering component used for the reaction mixture as indicated above substituted for HEPES-KOH (pH 7.4).

2.2.22.4 *Substrate Titration and Uracil Inhibition Assays*

Standard Ung assays were modified to determine the effect of varying substrate concentration and free uracil on enzyme activity. Ung or Ung H187D were diluted to ~0.13 units in UDB made with HEPES-KOH (pH 7.0 or 8.0). Diluted Ung was added as 25% of the final reaction volume to a mixture containing 70 mM HEPES-KOH (pH 7.0 or 8.0 to match UDB), 1 mM EDTA, and 1 mM DTT. For uracil inhibition assays, 0-1.0 mM uracil was included in the reaction mix. This reaction mixture (75 μ l) was added to 25 μ l of [*uracil*-³H]DNA diluted in 10 mM Tris-HCl (pH 7.5). The final substrate concentration was 0-3.7 μ g of [*uracil*-³H]DNA (180 cpm/pmol), 0-10 μ M with respect to [³H]uracil. The volume of Dowex 1-X8 columns was increased to 1.5 ml to avoid exceeding the resin's binding capacity.

2.2.22.5 *Assay for Substrate Specificity*

Ung activity was measured on single- or double-stranded [³²P]U-25-mer oligonucleotides in reaction mixtures (12.5 μ l) containing 70 mM HEPES-KOH (pH 7.0 or 8.0), 1 mM EDTA, 1 mM DTT, 4 pmol [³²P]U-25-mer, [³²P]U/A-25-mer, or [³²P]U/G-25-mer (15,500-22,000 cpm/pmol), and varying amounts of Ung or Ung H187D diluted in UDB (pH 7.0 or 8.0). After incubating for 30 min at 37°C, the reactions were terminated on ice by the addition of 0.8 μ g of Ugi protein. Alkaline lysis of apyrimidinic sites was performed by adding 3 M K₂HPO₄ (pH 13.7) to 10% (v/v) and heating for 3 h at 55°C. Samples were then neutralized with the addition of 3 μ l of 1.5 M KH₂PO₄, and mixed with 17.5 μ l of formamide dye (95% formamide, 10 mM EDTA, 0.1% bromophenol blue, 0.1% xylene cyanol). After heating at 95°C for

3 min, 10 μ l of each sample was analyzed by 12% denaturing polyacrylamide sequencing gel. Gels were dried and substrate and product bands were quantitated by “cutting and counting” as described above (Section 2.2.20).

2.2.22.6 *Ung/Ugi Binding Assay*

Ung/Ugi binding reactions (100 μ l) were prepared by mixing 300 pmol of [35 S]Ugi (15 μ l) with varying amounts of Ung or Ung H187D in DAB buffer. Samples were incubated for 10 min at 25°C, then 20 min at 4°C. Following complex formation, each sample was mixed with native gel loading dye and analyzed by 18% native polyacrylamide gel electrophoresis as described. Free and complexed [35 S]Ugi were detected by the previously described “cutting and counting” method (Section 2.2.20).

2.2.22.7 *Assay of DNA Binding by Ung Using UV-Catalyzed Crosslinking Reactions*

Time course reactions were performed in microcentrifuge tube or liquid scintillation vial caps. Caps were pre-irradiated for 45 min in the presence of DAB buffer. Reaction mixtures (135-150 μ l) consisted of 3.8 nmol of Ung or Ung H187D plus a 2-fold molar excess of 5'-end 32 P-labeled dT₂₀ oligonucleotide (1000 cpm/pmol). When indicated, uracil was included in the reaction at a 2 mM final concentration. Reaction mixtures were incubated on ice for 15 min then UV-irradiated ($\lambda_{\text{max}} = 254$ nm) in a Stratalinker 1800 (Stratagene Cloning Systems) with 15 μ l aliquots removed at various time points. Samples were mixed with an equal volume of SDS-PAGE loading dye, heated for 20 min at 42°C, and 25 μ l were analyzed by 12.5% SDS-PAGE.

Ung and Ung H187D binding to oligonucleotide containing uracil or apyrimidinic sites were measured in 15 μ l reactions containing dilutions of wild-type or mutant enzyme and various 5'-end 32 P-labeled oligonucleotides (0.028-2.28 nmol). Samples were incubated on ice for 15 min in a 96-well microtiter plate (Corning round-bottom well, low protein binding), pre-irradiated as described above, then UV-irradiated for 30 min. Following

crosslinking, 15 μ l of SDS-PAGE loading buffer was added to each well, the plate was incubated at 42°C for 20 min, and 25 μ l of each sample was analyzed by 12.5% SDS-PAGE.

After electrophoresis, the bottom portion of each gel was removed to eliminate uncrosslinked [32 P]oligonucleotide and reduce background radioactivity. Gels were stained with Coomassie Brilliant Blue to visualize free protein, then dried and processed as described above to quantitate the amount of radioactivity in Ung x [32 P]DNA crosslinked product.

2.2.23 Steady-State Fluorometry

Steady-state fluorescence measurements were performed with a Perkin Elmer Luminescence Spectrometer LS50 using an excitation wavelength of 310 nm and detecting emission at 370 nm. Double-stranded 2AP-27-mer oligonucleotide containing a 2-aminopurine:uracil basepair was diluted to various concentrations (20-4000 nM) in TE buffer and a 20 μ l aliquot was allowed to equilibrate with 400 μ l DAB (pH 7.4) for 60 sec while monitoring emission to establish a baseline. After 60 sec, 20 μ l of Ung or Ung H187D in DAB (pH 7.4) at 25°C was then added to a final concentration of 2 nM or 250 nM, respectively. Fluorescence was monitored for an additional 2 min for Ung or an additional 4 min for Ung H187D. The initial velocity of Ung was determined by calculating the slope of the line determined by linear regression from 70-90 sec reaction time. The initial velocity of Ung H187D was calculated in a similar manner, using the data from 70-300 sec reaction time.

2.2.24 Polyclonal Antiserum Production

After a 5-day quarantine, pre-immune serum was collected by performing test bleeds (3-5 ml) via cardiac puncture on female New Zealand White rabbits (2.1-2.5 kg). The blood was clotted by incubating for 1 h at 37°C, followed by 8-12 h at 4°C. The sample was centrifuged in an IEC clinical

centrifuge (setting #4) at room temperature for 20 min and the serum (2-2.5 ml) removed from the clot. Serum was stored at -20°C in 0.5 ml aliquots.

By using a Virtis "23" mixer, complete Freund's adjuvant was emulsified with an equal volume of purified *E. coli* Ung (0.3 mg in 0.5 ml DAB buffer) or Ugi inhibitor protein (0.38 mg in 0.5 ml DAB buffer).

Approximately 1.0 ml of antigen/adjuvant was injected subcutaneously into each rabbit at five separate sites.

Boost injections of Ung or Ugi plus incomplete adjuvant were performed every 5-6 weeks as described above. Test bleeds were taken approximately 10 days after each boost and serum was processed as described. After 4-6 boosts a terminal bleed was performed by cardiac puncture, yielding approximately 150 ml of blood. After clotting, the samples were centrifuged at 10,000xg for 10 min at 4°C to recover the serum (~75 ml).

Serum was assayed for Ung activity and the ability to inhibit Ung or Ugi activity in functional assays. The titer of anti-Ung or anti-Ugi antibody was determined by ELISA using the appropriate antigen.

2.2.25 Functional Assay of Serum

Pre-immune and polyclonal antisera were assayed for endogenous Ung activity and the ability to inhibit purified Ung or Ugi. Standard Ung and Ugi assays were performed with modifications. Sample additions consisted of 15 µl of serum serially diluted in UDB and 10 µl of Ugi dilution buffer or 0.1 units of Ugi. When assaying for serum inhibition of Ung or Ugi, ~0.12 units of enzyme per reaction was included in the reaction mixture. For detection of serum inhibition of Ugi, inhibitor was preincubated on ice for 5 min with diluted serum before adding 75 µl of reaction mix. Reactions were then incubated and processed as described for the standard Ung assays.

2.2.26 Immunoassay of Serum and Affinity-Purified Antibody

ELISA was performed to determine the titer of anti-Ung or anti-Ugi IgG as well as total IgG present in polyclonal antisera and affinity-purified

antibody preparations. When testing for antigen-specific IgG, Ung or Ugi was diluted in HN buffer (10 mM HEPES-KOH (pH 7.6), 150 mM NaCl) to 5 µg/ml. Wells of a microtiter plate were coated with 50 µl of antigen for 30 min to overnight. The antigen was removed and the plate washed with 200 µl of HN. Wells were then blocked with 100 µl of HNA buffer (10 mM HEPES-KOH (pH 7.6), 150 mM NaCl, 1% BSA) for 30 min. The plate was washed twice with 200 µl of HNAT buffer (10 mM HEPES-KOH (pH 7.6), 150 mM NaCl, 0.2% BSA, 0.02% Tween 80). Polyclonal antiserum or purified antibody was serially diluted in HNAT and 50 µl was incubated in the wells for 30 min. The plate was washed twice with 200 µl of HNAT and 50 µl of a 1:2000 dilution (in HNAT) of horseradish peroxidase-conjugated secondary antibody (goat anti-rabbit IgG, Boehringer Mannheim) was incubated in each well for 30 min. After extensive washing with HNAT, 100 µl of reaction mix (1 mM 2,2-azino-di-[3-ethylbenzthiazoline sulfonate] in ABTS buffer (3.25 mM sodium perborate, 39.8 mM citric acid, 60 mM disodium hydrogen phosphate, pH 4.5)) was added to each well and the reaction was allowed to develop for 20-40 min before reading absorbance at 405 nm with a microplate reader.

The protocol for surveying samples for total IgG was essentially the same as described above; however, dilutions of serum or antibody in HNAT were added directly to the wells of the microtiter plate without any preliminary binding of antigen.

2.2.27 Western Blot Analysis of Ung-Containing Samples

Following electrophoresis, proteins were transferred to nitrocellulose from the 12.5% SDS-polyacrylamide gel for Western blot analysis using a semi-dry transfer method. Ten sheets of Whatman (3MM CHR) chromatography filter paper and a 0.45 µm nitrocellulose membrane were cut to the dimensions of the resolving gel. MilliBlot-Graphite Electroblotter graphite plates were wet with Transblot buffer (48 mM Tris, 39 mM glycine, 1.3 mM SDS, 20% methanol) and the transfer apparatus was assembled by positioning on the anode plate 5 sheets of filter paper presoaked in Transblot

buffer followed by the nitrocellulose membrane presoaked in distilled water, the resolving gel, and 5 sheets of presoaked filter paper. A test tube was rolled across the top of the filter paper to remove air bubbles and the cathode plate was set in position to complete the apparatus. The gel was transblotted at 0.8 mA/cm^2 for 1 h.

All subsequent incubations were performed by shaking at room temperature. The nitrocellulose sheet was blocked overnight in 20-30 ml of HNAT (10 mM HEPES-KOH (pH 7.6), 150 mM NaCl, 0.2% BSA, 0.02% Tween-80). Anti-Ung serum or affinity-purified antibody was diluted (1:5000 and 1:200, respectively) in 10 ml of HNAT and incubated with the membrane for 1 h. The membrane was washed three times by incubating with 20 ml of HNAT for 5 min each wash. Alkaline phosphatase secondary antibody (goat anti-rabbit IgG, Boehringer Mannheim) was diluted 1:2000 in 10 ml of HNAT and incubated with the membrane for 1 h. The membrane was washed as described and then reacted with 10 ml of 100 mM NaHCO_3 (pH 9.8), 10 mM MgCl_2 containing 100 μl each of 30 mg/ml nitroblue tetrazolium in 70% DMF and 15 mg/ml 5-bromo-4-chloro-3-indolyl phosphate in 100% DMF for 15-30 min to develop a purple precipitate at sites of the alkaline phosphatase reaction. The reaction was terminated by washing the membrane with distilled H_2O . The membrane was air-dried and protected from light.

2.2.28 Antibody Purification

Conditions for the affinity purification of anti-Ung polyclonal IgG were optimized by suspending Ung-Sepharose resin in 10 mM phosphate buffer (pH 7.5). Polyclonal antiserum from a terminal bleed (50 μl) was mixed with 100 μl of Ung-Sepharose and incubated for 10 min at 25°C . Micro-purification columns were poured and washed as described in Section 2.2.15. Bound antibody was eluted as described in Table 3. The eluted antibody was assayed by ELISA for the presence of total and anti-Ung IgG as previously described. Aliquots (1.25 μl) were also analyzed by 12.5% SDS-polyacrylamide gel electrophoresis followed by silver staining.

Table 3

Buffer Conditions for Ung-Sepharose Affinity Chromatography

Wash Buffer ^a	Elution Buffer ^b	Neutralizing Buffer ^c
10 mM potassium phosphate (pH 6.8)	100 mM glycine (pH 2.0)	10 mM potassium phosphate (pH 8.0)
10 mM potassium phosphate (pH 6.8)	100 mM glycine (pH 1.8)	10 mM potassium phosphate (pH 8.0)
10 mM potassium phosphate (pH 8.0)	100 mM TEA (pH 11.5)	10 mM potassium phosphate (pH 6.8)
10 mM potassium phosphate (pH 7.2)	3.5 M MgCl ₂ , 10 mM potassium phosphate (pH 7.2)	
10 mM potassium phosphate (pH 7.2)	5 M LiCl, 10 mM potassium phosphate (pH 7.2)	

^a After incubation with sample as described under "Experimental Procedures", the affinity resin was washed 3 times with 200 µl of wash buffer applied in 100 µl aliquots.

^b Bound protein was eluted from the affinity resin with 100 µl of elution buffer.

^c When necessary, the eluted fraction was collected into 10 µl of neutralization buffer.

Once optimal purification conditions were determined, a large scale purification was performed by mixing 25 ml of Ung-Sepharose with 12.5 ml of serum. The slurry was mixed on a rocking table for 30 min at 25°C then transferred to a 1.5 cm diameter BioRad column. Fractions (1 ml) were collected at a rate of 15 ml/h at 4°C. The resin was washed with approximately 25 ml of 10 mM potassium phosphate buffer (pH 7.2) and bound antibody eluted with 3.5 M MgCl_2 in 10 mM potassium phosphate buffer (pH 7.2). Fractions were assayed for total protein by absorbance spectroscopy at 280 nm and for total and anti-Ung IgG by ELISA as described. Aliquots of a 1:50 dilution of flow through fractions (6.25 μl) and wash and elution fractions (1.25 μl) were analyzed by SDS-polyacrylamide gel electrophoresis and silver staining as previously described. Fractions containing the peak anti-Ung IgG were pooled and stored at -20°C.

3. RESULTS

3.1 Overproduction and Characterization of Uracil-DNA Glycosylase H187D

3.1.1 Verification of Ung and Ung H187D Overexpression Vectors

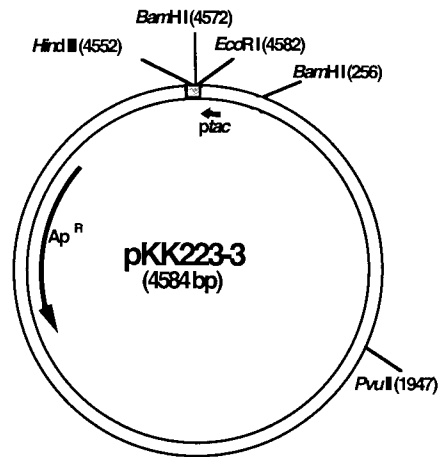
The plasmids used for overexpressing the *ung* and *ungH187D* genes are shown in Figure 1. They are based on the overexpression vector pKK223-3 (Figure 1A). The construction of pSB1051 and pUngH187D was performed by Dr. Sam Bennett as described previously (6, 10) and the vectors were provided as a gift by Dr. Bennett. pSB1051 consists of the *E. coli ung* gene cloned behind the IPTG-inducible *tac* promoter of pKK223-3 (Figure 1B). Site-directed mutagenesis of pSB1051 produced pUngH187D (Figure 1C), which carries a His to Asp mutation at codon 187 in the Ung protein.

These three vectors were electroporated into *E. coli* JM105, ampicillin-resistant bacteria were cultured, plasmid DNA was isolated, restriction enzyme digests performed and the restriction fragments were analyzed by 2% agarose gel electrophoresis (Figure 2). Plasmid DNA was also run on the same gel without subjecting it to restriction enzyme digestion to verify DNA recovery by minipreparation. A mixture of supercoiled and nicked circular plasmid was observed in lanes containing unrestricted DNA (Figure 2, lanes 1, 4, and 7). As expected, digestion of all three plasmids by *Pvu* II resulted in single linear fragments (Figure 2, lanes 2, 5, and 8). *Bam*H I digested pKK223-3 into two fragments that corresponded to the expected sizes of 4316 bp and 268 bp (Figure 2, lane 3). The banding pattern observed subsequent to digestion of pSB1051 by *Bam*H I corresponded to the expected three fragments of 4316, 811, and 486 bp (Figure 2, lane 6). The H187D mutation in the *ung* gene introduced a new *Bam*H I site in the *Bam*H I 811 bp fragment of pSB1051 (Figure 1B); thus, digestion of pUngH187D by *Bam*H I should result in fragments of 4316, 486, 442, and 369 bp (Figure 1C). The estimated size of the

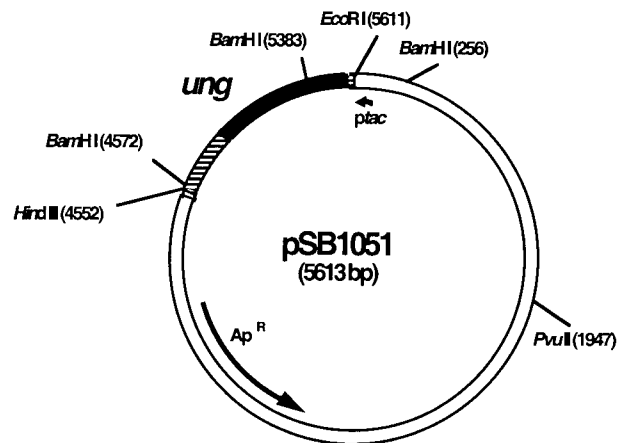
Figure 1. Restriction maps of pSB1051 and pUngH187D overexpression vectors. The *ung* and *ungH187D* genes were cloned into the overexpression plasmid pKK223-3 as described in (6, 10). The restriction sites pertinent to the cloning are indicated for pKK223-3 (A), pSB1051 (B), and pUngH187D (C).

Figure 1

A.



B.



C.

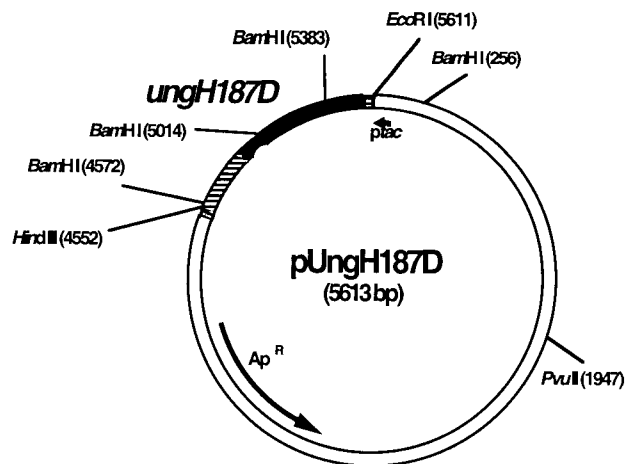
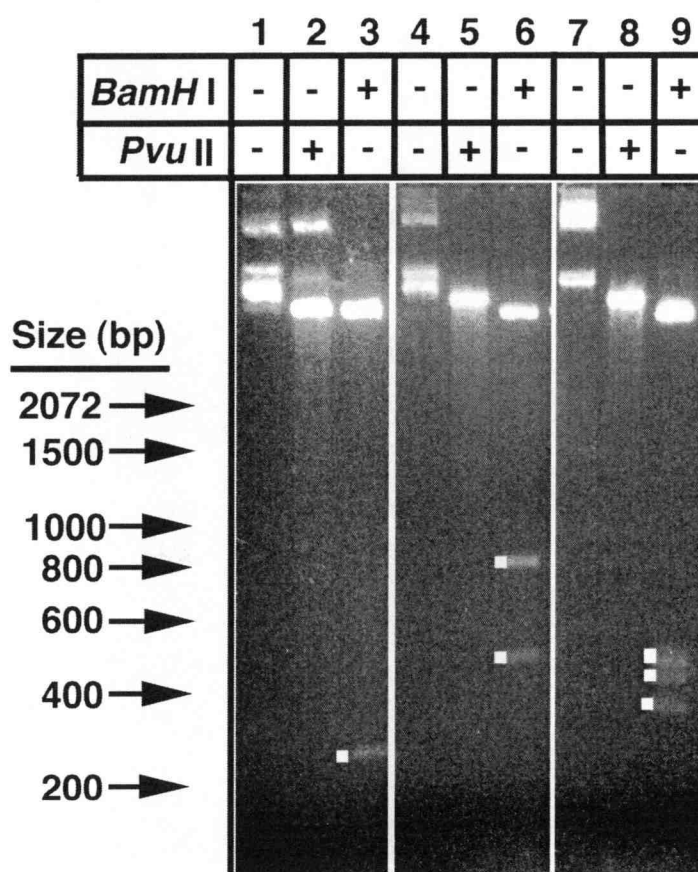


Figure 2. Restriction site analysis of overexpression vectors isolated from *E. coli* strain JM105. Isolates of pKK223-3 (lanes 1-3), pSB1051 (lanes 4-6), or pUngH187D (lanes 7-9) were recovered from *E. coli* strain JM105, treated with 10 units *Pvu* II or *Bam*H I restriction endonuclease as indicated, and analyzed by 2% agarose gel electrophoresis as described under "Experimental Procedures". Locations of DNA fragments have been highlighted by *white squares*.

Figure 2



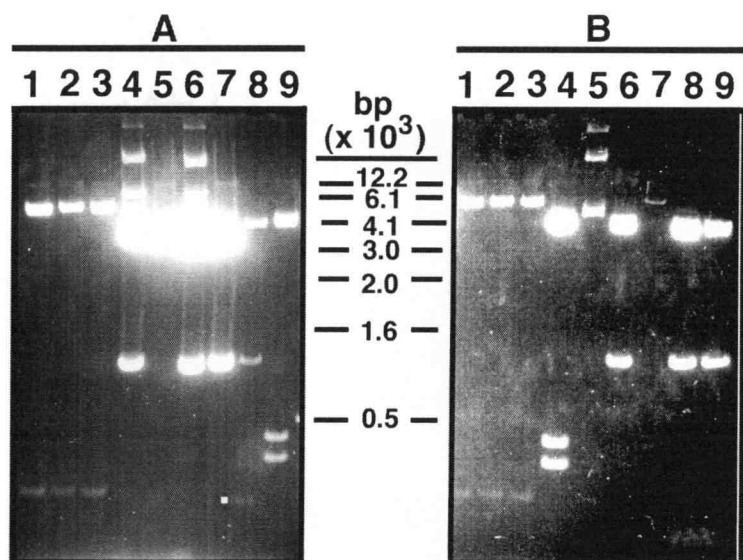
four fragments resulting from *Bam*H I digestion was in agreement with the expected sizes (Figure 2, lane 9).

3.1.2 Transformation of *E. coli* BD2314 (*ung*-152::Tn10) and BW310 (*ung*-1) with pKK223-3, pSB1051 and pUngH187D

Plasmid DNA from minipreparations of *E. coli* JM105 was introduced into *E. coli* strains BD2314 (*ung*-152::Tn10) and BW310 (*ung*-1) by electroporation in order to express *ungH187D* in an *ung*⁻ background. The plasmid DNA was isolated from ampicillin resistant colonies. The resultant DNA was analyzed following digestion with *Bam*H I restriction endonuclease by 2% agarose gel electrophoresis. While pKK223-3 vector recovered from *ung*⁻ strains produced fragments consistent with the expected sizes (4316 and 268 bp) upon *Bam*H I digestion (Figure 3A and B, lanes 1-3), the wild type and mutant Ung-containing vectors resulted in unexpected *Bam*H I restriction patterns. Two *E. coli* BD2314/pSB1051 clones yielded vector DNA that produced bands approximately 4100 and 800 bp long (Figure 3A, lanes 4 and 6), while a third produced a single restriction fragment of ~4100 bp (Figure 3A, lane 5). Digestion of one pUngH187D isolate from *E. coli* BD2314 also yielded ~4100 and ~800 bp fragments (Figure 3A, lane 7); in addition to these bands, a second isolate produced an additional ~250 bp fragment (Figure 3A, lane 8). A third pUngH187D sample yielded three bands approximately 4100, 450, and 350 bp in length (Figure 3A, lane 9). Similarly, one sample of pSB1051 recovered from *E. coli* BW310 produced ~4100, ~450, and ~350 bp fragments while a second was restricted into fragments of ~4100 and ~800 bp (Figure 3B, lanes 4 and 6, respectively). The third sample was not cleavable by *Bam*H I (Figure 3B, lane 5). Plasmid pUngH187D recovered from *E. coli* BW310 likewise produced unanticipated restriction patterns. In addition to an isolate which could not be digested by *Bam*H I (Figure 3B, lane 7), the pUngH187D recovered from *E. coli* BW310 resulted in the previously observed ~4100 and ~800 bp digestion pattern (Figure 3A, lanes 8 and 9).

Figure 3. *BamH* I restriction site analysis of overexpression vectors from *E. coli* strains BD2314 and BW310. The Δung strain BD2314 (A) and the *ung-1* strain BW310 (B) were transformed with the overexpression vectors. Three isolates each of pKK223-3 (lanes 1-3), pSB1051 (lanes 4-5), and pUngH187D (lanes 7-9) were isolated by miniprep, subjected to digestion with 10 units of *BamH* I, and analyzed by 2% agarose gel electrophoresis as described under "Experimental Procedures". Location of DNA fragment has been highlighted by *white square* (lane 7).

Figure 3



3.1.3 Construction of *E. coli recA ung* Strains for Overexpression of the *ungH187D* Gene

It was hypothesized that the pSB1051 and pUngH187D vectors were unstable or lethal to the *E. coli ung* strains. As a result pSB1051 and pUngH187D may have undergone rearrangements or deletions upon electroporation into strains BW310 and BD2314. In order to prevent this instability, *E. coli* BW310 was made *recA*-defective by P1*vir* transduction. A P1*vir* lysate of the *E. coli* JC10289 strain containing a Tn10 disruption of *recA* was incubated with a mid-log culture of *E. coli* BW310 at a multiplicity of infection of ~0.05. Transductants were selected for tetracycline resistance and one clone, designated MJS100, was isolated and screened for sensitivity to UV-irradiation. Saturated cultures of *E. coli* BW310, JC10289, and MJS100 were streaked onto LB agar then irradiated with UV light for various time intervals. Figure 4 shows that although *E. coli* BW310 was resistant to UV doses up to 57.6 J/m², JC10289 and the transductant MJS100 were equally sensitive to UV-irradiation, exhibiting inhibition of growth with UV doses of 9.6 J/m² and higher.

3.1.4 Transformation of *E. coli* MJS100 with pSB1051 and pUngH187D

pSB1051 and pUngH187D recovered from *E. coli* JM105 were transformed into *E. coli* MJS100 by electroporation. Tetracycline- and ampicillin-resistant clones were selected for minipreparation of plasmid DNA. The recovered vectors were analyzed by *Bam*H I digestion and 2% agarose gel electrophoresis. Samples of pSB1051 isolated from *E. coli* MJS100 displayed the expected *Bam*H I restriction fragments (4316, 811, and 486 bp) (Figure 5, lanes 1-3). Unexpectedly, digestion of pUngH187D recovered from *E. coli* MJS100 with *Bam*H I resulted in DNA fragments ~2200 and ~800 bp in length (Figure 5, lanes 5-7). Although it was preferable to express the *ungH187D* gene in an *ung* background, these efforts did not resolve the problem of plasmid instability in an *E. coli ung* strain; thus, Ung H187D was overproduced in *E. coli* JM105 in order to purify the mutant form of the enzyme.

Figure 4. UV light sensitivity of *E. coli* BW310, JC10289, and MJS100. Saturated cultures of *E. coli* BW310 (A), MJS100 (B), and JC10289 (C) were streaked onto LB agar, exposed to various doses of UV-irradiation, and incubated at 37°C in the dark. Columns 1-6 correspond to UV doses of 4.8, 9.6, 14, 19, 38, and 58 J/m², respectively. The unirradiated controls are designated Column C.

Figure 4

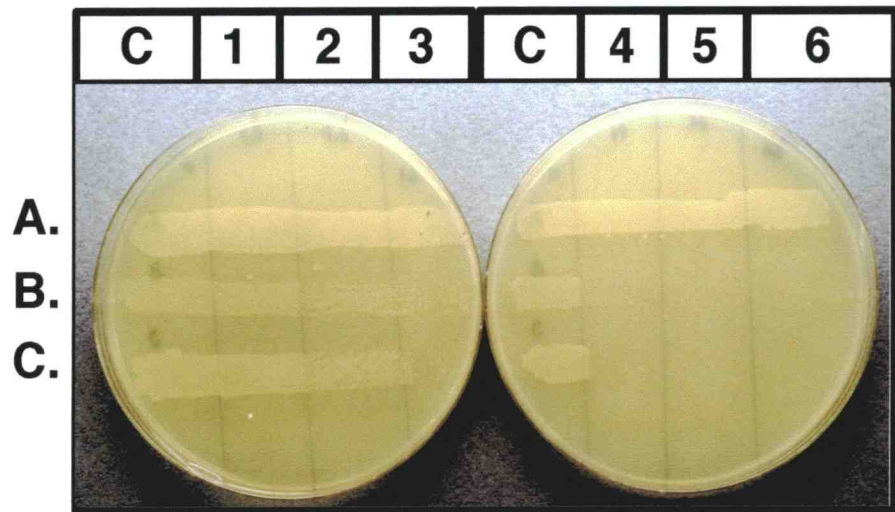
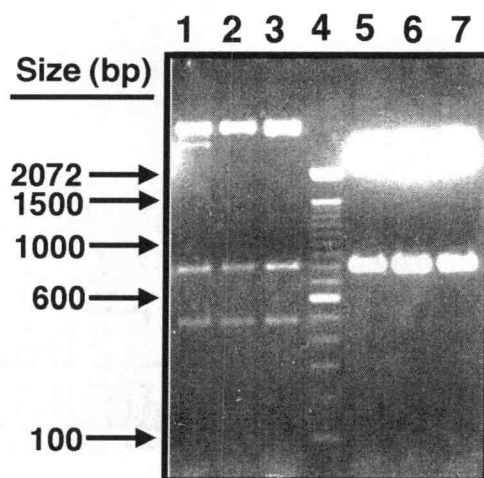


Figure 5. *BamH* I restriction site analysis of *ung* overexpression vectors isolated from *E. coli* MJS100. Plasmids pSB1051 (lanes 1-3) and pUngH187D (lanes 5-6) were transformed into the $\Delta ung \Delta recA$ strain MJS100. Plasmid DNA was isolated by minipreparation and three isolates of each plasmid were subjected to *BamH* I digestion and analyzed by 2% agarose gel electrophoresis as described under "Experimental Procedures". Lane 4 contains a 1 kb DNA ladder (Life Technologies).

Figure 5



3.1.5 Overproduction of the Ung H187D Protein

To assess the level of Ung H187D overproduction, three mid-log cultures of *E. coli* JM105 cells transformed with either pKK223-3, pSB1051, or pUngH187D were each divided in half and grown in the presence or absence of 1 mM IPTG to induce *ung* gene expression. Cell-free extracts were analyzed by 12.5% SDS-polyacrylamide gel electrophoresis as shown in Figure 6. A Coomassie Brilliant Blue stainable protein band corresponding to the approximate molecular weight of Ung ($M_r = 25,000$) was observed to be IPTG-induced in *E. coli* containing pSB1051 (Figure 6, lane 4) and pUngH187D (Figure 6, lane 6).

The specific activity of uracil-DNA glycosylase was determined for each cell-free extract (Figure 6). As expected, *E. coli* JM105 cells transformed with pSB1051 displayed an IPTG-inducible Ung activity. Overproduction of Ung in *E. coli* JM105/pSB1051 cells produced 130,000 units/mg of cellular protein, which was ~11-fold higher than that of uninduced cells (Figure 6, lanes 3 and 4) and ~930-fold higher than cells containing the vector control (Figure 6, lanes 2 and 4). In contrast, *E. coli* JM105/pUngH187D cells treated with or without IPTG did not show significantly increased specific activity of uracil-DNA glycosylase relative to the cells containing the vector control (Figure 6, lanes 2 and 6, 1 and 5, respectively). In each case, the specific activity was approximately 1.5 times the corresponding vector control, though the Ung H187D protein was overproduced to a much greater extent. These results implied that the UngH187D protein was defective in uracil-DNA glycosylase activity.

3.1.6 Purification of the Ung H187D Protein

To facilitate characterization of Ung H187D, the protein was overproduced in *E. coli* JM105/pUngH187D and purified as outlined in Figure 7. Typically, a mid-log culture of *E. coli* JM105/pUngH187D was incubated 3 h at 37°C in the presence of 1 mM IPTG to induce *ungH187D* gene expression. Cells were harvested by centrifugation and lysed by sonication. The cell

Figure 6. Overproduction of Ung and Ung H187D. *E. coli* JM105 transformed with pKK223-3 (lanes 1 and 2), pSB1051 (lanes 3 and 4), or pUngH187D (lanes 5 and 6) were grown in the presence (+) or absence (-) of 1 mM IPTG as indicated. Cell-free extracts were prepared, samples (50 μ g total protein) were analyzed on a 12.5% SDS-polyacrylamide gel, and protein bands were visualized by Coomassie Brilliant Blue staining as described under "Experimental Procedures". The molecular weight standards for bovine serum albumin, ovalbumin, glyceraldehyde-3-phosphate dehydrogenase, carbonic anhydrase, trypsinogen, and α -lactalbumin are indicated by *arrows* from *top* to *bottom*. The positions of Ung and the tracking dye (TD) are indicated by *arrows*. The specific activity of uracil-DNA glycosylase in each cell-free extract was determined by using standard assay conditions and the results are indicated.

Figure 6

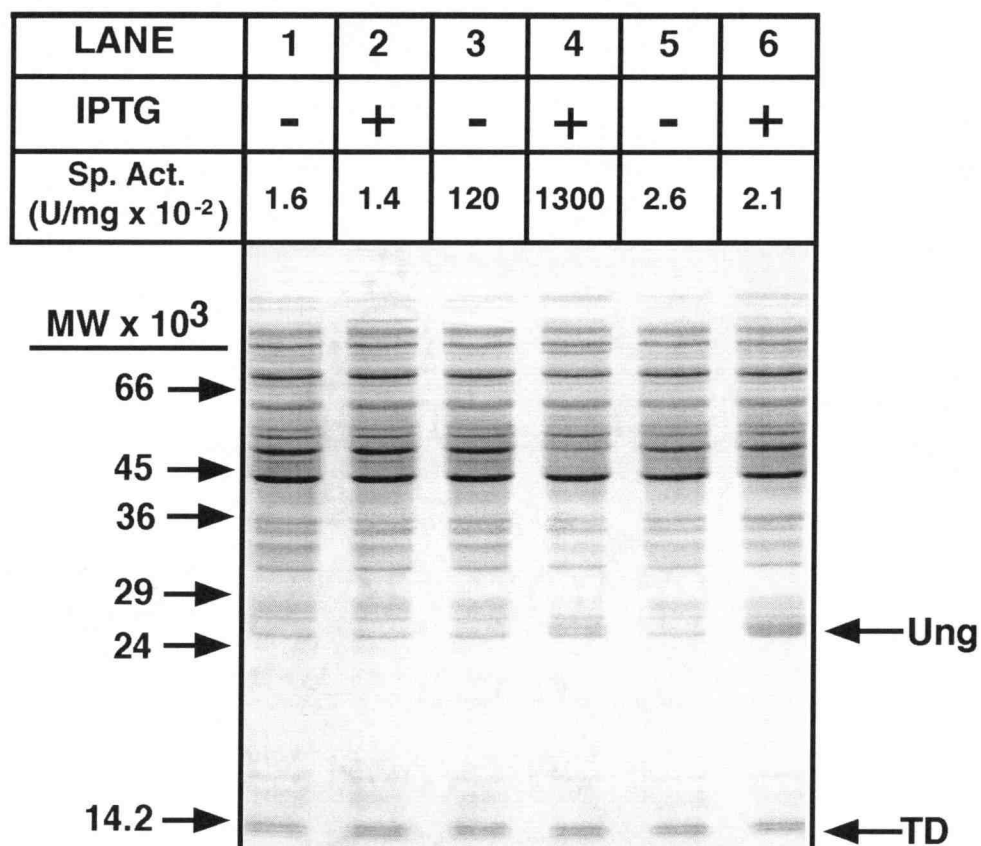
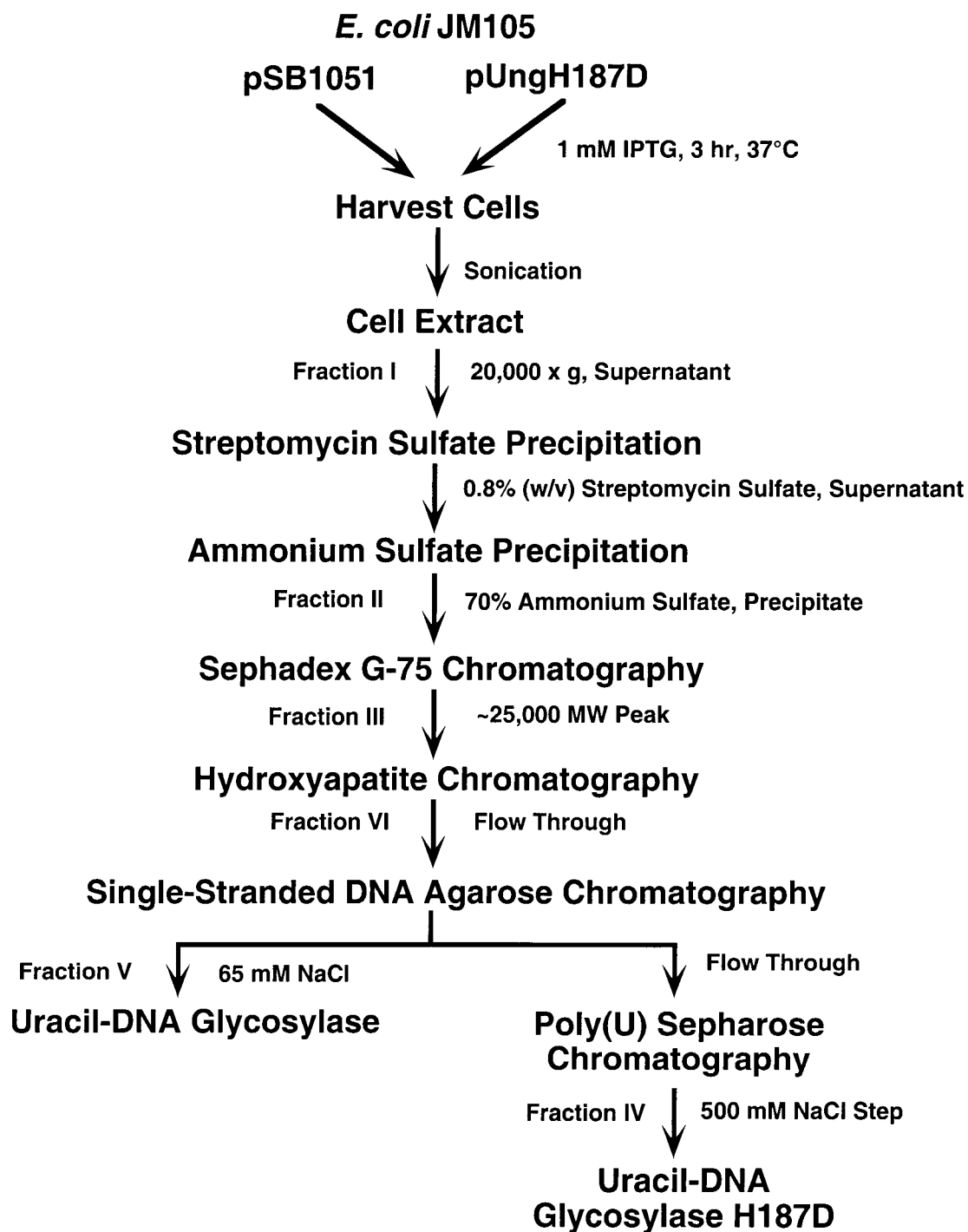


Figure 7. Scheme for purification of Ung and Ung H187D from *E. coli* JM105. Ung and Ung H187D were purified from *E. coli* JM105 containing pSB1051 or pUngH187D, respectively, according to the protocol outlined here and described under “Experimental Procedures”.

Figure 7



extract was treated with an equal volume of 1.6% streptomycin sulfate and the precipitate removed by centrifugation at 20,000xg for 15 min. The supernatant was adjusted to 70% (saturation) ammonium sulfate. Precipitated proteins were recovered by centrifugation at 10,000xg for 15 min then resuspended and dialyzed in UEB buffer. UngH187D was subjected to size exclusion chromatography using Sephadex G-75 resin. This resulted in a single activity peak at fraction 58 (Figure 8), which is characteristic of wild type Ung. Presumably, a large portion of the activity detected in the peak fractions was due to the wild type Ung endogenous to *E. coli* JM105. Analysis of fractions across the peak by 12.5% SDS polyacrylamide gel electrophoresis revealed that the activity peak was coincident with the overproduced Ung H187D protein of ~25,000 molecular weight (data not shown). Peak fractions (53-63) were pooled and applied to a hydroxyapatite column. After washing the column, uracil-DNA glycosylase activity eluted as a peak at fraction 6 (Figure 9). Fractions (5-9) containing overproduced UngH187D were pooled and applied to a single-stranded DNA agarose column, where two peaks of Ung activity were detected (Figure 10A). The major activity peak containing a relatively small amount of protein eluted from the column at a NaCl concentration (~100 mM) characteristic of wild type Ung. The minor activity peak found in the flow through fractions constituted ~9% of the recovered activity but contained a relatively large amount of protein. Analysis of the flow through fractions using 12.5% SDS-polyacrylamide gel electrophoresis revealed a large protein band (M_r ~25,000) corresponding to the overproduced Ung H187D protein. Additionally, several minor contaminants were observed corresponding to ~26,000 and ~22,000 molecular weight species, plus a low molecular weight species which migrated on the dye front (data not shown).

It was predicted that although Ung H187D had reduced affinity for single-stranded DNA, it might retain the ability to bind uracil. Thus, additional purification of Ung H187D was carried out using poly(U) Sepharose. Flow through fractions (62-102) from single-stranded DNA agarose chromatography containing the overproduced Ung H187D were pooled and

Figure 8. Sephadex G-75 chromatography of Ung H187D. A culture (2 L) of *E. coli* JM105 containing pUngH187D was grown, induced with IPTG, and the cells harvested and sonicated as outlined in Figure 7 and described under "Experimental Procedures". After streptomycin sulfate and ammonium sulfate precipitations, Fraction II (~25 ml) was applied to a Sephadex G-75 column (6 cm² x 88 cm) equilibrated in UEB buffer. Fractions (5 ml) were collected and 25 µl aliquots (1/50 dilution in UDB buffer) were assayed for uracil-DNA glycosylase activity by using standard reaction conditions. Peak fractions were pooled, concentrated (~2-fold), and diafiltered against HAB buffer to obtain Fraction III.

Figure 8

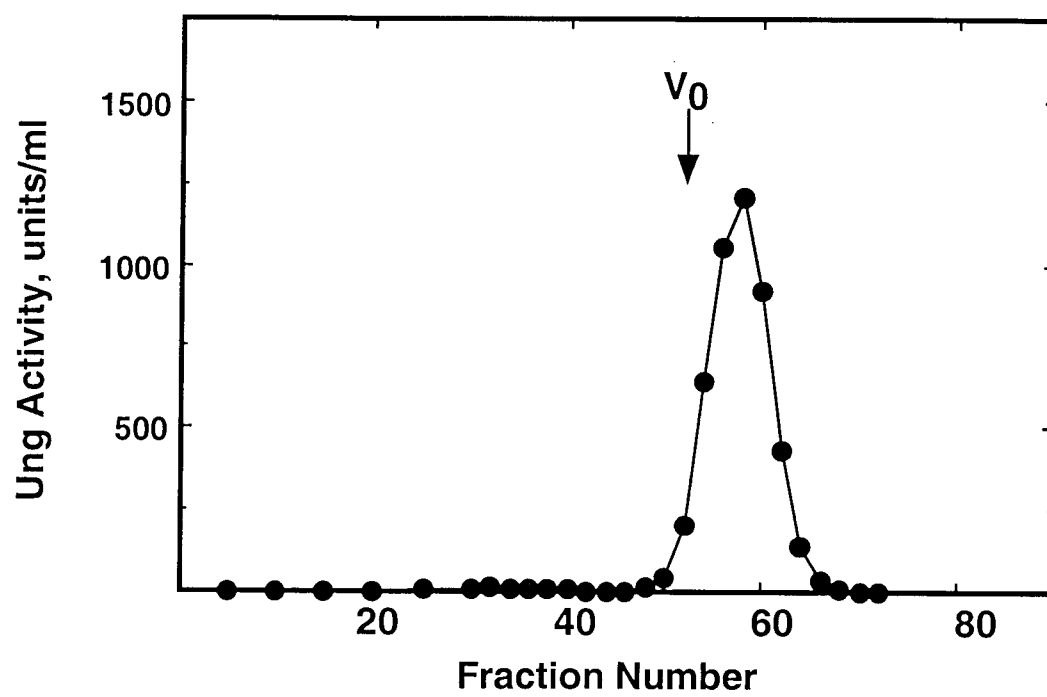


Figure 9. Hydroxylapatite chromatography of Ung H187D. Fraction III (~25 ml) was applied to a hydroxylapatite column (2 cm² x 10 cm) equilibrated with HAB buffer. Fractions (5 ml) were collected and 25 µl aliquots (1/50 dilution) were assayed for uracil-DNA glycosylase activity using standard reaction conditions as described under "Experimental Procedures". Peak fractions were pooled and designated Fraction IV.

Figure 9

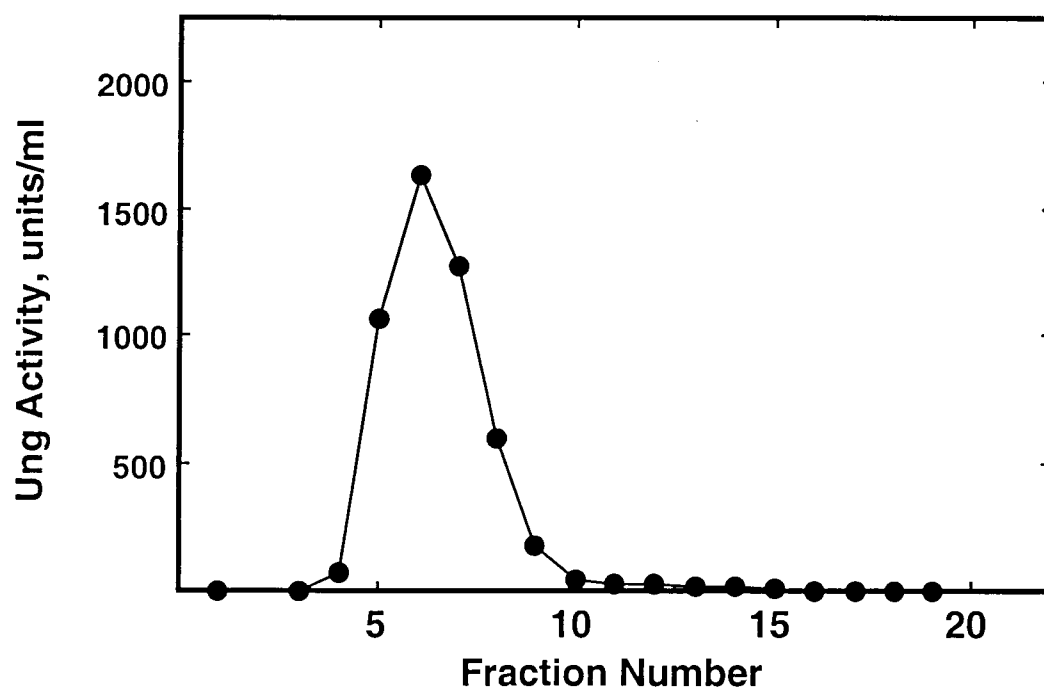
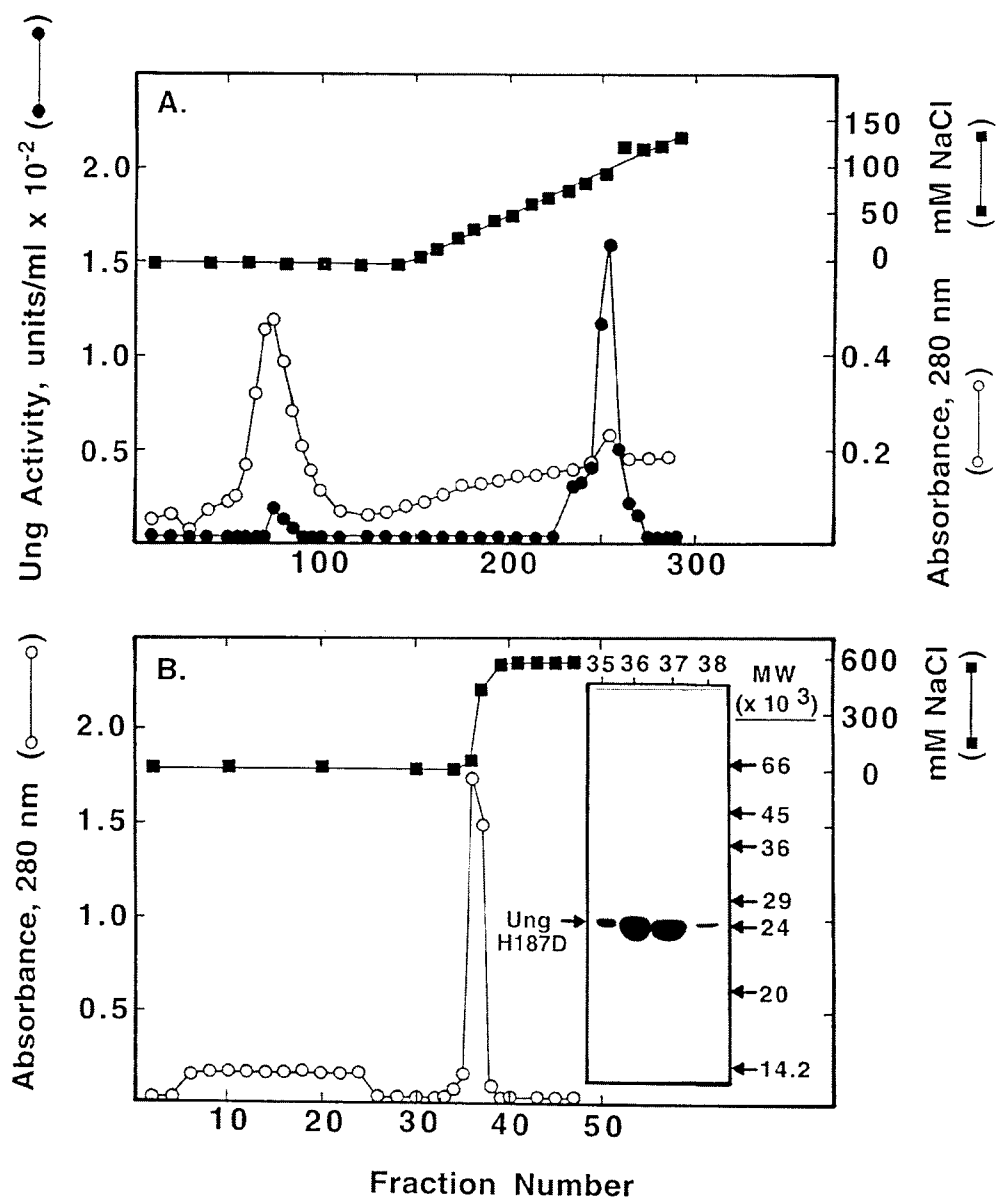


Figure 10. Single-stranded DNA agarose and Poly(U) Sepharose chromatography of Ung H187D. (A) Fraction IV (17 mg) was dialyzed against DAB buffer and applied to a single-stranded DNA agarose column (19.6 cm² x 42 cm) equilibrated in DAB buffer. The column was then washed and eluted with a linear gradient of 0-150 mM NaCl in DAB buffer. Fractions (2.5 ml) were collected, 25 μ l aliquots were assayed for Ung activity (●), and absorbance (OD_{280 nm}) was measured (○). NaCl concentration (■) was determined by measuring the conductivity of fractions (100 μ l) diluted 1/10 in distilled water at room temperature. Flow through fractions (62-102) were pooled and dialyzed against TMEG buffer, which constituted Fraction V. (B) Fraction V (8 mg) was loaded onto a poly(U) Sepharose column equilibrated in TMEG buffer. The column was washed and eluted step-wise with 500 mM NaCl in TMEG buffer. Fractions (2 ml) were collected and the absorbance at 280 nm measured (○). NaCl concentration (■) was determined by measuring conductivity as described in (A). Peak fractions (35-38) were analyzed on a 12.5% SDS-polyacrylamide gel (*insert*) as described under "Experimental Procedures". The location of Ung H187D is indicated by an *arrow*.

Figure 10



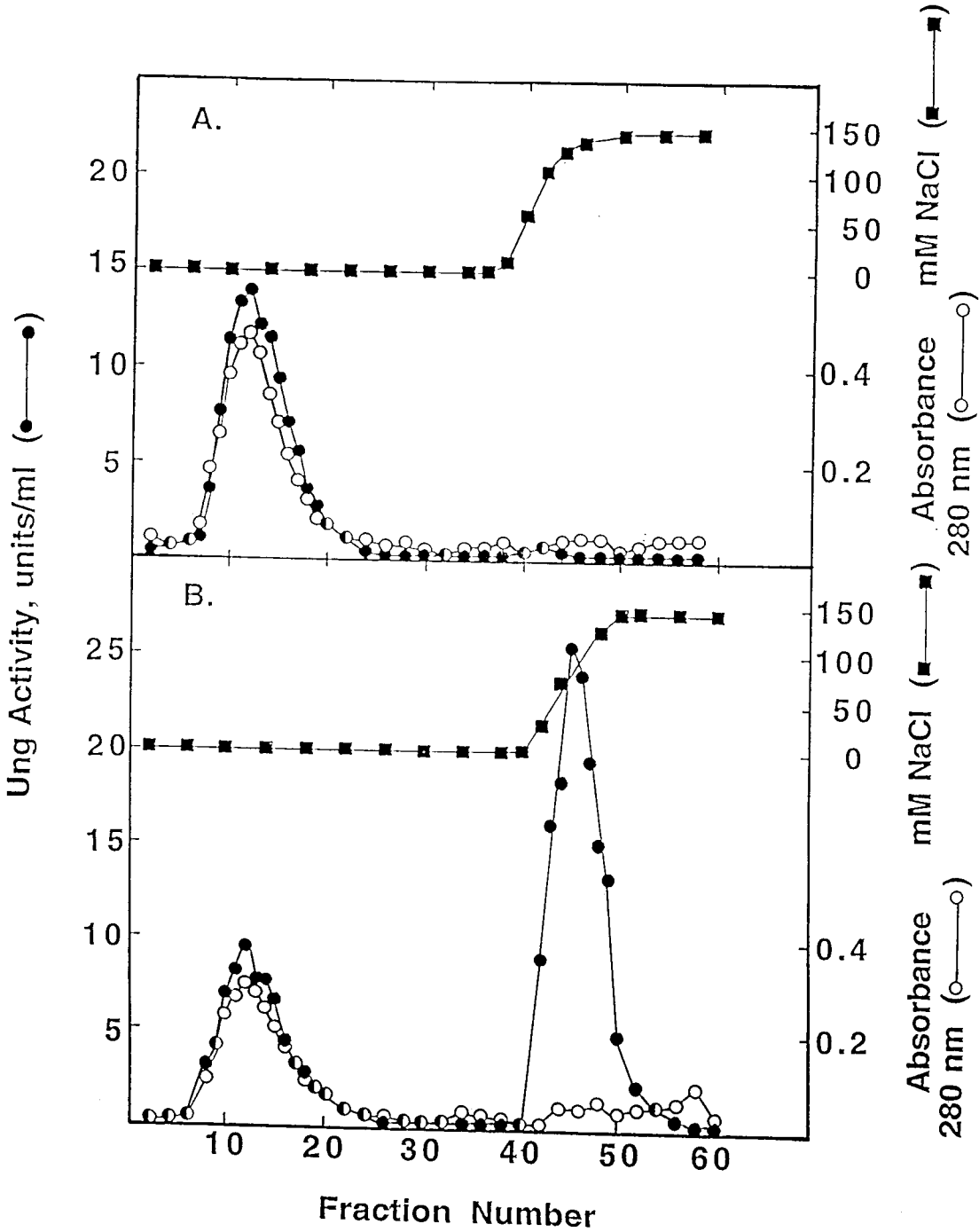
designated Fraction V. An aliquot of Fraction V (8 mg) was applied to a poly(U) Sepharose column. After washing the column, protein which bound to the matrix was eluted stepwise by using 500 mM NaCl. Fractions were analyzed for the presence of protein by absorbance spectroscopy at 280 nm. A broad protein peak was observed in the wash fractions while a sharp, relatively concentrated protein peak was detected at fraction 36 subsequent to the step elution (Figure 10B). Analysis of peak fractions by SDS-polyacrylamide gel electrophoresis revealed that the protein contained in the elution fractions was the overproduced Ung H187D, yielding an apparently homogeneous preparation of the mutant enzyme (Figure 10B, *insert*). After pooling the peak fractions, the specific activity of Ung H187D was determined to be 37 units/mg, whereas wild type Ung was determined to have a specific activity of 2.1×10^6 units/mg under standard reaction conditions.

3.1.7 Rechromatography of Ung H187D on Single-Stranded DNA Agarose

Although single-stranded DNA agarose chromatography appeared to separate Ung H187D from wild type Ung (Figure 10A), this observation alone did not eliminate the possibility that the activity detected in the Ung H187D preparation was due to a trace contaminant of Ung. To determine whether residual Ung was present in Ung H187D (Fraction VI), a sample (167 units) of Ung H187D was rechromatographed on a single-stranded DNA agarose column (Figure 11A). A single peak of activity was detected in the flow through fractions and no significant activity was observed binding to the matrix with characteristics of wild type Ung. In order to verify that this chromatographic system would have resolved an Ung contaminant, if present, the experiment was repeated using an identical sample of Ung H187D to which 167 units of Ung was added. Following chromatography, two peaks of activity corresponding to Ung H187D and Ung were resolved (Figure 11B). The specific activity of the flow through fractions shown in Figure 11A was calculated to be 49 units/mg of protein. Likewise, the flow through fractions shown in Figure 11B had a specific activity of 49 units/mg of protein despite

Figure 11. Rechromatography of Ung H187D on single-stranded DNA agarose. (A) Ung H187D (Fraction VI, 167 units) was applied to a single-stranded DNA agarose column (5.7 cm x 1.8 cm²) equilibrated in DAB buffer. The column was washed and then step-eluted with DAB buffer containing 150 mM NaCl as described under "Experimental Procedures". (B) A sample containing Ung H187D (Fraction VI, 167 units) and wild type Ung (Fraction V, 167 units) in DAB buffer was prepared and single-stranded agarose chromatography performed as described in (A). Fractions (1 ml) were collected, assayed under standard reaction conditions for uracil-DNA glycosylase activity (●), measured for absorbance at 280 nm (○), and monitored for conductivity (■).

Figure 11



being mixed with wild type Ung. Together these observations suggest that the activity detected in the Ung H187D preparation was inherent to the mutant enzyme.

3.1.8 Ability of Ung and Ung H187D to Bind the Uracil-DNA Glycosylase Inhibitor

To determine whether the Ugi inhibitor protein was able to bind Ung H187D, band shift assays were performed using radioactively labeled Ugi. [³⁵S]Ugi (300 pmol) was incubated with increasing molar amounts of Ung or Ung H187D (75-1,500 pmol). Enzyme-inhibitor complex was resolved from the individual components by native polyacrylamide gel electrophoresis. [³⁵S]Ugi was included as a control to indicate the location of uncomplexed inhibitor (Figure 12A and C, lane C). Autoradiography was performed to determine the location of free and complexed [³⁵S]Ugi (Figure 12A and C). At a molar ratio of Ung to Ugi of 1:1, 66% of the [³⁵S]Ugi was detected in complex (Figure 12B). In contrast, 87% of the [³⁵S]Ugi complexed with Ung H187D at the same molar ratio (Figure 12D). Wild type Ung complex formation reaches a plateau at ratios higher than 2:1 while Ung H187D complex formation plateaus at a 0.75 ratio with [³⁵S]Ugi. In both cases, a small fraction of the [³⁵S]Ugi preparation appears to be incapable of forming complex with enzyme (Figure 12B and D).

3.1.9 pH Optimum of Ung H187D Activity

The specific activity of Ung H187D and Ung was determined in Tris-HCl and HEPES-KOH buffers over a pH range of 6.5-9.5 (Figure 13). Maximal activity of Ung H187D was observed with HEPES-KOH at pH 7.0 which was one pH unit lower than the pH optimum for Ung (pH 8.0).

3.1.10 Substrate Specificity of Ung and Ung H187D

The relative ability of Ung and Ung H187D to remove uracil from either a single-stranded or double-stranded oligonucleotide containing a U/A

Figure 12. Binding of Ung and Ung H187D by uracil-DNA glycosylase inhibitor protein. (A) Ung•Ugi complex formation was studied in binding reaction mixtures (100 μ l) containing 300 pmol of [35 S]Ugi and 0, 75, 150, 225, 300, 375, 450, 600, or 1,500 pmol of Ung (lanes C, 1-8, respectively). Samples were incubated at 25°C for 10 min and 4°C for 20 min, then analyzed by 18% nondenaturing polyacrylamide gel electrophoresis and autoradiography. *Arrows* indicate the location of [35 S]Ugi and Ung•[35 S]Ugi. (B) Following electrophoresis the gel was dried, autoradiography performed, radioactive bands containing [35 S]Ugi and Ung•[35 S]Ugi were detected and excised from the gel. The 35 S radioactivity was measured in each gel slice as described under "Experimental Procedures". The amount of unbound [35 S]Ugi (\square) and Ung•[35 S]Ugi complex (\blacksquare) was measured as the percentage of the total amount of 35 S radioactivity detected. (C) Complex formation between Ung H187D and Ugi was similarly examined in identical reaction mixtures containing 300 pmol of [35 S]Ugi and 0, 75, 150, 225, 300, 375, 450, 600, or 1,500 pmol of Ung H187D (lanes C, 1-8, respectively). (D) The amount of unbound [35 S]Ugi and Ung H187D•[35 S]Ugi complex was determined as described above.

Figure 12

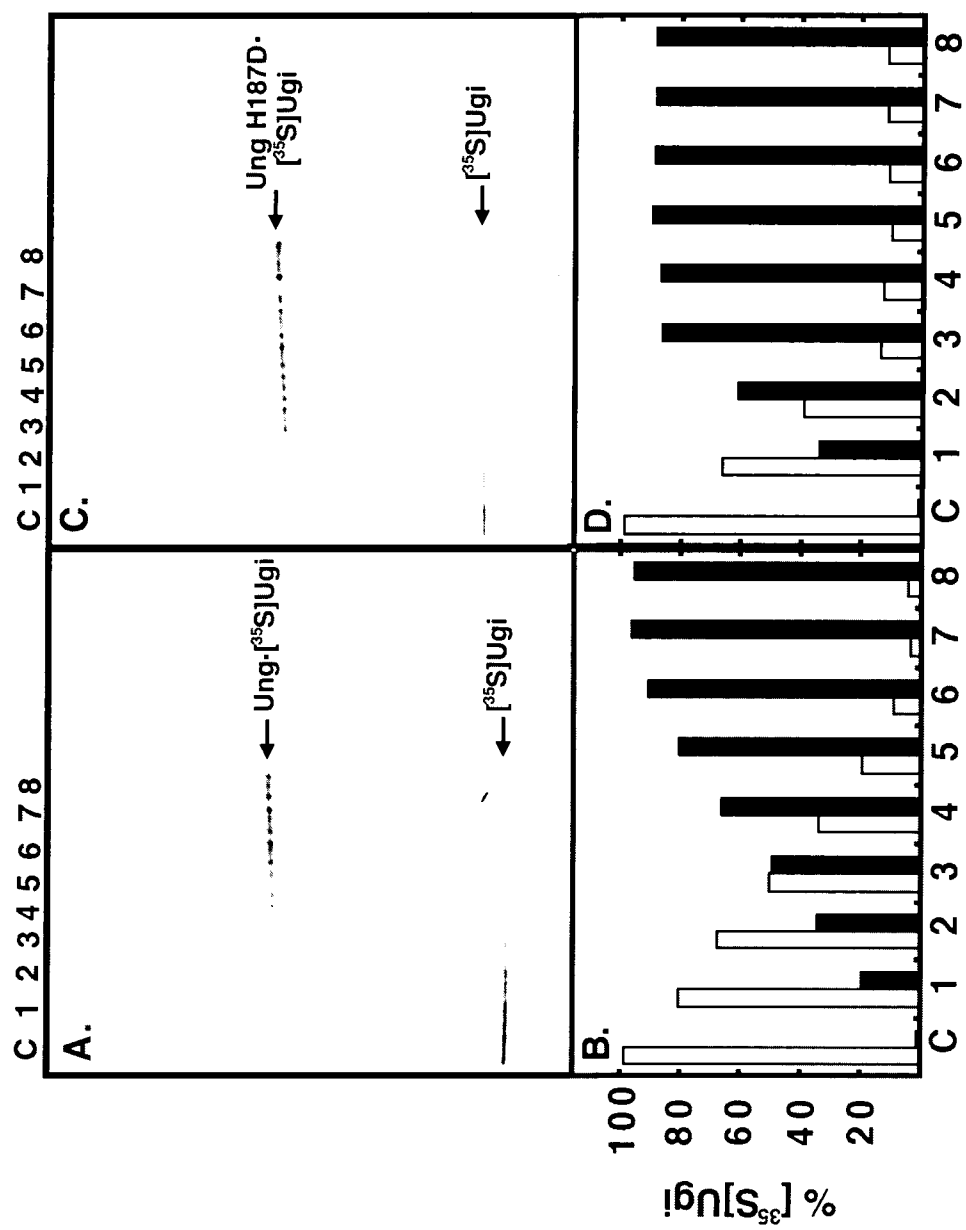
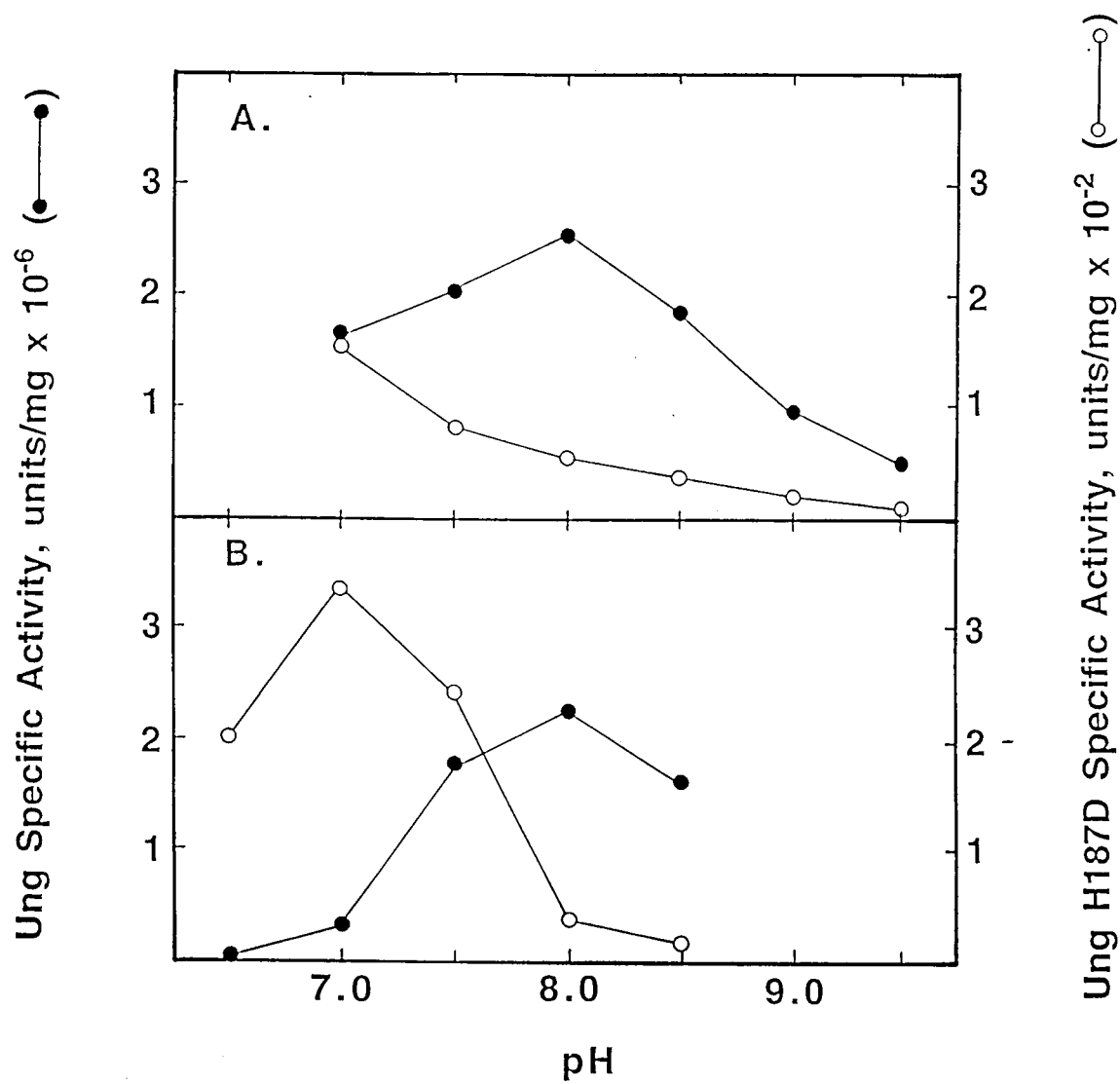


Figure 13. Comparison of pH optima of wild type Ung and Ung H187D activity. Four sets of standard uracil-DNA glycosylase reaction mixtures containing Ung (●) or Ung H187D (○) were prepared except that either (A) 70 mM Tris-HCl (pH 7.0-9.5) or (B) 70 mM HEPES-KOH (pH 6.5-8.5) was used as a buffer as indicated. Three concentrations (0.03-0.13 units) of enzyme were assayed at each pH and were used to determine the specific activity for each reaction condition.

Figure 13



base pair or U/G mispair was examined. A 5'-end ^{32}P -labeled oligonucleotide (^{32}P U-25-mer) with a site-specific uracil residue at position 11 was annealed to one of two complementary oligonucleotides producing either a ^{32}P U/A-25-mer or ^{32}P U/G-25-mer DNA substrate. Each of the three substrates (U, U/A, U/G) was incubated with Ung at pH 8.0 to catalyze uracil excisions, producing apyrimidinic sites. After alkali-induced cleavage of the deoxyribose-phosphate bond, an AP site-containing ^{32}P 11-mer was resolved by denaturing polyacrylamide gel electrophoresis as the reaction product (Figure 14A-C). The rate of uracil excision was determined for each DNA substrate, and the wild type Ung was found to hydrolyze the single-stranded U-25-mer about 3- and 5-fold faster than the U/G- and U/A-25-mer, respectively (Figure 14D). Interestingly, when Ung H187D was examined under the same reaction conditions, the U/G-25-mer was found to be the preferred substrate. Activity on the single-stranded U-25-mer and the U/A-25-mer was reduced by ~1.5- and 2.3-fold, respectively, compared to the U/G-25-mer substrate (Figure 14E-H). When wild type Ung was assayed at the suboptimal pH of 7.0, its activity on U-25-mer was reduced ~2.6-fold relative to standard assay conditions (pH 8.0) and activity on double-stranded substrate was not detected (Figure 15A-D). When Ung H187D was assayed at its optimal pH of 7.0, all three substrates were processed with similar efficiencies (Figure 15E-H). Activity on the U/G- and U/A-25-mer was determined to be 75% and 86% of the rate of activity on the U-25-mer which was increased ~3-fold relative to the assay at pH 8.0.

3.1.11 Effect of Uracil on Ung and Ung H187D Activity

Inhibition studies were conducted to determine whether the H187D mutation of Ung affected the binding of uracil to the enzyme. Standard assays were conducted using Ung or Ung H187D in the presence of various amounts of free uracil, 6-amino uracil or 5-fluorouracil and the percent of activity relative to the control was determined as shown in Figure 16. At pH 8.0, Ung activity appeared to be 50% inhibited by ~0.15 mM uracil. In contrast, Ung

Figure 14. Substrate specificity of Ung and Ung H187D at pH 8.0. Three sets of standard uracil-DNA glycosylase reaction mixtures (125 μ l) each containing 0.3 units of Ung and either [32 P]U-25-mer (A), [32 P]U/A-25-mer (B), or [32 P]U/G-25-mer (C) were incubated at 37°C for 0, 10, 20, 30, 40, 50, or 60 min (lanes 1-7, respectively). Reactions were conducted using 70 mM HEPES-KOH (pH 8.0) as a buffer. A control reaction (lane C) was prepared which was incubated without Ung on ice for 60 min. After incubation, each reaction was terminated, AP-sites were hydrolyzed by alkaline treatment, and samples were analyzed by denaturing 12% urea-polyacrylamide gel electrophoresis. Arrows indicate the locations of 25-mer substrate (S) and 11-mer product (P) on the autoradiogram. (D) Radioactive bands were excised from the dried gel, the amount of 32 P radioactivity was measured for bands S and P, and the percent of 25-mer hydrolyzed for the U (●), U/A (▲), and U/G (■) containing oligonucleotide was calculated. Three similar sets of reaction mixtures each containing Ung H187D and either [32 P]U-25-mer (E), [32 P]U/A-25-mer (F), or [32 P]U/G-25-mer (G) were incubated. (H) The percent of 25-mer hydrolyzed for each substrate was determined as described above.

Figure 14

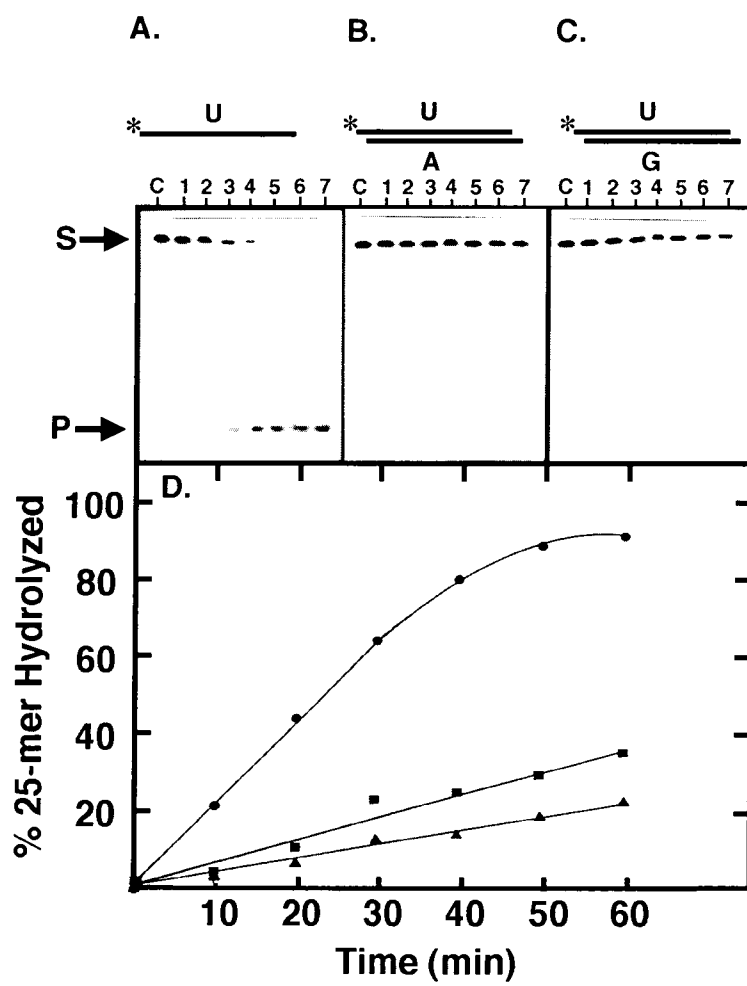


Figure 15. Substrate specificity of Ung and Ung H187D at pH 7.0. Three sets of standard uracil-DNA glycosylase reaction mixtures (125 μ l) each containing 0.3 units of Ung and either [32 P]U-25-mer (A), [32 P]U/A-25-mer (B), or [32 P]U/G-25-mer (C) were incubated at 37°C for 0, 10, 20, 30, 40, 50, or 60 min (lanes 1-7, respectively). Reactions were conducted using 70 mM HEPES-KOH (pH 7.0) as a buffer. A control reaction (lane C) was prepared which was incubated without Ung on ice for 60 min. After incubation, each reaction was terminated, AP-sites were hydrolyzed by alkaline treatment, and samples were analyzed by denaturing 12% urea-polyacrylamide gel electrophoresis. *Arrows* indicate the locations of 25-mer substrate (S) and 11-mer product (P) on the autoradiogram. (D) Radioactive bands were excised from the dried gel, the amount of 32 P radioactivity was measured for bands S and P, and the percent of 25-mer hydrolyzed for the U (●), U/A (▲), and U/G (■) containing oligonucleotide was calculated. Three similar sets of reaction mixtures each containing Ung H187D and either [32 P]U-25-mer (E), [32 P]U/A-25-mer (F), or [32 P]U/G-25-mer (G) were incubated. (H) The percent of 25-mer hydrolyzed for each substrate was determined as described above.

Figure 15 (Continued)

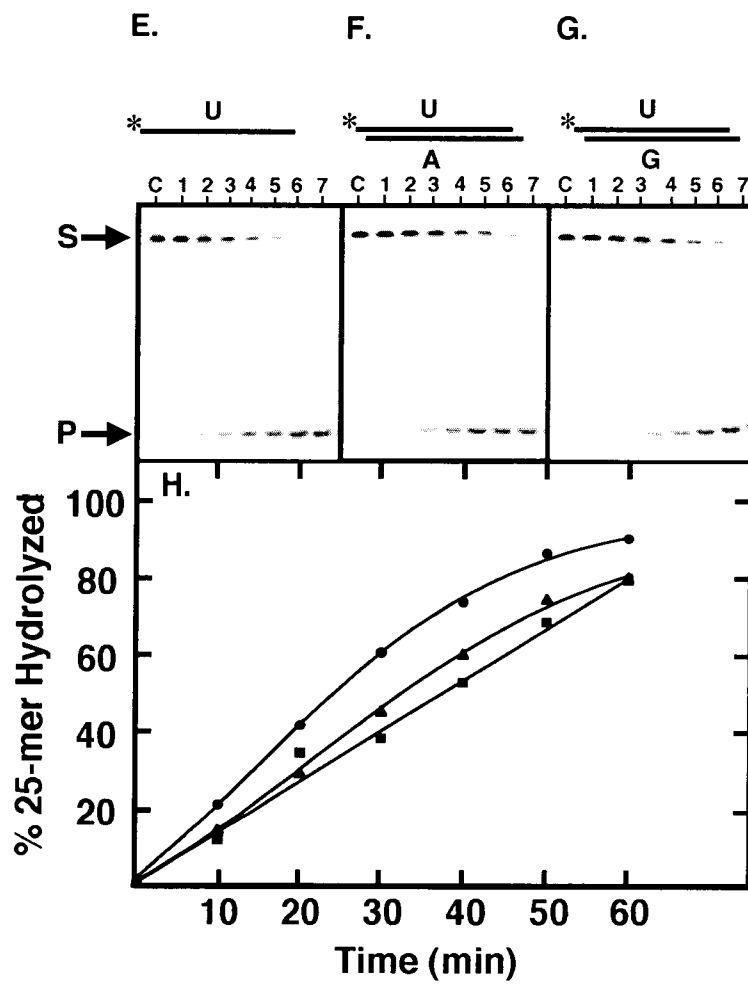
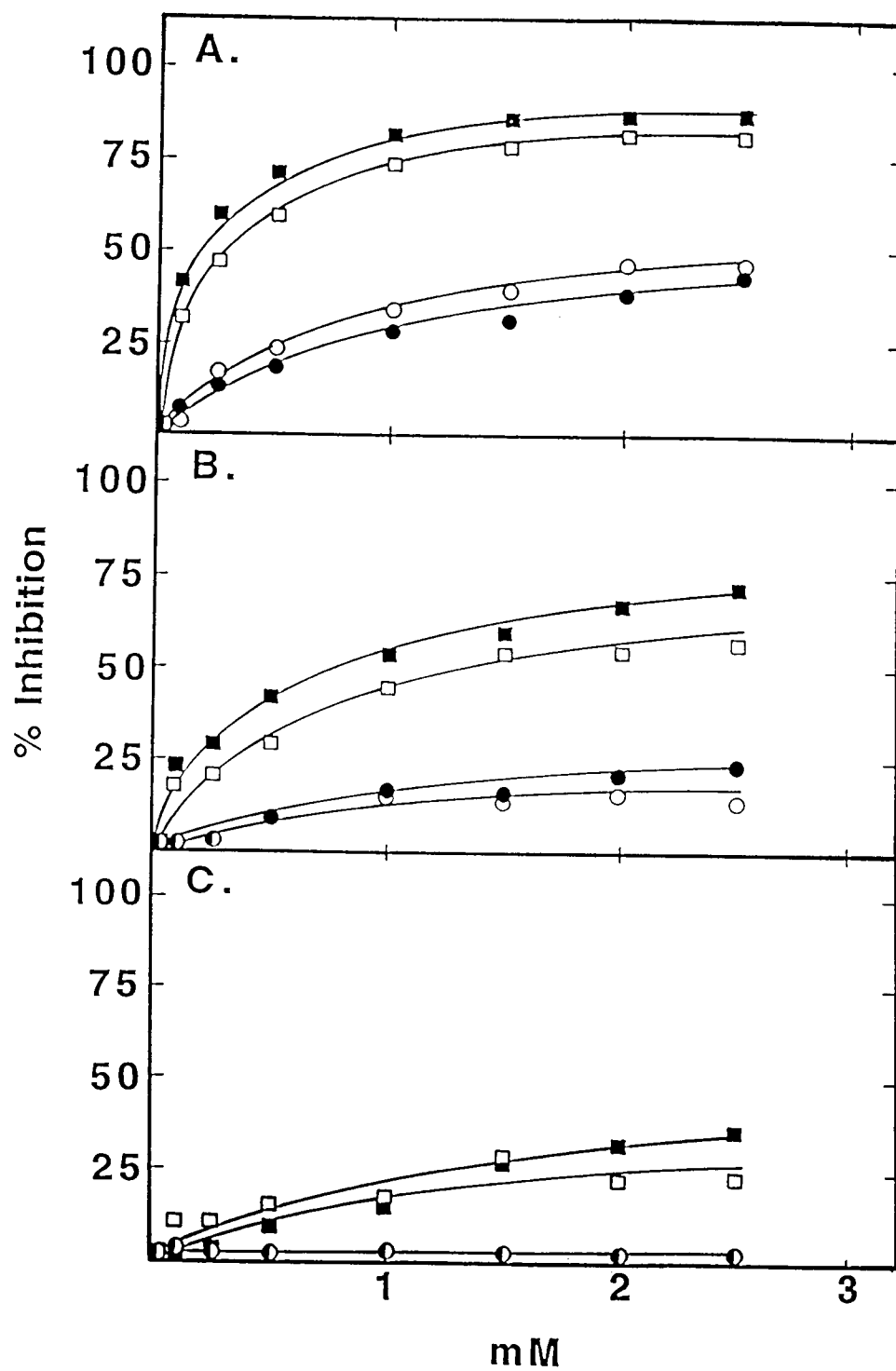


Figure 16. Effect of uracil on wild type Ung and Ung H187D activity. (A) Four sets of standard uracil-DNA glycosylase reaction mixtures (100 μ l) were prepared containing either 1.3 units of Ung (\square, \blacksquare) or 0.6 units of Ung H187D (\circ, \bullet). Reactions were conducted using 70 mM HEPES-KOH (pH 8.0) (\blacksquare, \bullet) or 70 mM HEPES-KOH (pH 7.0) (\square, \circ) and each reaction was supplemented with various amounts of uracil as indicated. (B) Similarly, four sets of reaction mixtures were prepared and supplemented with different amounts of 6-amino uracil or (C) 5-fluorouracil as indicated. After incubation at 37°C for 30 min, the amount of [3 H]uracil released from the DNA substrate was measured. The percent of Ung activity inhibited was determined relative to the control lacking uracil.

Figure 16



H187D was much more resistant and showed about 7.5% inhibition at the same uracil concentration (Figure 16A). Similar results for inhibition by uracil were observed for reactions conducted at pH 7.0 (Figure 16A). Substitution of 6-amino uracil in place of uracil also demonstrated that Ung was more sensitive to the inhibitor than Ung H187D, and that the observed level of inhibition was not significantly affected by the change of pH (Figure 16B). Inhibition of Ung by 5-fluorouracil (Figure 16C) was least pronounced, regardless of pH: ~20% at 1 mM 5-fluorouracil. Moreover, inhibition of Ung H187D was not observed at any of the 5-fluorouracil concentrations tested (Figure 16C).

3.1.12 Ability of Ung and Ung H187D to Bind DNA

To assess the relative affinity of Ung and Ung H187D for DNA, UV-catalyzed cross-linking experiments were conducted using three different oligonucleotides. Nonspecific DNA interactions were analyzed after mixing [^{32}P]dT₂₀ with either Ung or Ung H187D, irradiating with UV light for various times, and resolving the reaction products using SDS-polyacrylamide gel electrophoresis. Autoradiography was used to detect the enzyme x [^{32}P]dT₂₀ bands as shown in Figure 17A. The rate of cross-linking was determined by measuring the amount of ^{32}P radioactivity contained in the enzyme x dT₂₀ bands as a function of UV irradiation time (Figure 17B). A comparison of the cross-linking rates indicated that Ung (0.36 pmol/min) was ~2.2-fold more efficient than Ung H187D (0.16 pmol/min) at forming a protein x dT₂₀ complex. Enzyme saturation experiments using various concentrations of oligonucleotide to perform UV-catalyzed cross-linking revealed the extent of Ung and Ung H187D x dT₂₀ product formation (Figure 18A). In both cases, cross-linking increased with increasing dT₂₀ concentration until reaching a plateau where ~1.5-fold more Ung x dT₂₀ than Ung H187D x dT₂₀ was produced. The experiment was also conducted using [^{32}P]dT₁₉-U, a uracil-containing oligonucleotide (20-mer) possessing a uracil residue 12 nucleotides from the 5'-end (Figure 18B). With this DNA substrate, the ability of Ung

Figure 17. Relative ability of Ung and Ung H187D to form UV-catalyzed cross-links with dT₂₀. (A) Two reaction mixtures (150 μ l) containing DAB buffer, 3.8 nmol of either Ung or Ung H187D were UV-irradiated on ice as described under "Experimental Procedures". At the times indicated, 15 μ l samples were removed and analyzed by 12.5% SDS-polyacrylamide gel electrophoresis. The protein bands were visualized by Coomassie Brilliant Blue staining and the enzyme x [³²P]dT₂₀ (*arrow*) was detected by autoradiography. Lanes 1-7 correspond to UV-light exposure times of 0, 2.5, 5, 10, 20, 30, and 45 min, respectively. (B) The amount of [³²P]dT₂₀ cross-linked to Ung (●) and Ung H187D (○) was quantitated by excising the radioactive bands from the dried gel, solubilizing the gel with 30% H₂O₂ at 55°C, and measuring the ³²P radioactivity in a liquid scintillation counter using 5 ml of Formula 989 fluor.

Figure 17

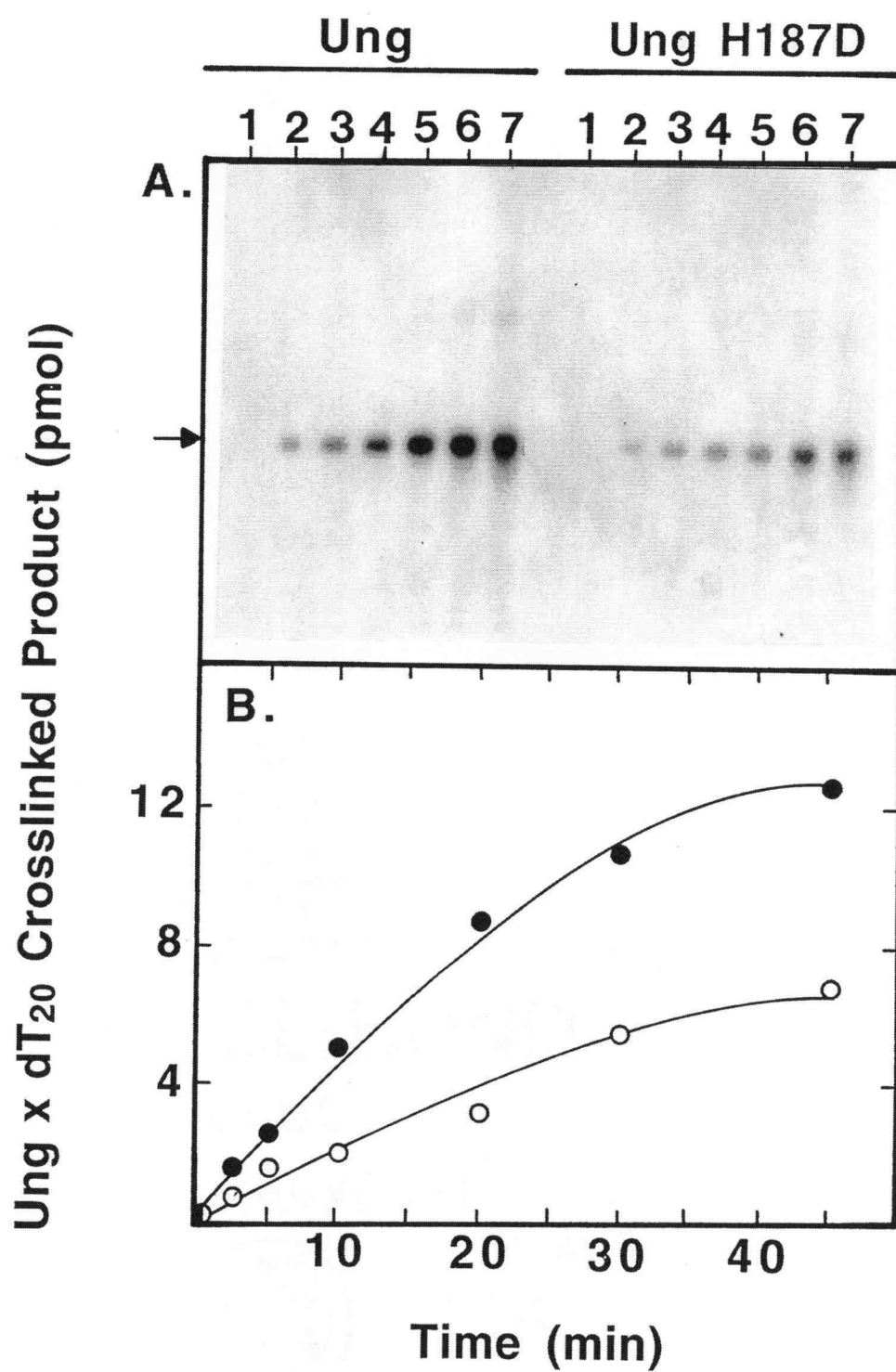
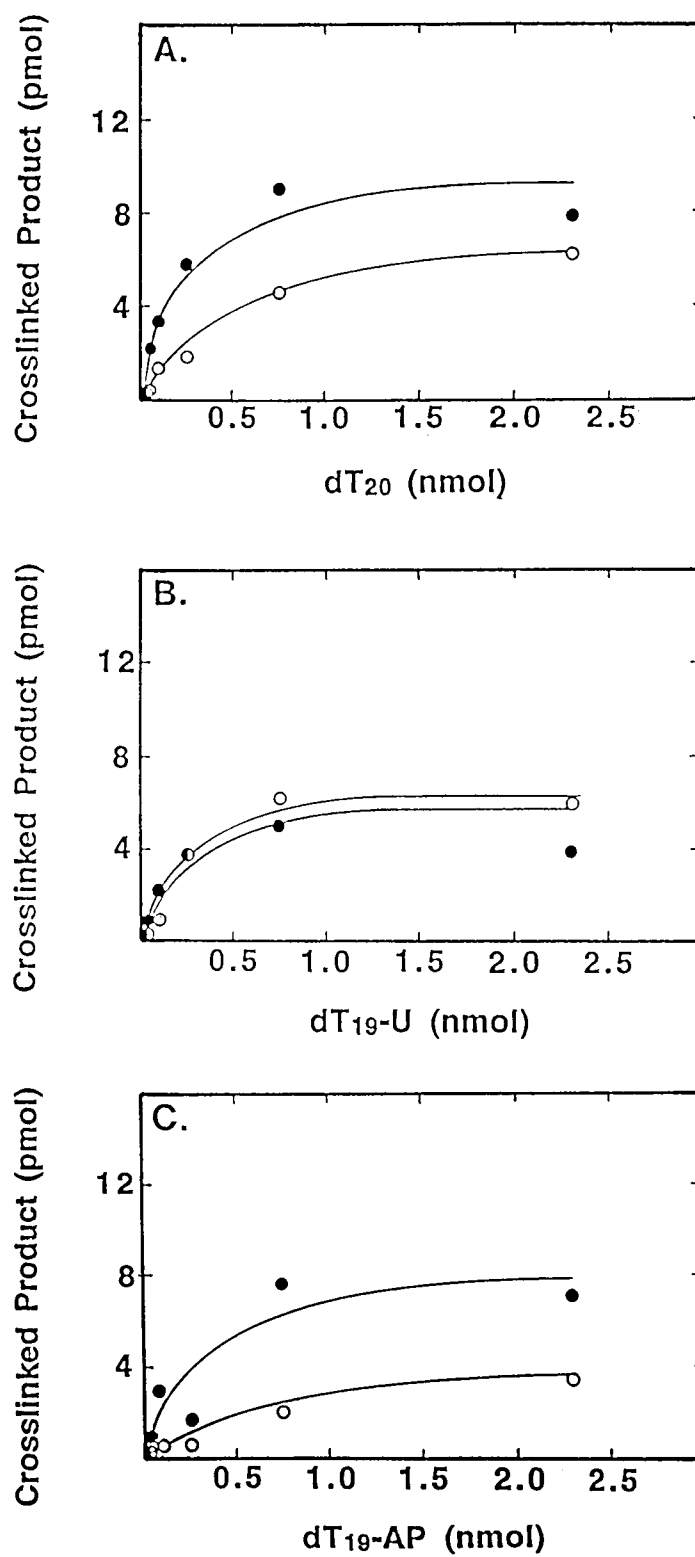


Figure 18. Effect of uracil- and AP-sites on UV-catalyzed cross-linking of Ung and Ung H187D to dT₂₀. (A) Samples (15 μ l) containing 0.38 nmol of Ung (●) or Ung H187D (○) and 0.028, 0.084, 0.25, 0.76, or 2.28 nmol of [³²P]dT₂₀ were UV-irradiated for 30 min as described under "Experimental Procedures". Identical UV-catalyzed cross-linking reactions were carried out except that [³²P]dT₁₉-U (B) or [³²P]dT₁₉-AP (C) was substituted as the oligonucleotide. After UV irradiation, samples were analyzed by 12.5% SDS-polyacrylamide gel electrophoresis and the amount of enzyme cross-linked to [³²P]oligonucleotide was determined by liquid scintillation counting as described in Figure 17.

Figure 18



H187D, relative to Ung, to form a cross-linked complex was nearly identical. In addition, the cross-linking efficiency was measured by using [^{32}P]dT₁₉-AP, which contained an apyrimidinic site in place of the site-specific uracil residue of dT₁₉-U (Figure 18C). Recognition of dT₁₉-AP by Ung was ~2-fold greater than by Ung H187D, due primarily to the decreased ability of Ung H187D to cross-link to this oligonucleotide relative to either dT₂₀ or dT₁₉-U.

3.1.13 Effect of Uracil on DNA Binding

To determine the effect of free uracil on the DNA affinity of Ung and Ung H187D, UV-catalyzed cross-linking experiments were carried out in the presence of [^{32}P]dT₂₀ and 2 mM uracil (Figure 19). Inspection of the respective autoradiographs (Figure 19A and B) and cross-linking rates (Figure 19C) shows that, in the absence of uracil, the extent of UV-catalyzed oligonucleotide cross-linking to Ung was approximately twice that of Ung H187D. However, in the presence of the highly inhibitory concentration of free uracil, the extent of Ung cross-linking remained unaffected, whereas Ung H187D cross-linking was reduced more than two-fold.

3.1.14 Enzyme Kinetics of Ung and Ung H187D

The effect of substrate concentration on enzyme activity was examined by titrating various amounts of calf thymus [*uracil*- ^3H] DNA substrate into the standard uracil-DNA glycosylase assay. V_{max} and K_{m} values were calculated from the double reciprocal plot shown in Figure 20 and are summarized in Table 4. The Ung H187D mutation increased V_{max} and K_{m} at standard conditions by 1.9- and 4.3-fold, respectively. The reaction pH affected these values, with larger V_{max} corresponding to pH 8.0. Similarly the K_{m} was increased for wild type Ung from 0.32 μM at pH 7.0 to 0.88 μM at pH 8.0. The Ung H187D K_{m} increased from 1.7 μM to 3.8 μM at pH 7.0 and pH 8.0, respectively. The values for k_{cat} were compared and the substitution of Asp-187 for His-187 led to a reduction of approximately five orders of magnitude,

Figure 19. Effect of free uracil on UV-catalyzed cross-linking of Ung and Ung H187D to dT₂₀. (A) Two reaction mixtures (135 μ l) containing 3.4 nmol of Ung and 6.8 nmol of [³²P]dT₂₀ were UV-irradiated with UV-light in the presence or absence of 2 mM uracil. Samples (15 μ l) were removed after the irradiation times indicated and subsequently analyzed by 12.5% SDS-polyacrylamide gel electrophoresis. (B) An identical set of reaction mixtures was prepared except that 3.4 nmol of Ung H187D was substituted as the enzyme. Autoradiogray was conducted to locate the cross-linked enzyme x [³²P]dT₂₀ species. Lanes 1-7 correspond to irradiation times of 0, 2.5, 5, 10, 20, 30, and 45 min, respectively. (C) The amount of enzyme x [³²P]dT₂₀ produced was quantitated by liquid scintillation counting as previously described for Ung (●) and Ung H187D (■) in the presence and Ung (○) and Ung H187D (□) in the absence of uracil.

Figure 19

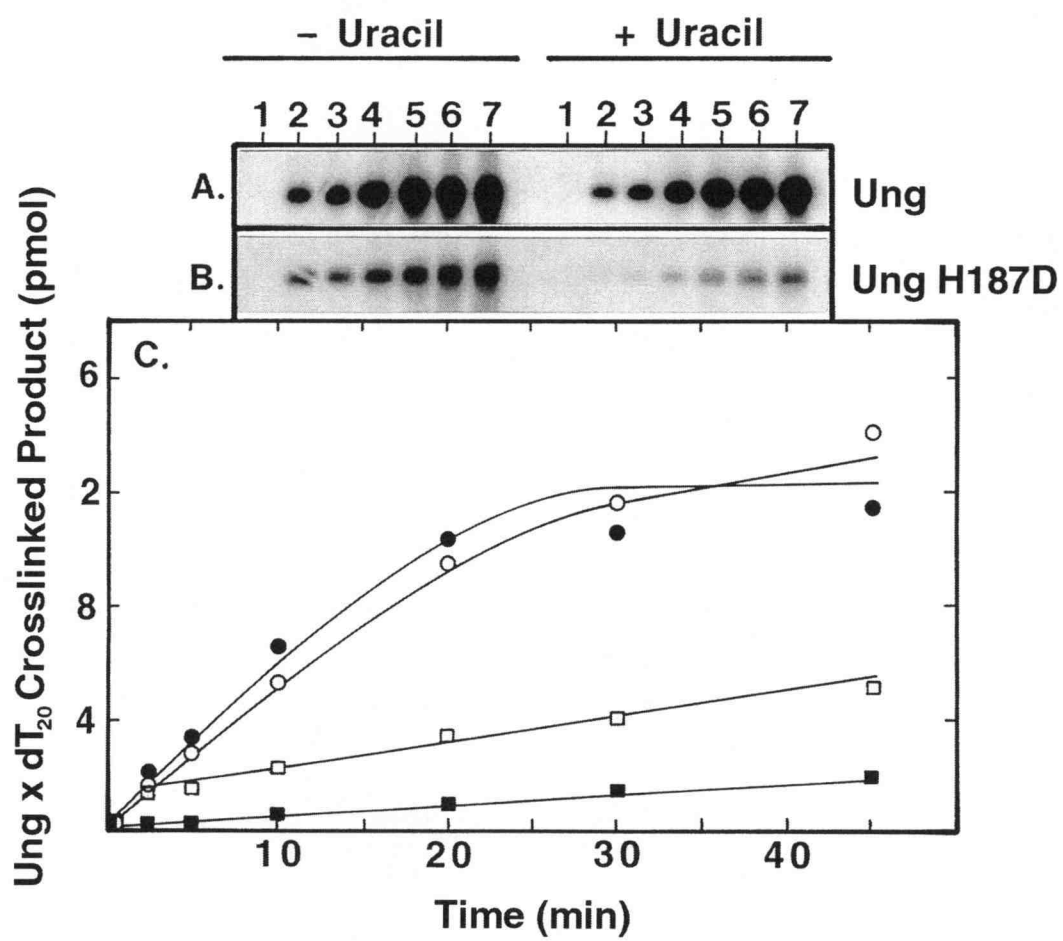


Figure 20. Effect of substrate concentration on Ung and Ung H187D activity. Modified uracil-DNA glycosylase reaction mixtures containing Ung (□,■) or Ung H187D (○,●) were diluted in UDB buffers by using 70 mM HEPES-KOH (pH 8.0) (■,●) or 70 mM HEPES-KOH (pH 7.0) (□,○) and calf thymus [*uracil*-³H] DNA concentrations of 0-10 μM with respect to [³H]uracil as described under "Experimental Procedures, Section 2.2.22.4". After incubation at 37°C for 30 min, the reaction was stopped with 10 mM ammonium formate buffer (pH 4.2), free [³H]uracil was recovered by Dowex chromatography and the amount of [³H]uracil released from the DNA substrate was determined by liquid scintillation counting.

Figure 20

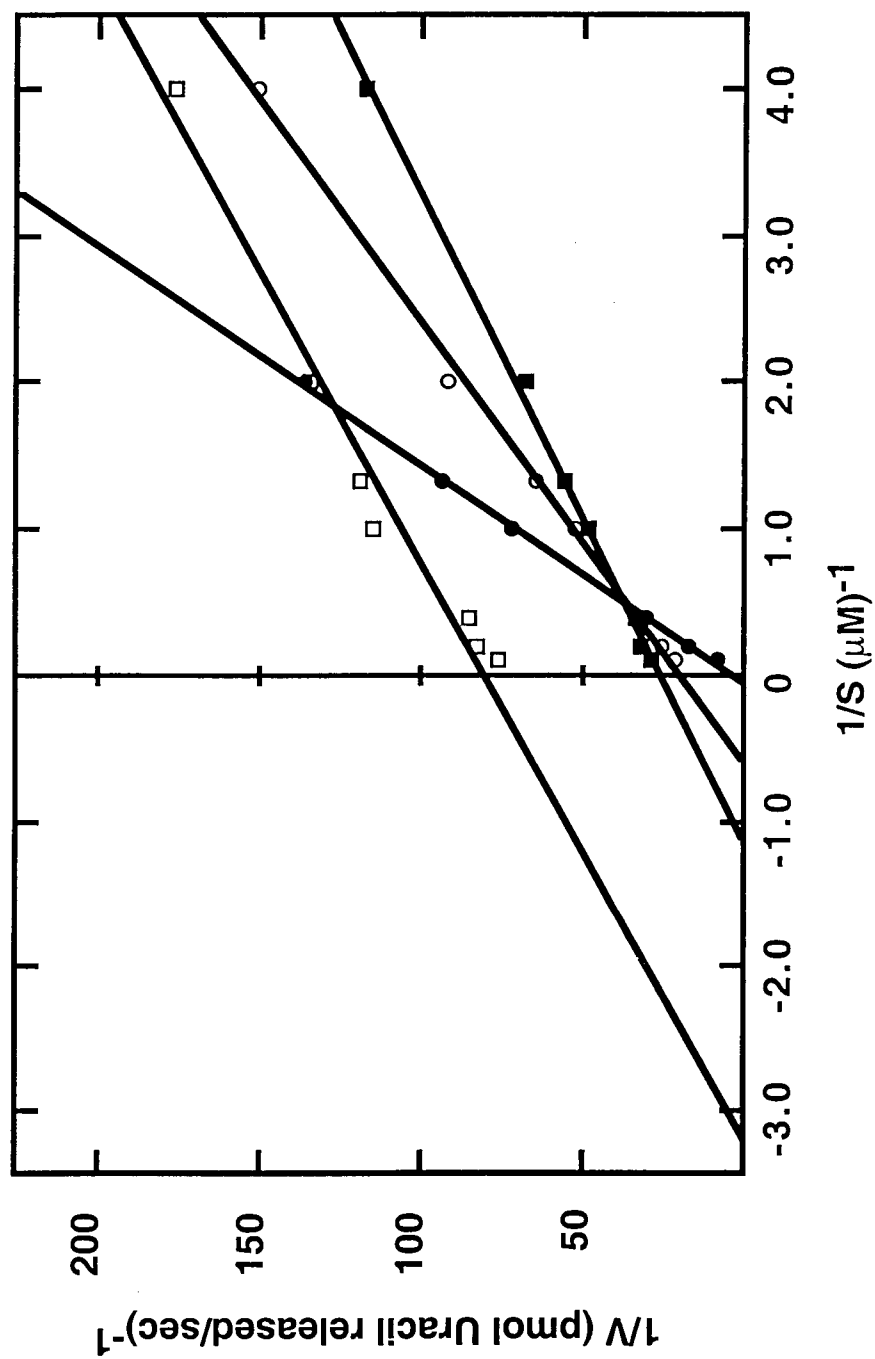


Table 4

Kinetic Parameters for Wild Type and H187D Mutant Uracil-DNA Glycosylases on Calf Thymus [uracil-³H] DNA Substrate^a

Enzyme (pH) ^b	V _{max} (M/sec × 10 ⁻¹⁰)	K _m (M × 10 ⁻⁶)	k _{cat} (sec ⁻¹)	k _{cat} /K _m (M ⁻¹ sec ⁻¹ × 10 ³)	V _{max} /K _m (sec ⁻¹ × 10 ⁻⁴)
Ung (7.0)	1.3	0.32	1.3	4100	4.1
Ung (8.0)	3.9	0.88	12	14000	4.4
Ung H187D (7.0)	5.1	1.7	0.0023	1.4	3.0
Ung H187D (8.0)	7.3	3.8	0.00025	0.066	1.9

^a The reaction mixture (75 μl) was added to 25 μl of [uracil-³H] DNA diluted in 10 mM Tris-HCl (pH 7.5). The final substrate concentration was 0-3.7 μg of [uracil-³H] DNA (180 cpm/pmol), 0-10 μM with respect to [³H]uracil.

^b Ung or Ung H187D (~0.13 units in UDB with HEPES-KOH (pH 7.0 or 8.0, as indicated)) was included in a modified reaction mixture as described under "Experimental Procedures".

from 12 sec^{-1} to 0.00025 sec^{-1} , under standard conditions. In contrast, pH and the H187D mutation had relatively minor effects on V_{max}/K_m . The values of V_{max}/K_m for Ung at pH 7.0 and pH 8.0 were nearly identical at 4.1×10^{-4} and $4.4 \times 10^{-4} \text{ sec}^{-1}$, respectively. The Ung H187D mutant V_{max}/K_m at pH 8.0 was reduced 2.3-fold to $1.9 \times 10^{-4} \text{ sec}^{-1}$. At the mutant's pH optimum, V_{max}/K_m was calculated to be $3.0 \times 10^{-4} \text{ sec}^{-1}$, which is only 1.4-fold less than that of the wild type enzyme at the same pH.

The kinetics of the wild type and mutant enzymes on double stranded oligonucleotide containing a 2-aminopurine·dU basepair were also studied using steady-state fluorometry. 2-Aminopurine (2-APu) is an adenine isomer which is fluorescent but exhibits quenching within duplex DNA (145). Thus, upon excision of uracil by the action of Ung or Ung H187D, the 2-APu residue becomes unpaired and fluorescent with an emission wavelength of 370 nm. Various amounts of double-stranded 2AP-27-mer substrate were equilibrated in DAB buffer (pH 7.4) for 60 sec and emission was monitored to establish a baseline. After 60 sec, Ung or Ung H187D was added to the reaction chamber at a final concentration of 2 nM or 250 nM, respectively. A large spike in fluorescence was detected due to sample addition and mixing from ~60-70 sec. After enzyme addition, the fluorescence was monitored for an additional 2 min for wild type Ung and an additional 4 min for Ung H187D. The initial reaction velocity for Ung was determined from the slope of the line ($\Delta I/\Delta t$) from 70-90 sec at each oligonucleotide concentration (Figure 21). The initial velocity for Ung H187D was determined from the slope of the line from 70-300 sec at each oligonucleotide concentration (Figure 22). Double reciprocal plots were produced by using these calculated values. Representative double reciprocal plots are shown in Figure 23. Four trials were performed with wild type Ung, and the average value of K_m was determined to be $55 (\pm 3) \text{ nM}$ (Figure 23A). The K_m of Ung H187D was calculated to be $1700 (\pm 300) \text{ nM}$, which is the average of three trials (Figure 23B). These values are considerably lower than those determined using calf thymus [*uracil*- ^3H] DNA. The k_{cat} of Ung and Ung H187D were calculated as 0.59 sec^{-1} and $0.68 \times 10^{-3} \text{ sec}^{-1}$, respectively.

Figure 21. Steady state kinetics of Ung with a 2-aminopurine-containing double-stranded oligonucleotide. Steady-state fluorescence measurements were performed using double-stranded 2AP-27-mer oligonucleotide containing a 2-aminopurine:uracil basepair with an excitation wavelength of 310 nm and emission wavelength of 370 nm. An aliquot (20 μ l) of the oligonucleotide was mixed with 400 μ l of DAB buffer (pH 7.4) and fluorescence was monitored for 60 sec to establish a baseline. Oligonucleotide concentrations were 20, 40, 50, 60, 80, 100, 120, 150, 200, 250, 300, 400, 500, 800, or 1000 nM (A-O, respectively). After 60 sec, 20 μ l of Ung (2 nM) was added to the reaction cuvette (*arrows* indicate Ung addition). Fluorescence was monitored for an additional 2 min and the intensity of fluorescence was plotted versus time. The initial velocity ($\Delta I/\Delta t$) of the reaction was determined from the slope of the line calculated by linear regression from the data points encompassing 70-90 sec incubation time.

Figure 21

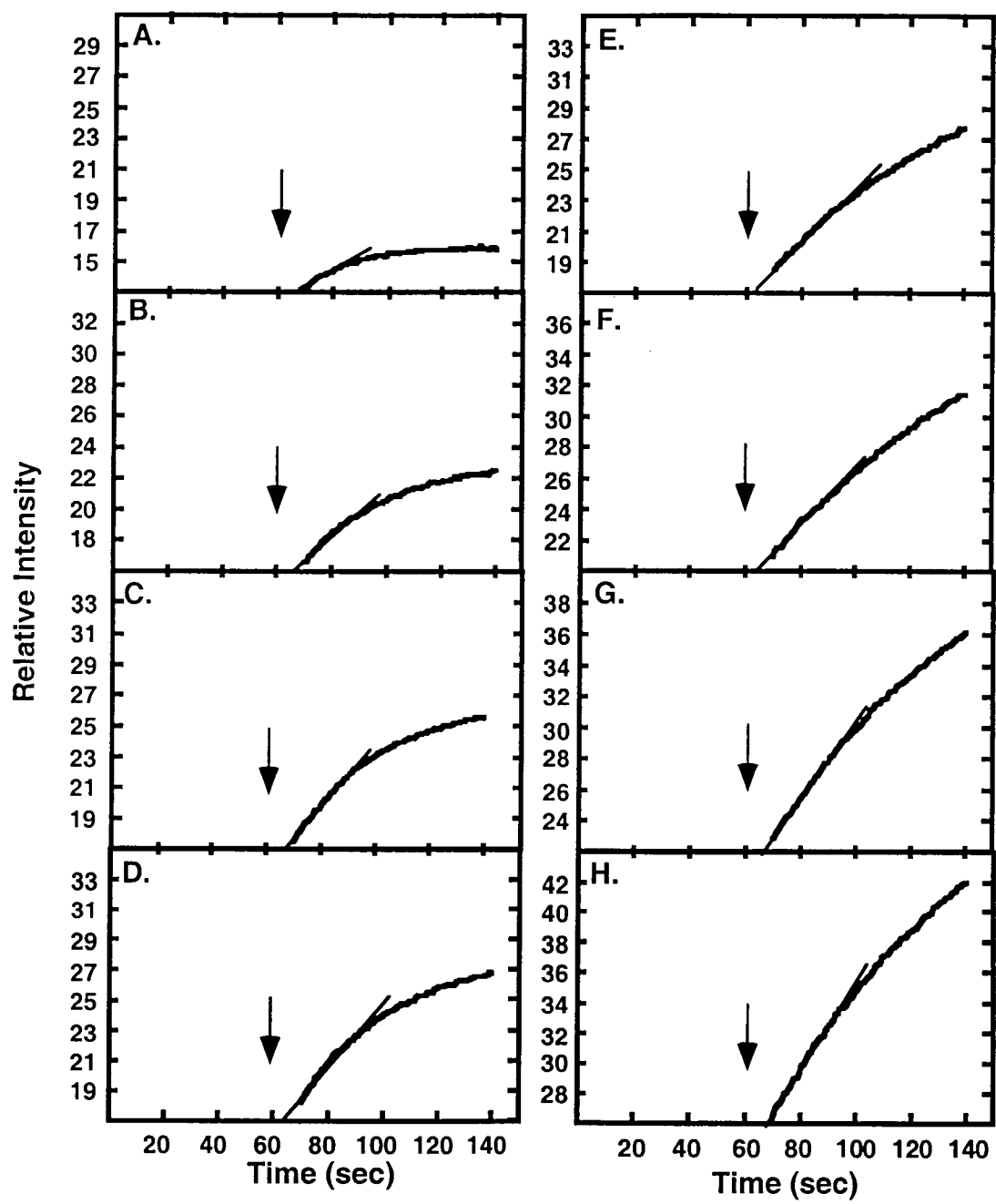


Figure 21 (Continued)

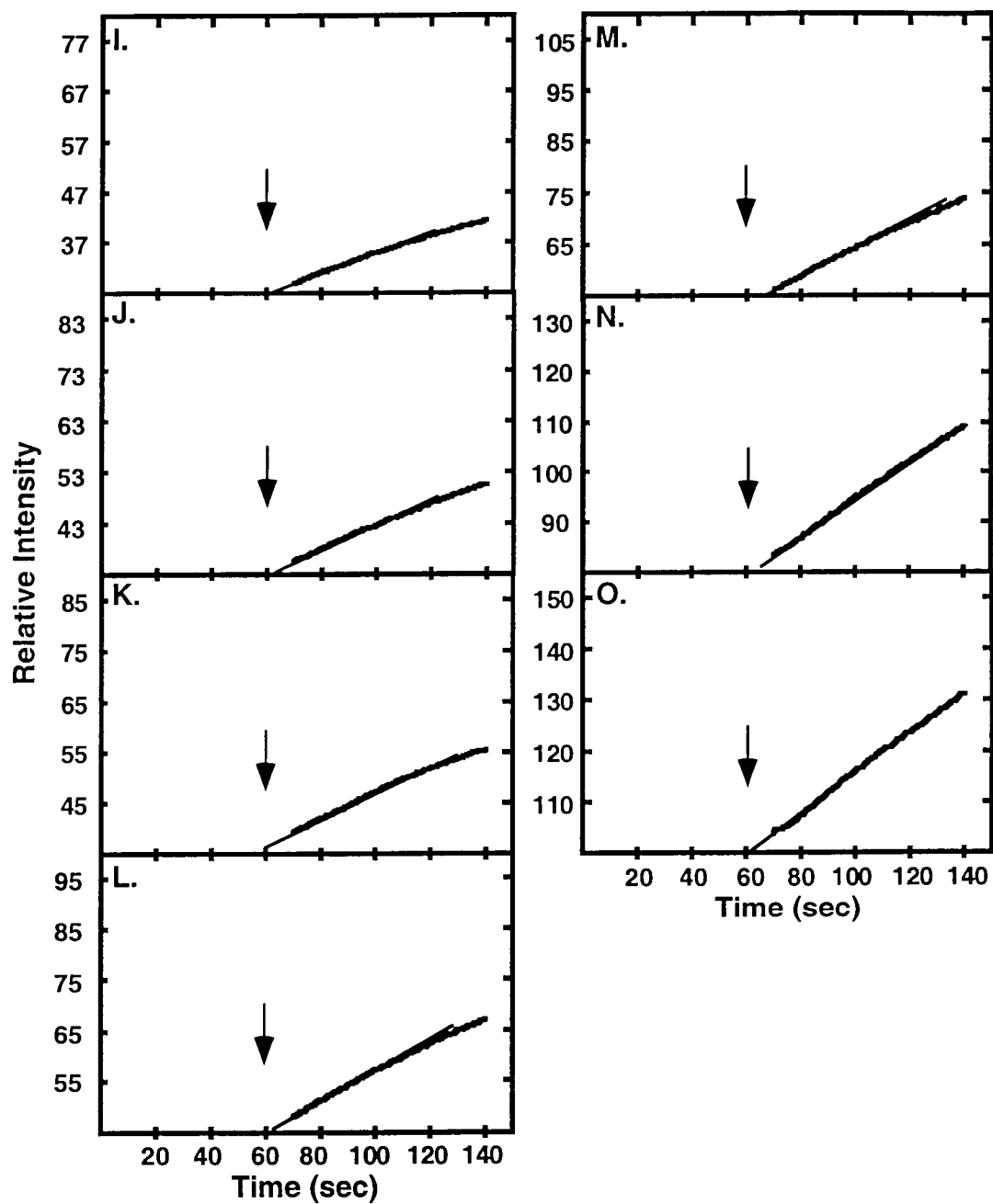


Figure 22. Steady state kinetics of Ung H187D with a 2-aminopurine-containing double-stranded oligonucleotide. Steady-state fluorescence measurements were performed using double-stranded 2AP-27-mer oligonucleotide containing a 2-aminopurine:uracil basepair with an excitation wavelength of 310 nm and emission wavelength of 370 nm. An aliquot (20 μ l) of the oligonucleotide was mixed with 400 μ l of DAB buffer (pH 7.4) and fluorescence was monitored for 60 sec to establish a baseline. Oligonucleotide concentrations were 500, 1000, 1500, 2000, 2500, 3000, or 3500 nM (A-G, respectively). After 60 sec, 20 μ l of Ung H187D (250 nM) was added to the reaction cuvette (*arrows* indicate Ung addition). Fluorescence was monitored for an additional 4 min and the intensity of fluorescence was plotted versus time. The initial velocity ($\Delta I/\Delta t$) of the reaction was determined from the slope of the line calculated by linear regression from the data points encompassing 70-300 sec incubation time.

Figure 22

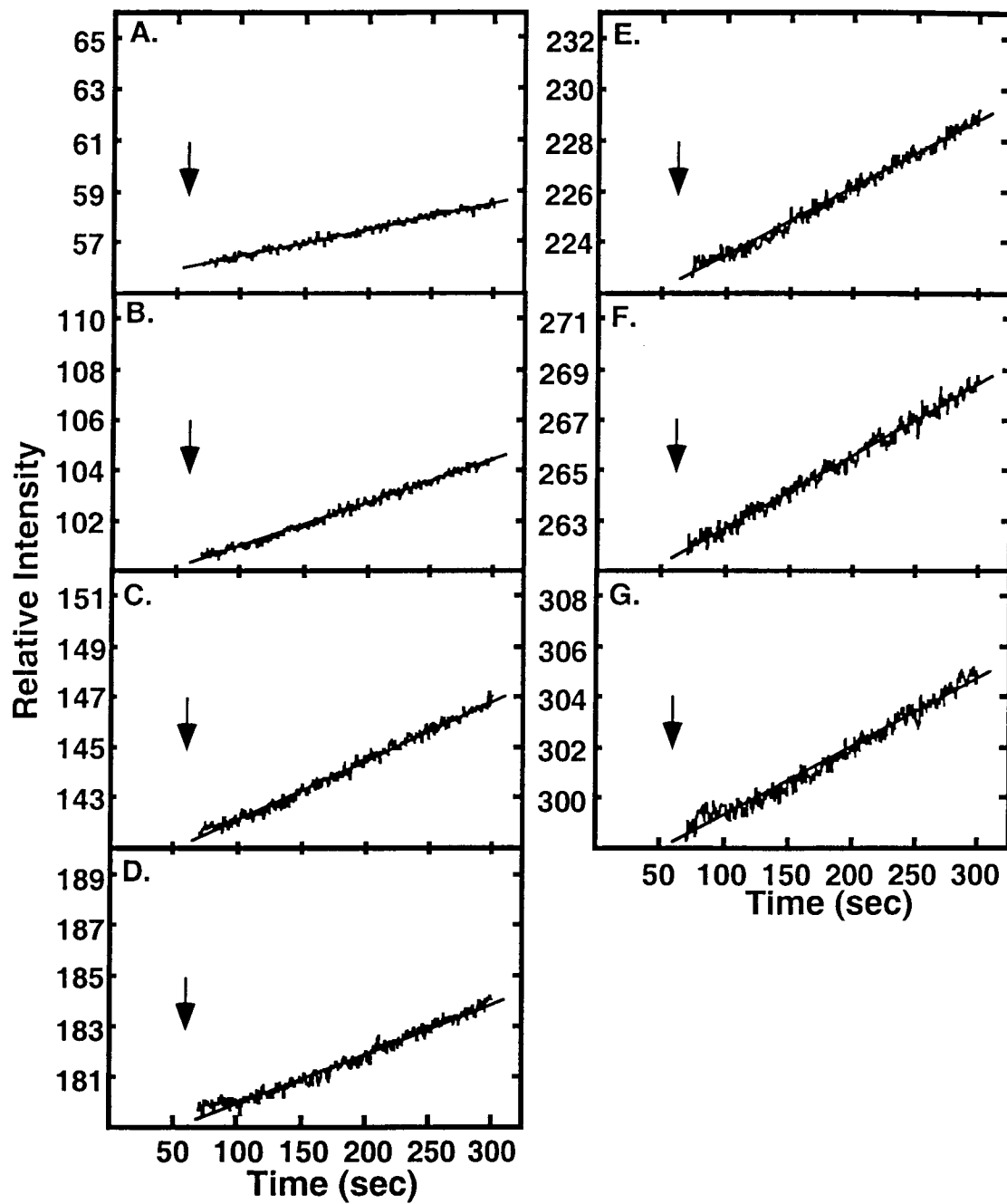
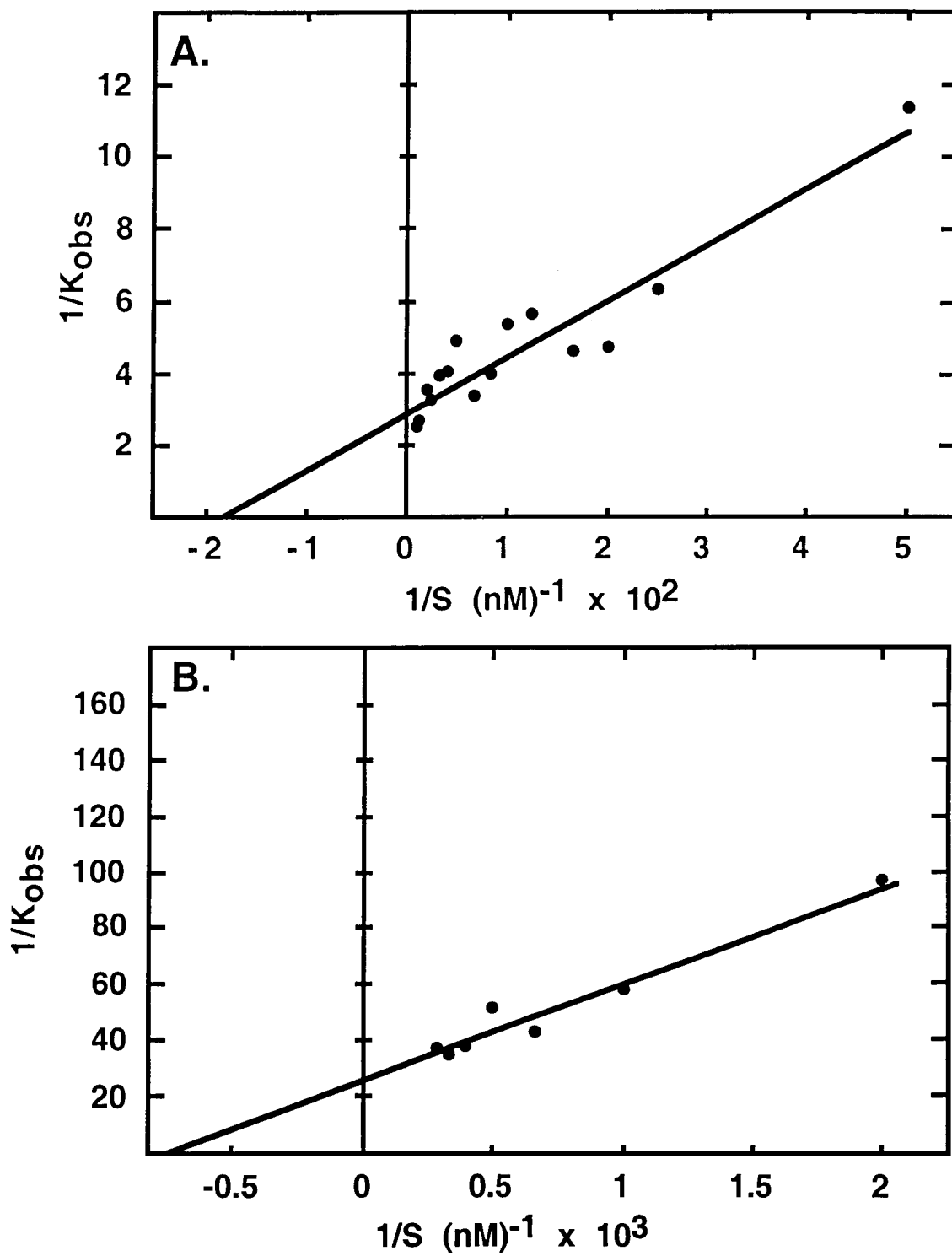


Figure 23. Double reciprocal plots of Ung and Ung H187D hydrolysis of a 2-aminopurine-containing double-stranded oligonucleotide. Steady-state fluorescence measurements were performed using double-stranded oligonucleotide containing a 2-aminopurine:uracil basepair incubated with (A) Ung or (B) Ung H187D as described in "Figures 21 and 22". Reaction velocity was calculated from the data in "Figures 21 and 22" and double reciprocal plots were produced.

Figure 23



3.2 Ugi-Affinity Purification of Mitochondrial Uracil-DNA Glycosylases

3.2.1 Production of Polyclonal Antisera to Uracil-DNA Glycosylase and Uracil-DNA Glycosylase Inhibitor

Polyclonal antibody was raised to *E. coli* uracil-DNA glycosylase and PBS2 uracil-DNA glycosylase inhibitor by injecting rabbits with 0.30 mg of purified Ung (Fraction V) or 0.38 mg of purified Ugi (Fraction IV), respectively. Boost injections were performed every 5-6 weeks and blood samples were taken 10 days subsequently to assay for the presence of inhibiting antibody. Tables 5 and 6 summarize the results of these assays. After 2-3 injections, sera immunized to Ung typically inhibited 60-70% of the Ung activity in a standard uracil-DNA glycosylase assay. When the antigen was Ugi, one animal produced a relatively weak immune response, resulting in serum that was capable of inhibiting only 16% of the Ugi activity relative to the control after 6 injections (Table 6, Rabbit #77). In contrast, a second animal produced a very strong response (Table 6, Rabbit #76), inhibiting greater than 98% of the Ugi activity after only 2 injections. Subsequent boosts resulted in a decrease in Ugi inhibition to 56-59%. A 1:100 dilution of serum from Rabbit #78 also inhibited 52% of human Δ 84UDG uracil-DNA glycosylase activity (data not shown).

3.2.2 Preparation of Ugi- and Ung-Sepharose

Ugi was coupled to Sepharose 4B to make affinity resin for purification of polyclonal antibody raised to Ugi and uracil-DNA glycosylases from varied biological sources. Additionally, Ung was coupled to Sepharose 4B to produce affinity resin to be used in the affinity purification of anti-Ung polyclonal antibody. CNBr-activated Sepharose 4B was incubated with purified Ung or Ugi (30 mg protein/g of Sepharose) for 2 h at room temperature. Unreacted active sites on the resin were then blocked by incubating with 0.1 M Tris-HCl (pH 8.0) and uncoupled ligand was removed by extensive washing with alternating cycles of low and high pH buffer. The amounts of Ugi and Ung

Table 5

*Inhibition of Uracil-DNA Glycosylase by Polyclonal Antisera to E. coli
Uracil-DNA Glycosylase*

Rabbit #78				Rabbit #79			
Boost	Uracil Released (pmol) ^a		% Control ^d	Boost	Uracil Released (pmol) ^a		% Control ^d
	Ung ^b	Ung + Serum ^c			Ung ^b	Ung + Serum ^c	
0 ^e	31	35	>100	0 ^e	23	33	>100
1	63	58	92	1	73	32	46
2	93	29	31	2	90	36	40
3	66	21	32	3	64	17	27
4 ^f	70	28	40	4	72	25	35
				5	60	22	37
				6 ^f	57	21	37

^a *E. coli* Ung activity was determined by quantitating the release of [³H]uracil (180 cpm/pmol) from uracil-containing calf thymus DNA in modified Ung assays as described under "Experimental Procedures, Section 2.2.25".

^b The activity of *E. coli* Ung (~0.12 units) was determined in the absence of serum with the addition of UDB buffer.

^c The activity of *E. coli* Ung (~0.12 units) was determined in the presence of polyclonal antiserum (10⁻³ dilution) in UDB buffer.

^d Percent control was calculated by dividing pmol of uracil released with samples containing Ung + Serum by pmol uracil released with samples containing Ung. Stimulation of Ung activity was seen in the presence of serum.

^e Pre-immune sera were sampled and assayed prior to immunizations with *E. coli* Ung.

^f Terminal bleeds were performed subsequent to the final injection.

Table 6

*Inhibition of Uracil-DNA Glycosylase Inhibitor by Polyclonal Antisera to PBS2
Uracil-DNA Glycosylase Inhibitor*

Rabbit #76				Rabbit #77			
Boost	Uracil Released (pmol) ^a		% Control ^d	Boost	Uracil Released (pmol) ^a		% Control ^d
	Ugi ^b	Ugi + Serum ^c			Ugi ^b	Ugi + Serum ^c	
0 ^e	77	82	>100	0 ^e	77	73	95
1	74	9	12	1	72	59	82
2	62	<1.2 ^f	<2	2	57	37	65
3	56	23	41	3	47	45	96
4 ^g	71	31	44	4	73	71	97
				5	55	53	96
				6 ^g	56	47	84

^a Ugi activity was determined by quantitating the inhibition of [³H]uracil (180 cpm/pmol) release from uracil-containing calf thymus DNA by *E. coli* Ung (~0.12 units) in assays modified as described under "Experimental Procedures, Section 2.2.25".

^b The activity of Ugi (~0.1 units) was determined in the absence of serum with the addition of UDB buffer.

^c The activity of Ugi (~0.1 units) was determined in the presence of polyclonal antiserum (10⁻³ dilution) in UDB buffer.

^d Percent control was calculated by dividing pmol of uracil released by Ung in samples containing Ugi + Serum by pmol uracil released by Ung in samples containing Ugi. Stimulation of Ung activity was seen in the presence of serum.

^e Pre-immune sera were sampled and assayed prior to immunizations with *E. coli* Ung.

^f This value represents the assay's lower limit of detection.

^g Terminal bleeds were performed subsequent to the final injection.

coupled to Sepharose 4B resin were estimated to be 220 nmol/ml and 97 nmol/ml of packed resin, respectively, based on the amount of uncoupled ligand recovered during the coupling process. The binding capacity of Ugi-Sepharose was determined by incubating 100 μ l of resin (25% (v/v) slurry) with varying amounts of [3 H]Ung (13.5 cpm/pmol). The resin was washed and bound protein removed with gel loading dye containing 1% SDS and boiling for 10 min. Flow through, wash, and elution fractions were analyzed by 12.5% SDS-polyacrylamide gel electrophoresis as described (Figure 24). The amount of [3 H]Ung in the flow through (Figure 24A-E, lane 1) increased with increasing Ung concentrations. In contrast, the size of the protein band in the elution fractions increased with increasing Ung addition up to 3900 pmol, where it appeared to plateau (Figure 24D, lanes 4-6). Quantitation of 3 H-radioactivity recovered by SDS elution via liquid scintillation counting revealed that protein binding increased with increasing Ung addition until the capacity of the resin was reached at \sim 90 nmol of Ung per ml of Ugi-Sepharose resin (Figure 24F). Binding capacity was similarly estimated for Ung-Sepharose by incubating coupled resin with [35 S]Ugi. The binding capacity of Ung-Sepharose was determined to be \sim 40 nmol of Ugi per ml of Ung-Sepharose resin (Figure 25). In both cases, a small fraction (<1%) of radioactive protein remained bound to the resin after SDS elution. The amount of [3 H]Ung which could not be eluted from the Ugi-Sepharose resin was 19 pmol, while the amount of unrecovered [35 S]Ugi was 36 pmol (data not shown).

3.2.3 Affinity Chromatography of Uracil-DNA Glycosylase

In order to determine whether Ung could be detected at physiological concentrations in whole cell extracts by Ugi-Sepharose, *E. coli* JM105 crude cell extract was incubated with Ugi-Sepharose beads. In addition, cell extract mixed with 5 or 50 μ g of purified *E. coli* Ung (Fraction V) was incubated with Ugi-Sepharose resin in case the endogenous levels of Ung were below the limits of detection for the purification system. The resin was washed and

Figure 24. Binding capacity of Ugi-Sepharose. The binding capacity of Ugi-Sepharose was determined by incubating 975 (A), 1950 (B), 2930 (C), 3900 (D), or 4870 (E) pmol of [^3H]Ung (13.5 cpm/pmol) with 100 μl of a 25% (v/v) resin slurry in DAB buffer for 10 min at 25°C as described under “Experimental Procedures”. The resin was washed three times with 200 μl of DAB buffer and the bound Ung was eluted by the addition of 100 μl of SDS sample buffer (50 mM Tris-HCl (pH 6.8), 1% SDS, 143 mM β -mercaptoethanol, 10% (w/v) glycerol, and 0.04% bromophenol blue) and incubating at 100°C for 10 min. Aliquots (25 μl) of flow through (lane 1) and wash (lanes 2 and 3) were analyzed by 12.5% SDS polyacrylamide gel electrophoresis along with 50 μl of elution fractions (lanes 4-6). The molecular weight standards for bovine serum albumin, ovalbumin, glyceraldehyde-3-phosphate dehydrogenase, carbonic anhydrase, trypsinogen, trypsin inhibitor and α -lactalbumin are indicated by *arrows* from *top* to *bottom*. (F) Flow through (100 μl), wash (100 μl), and SDS sample buffer eluted fractions (25 μl) and the resin were quantitated for ^3H -radioactivity by liquid scintillation counting using Formula 989 fluor. The total amount of bound [^3H]Ung was calculated by summing the amount of radioactivity detected in SDS sample buffer eluted fractions and resin.

Figure 24

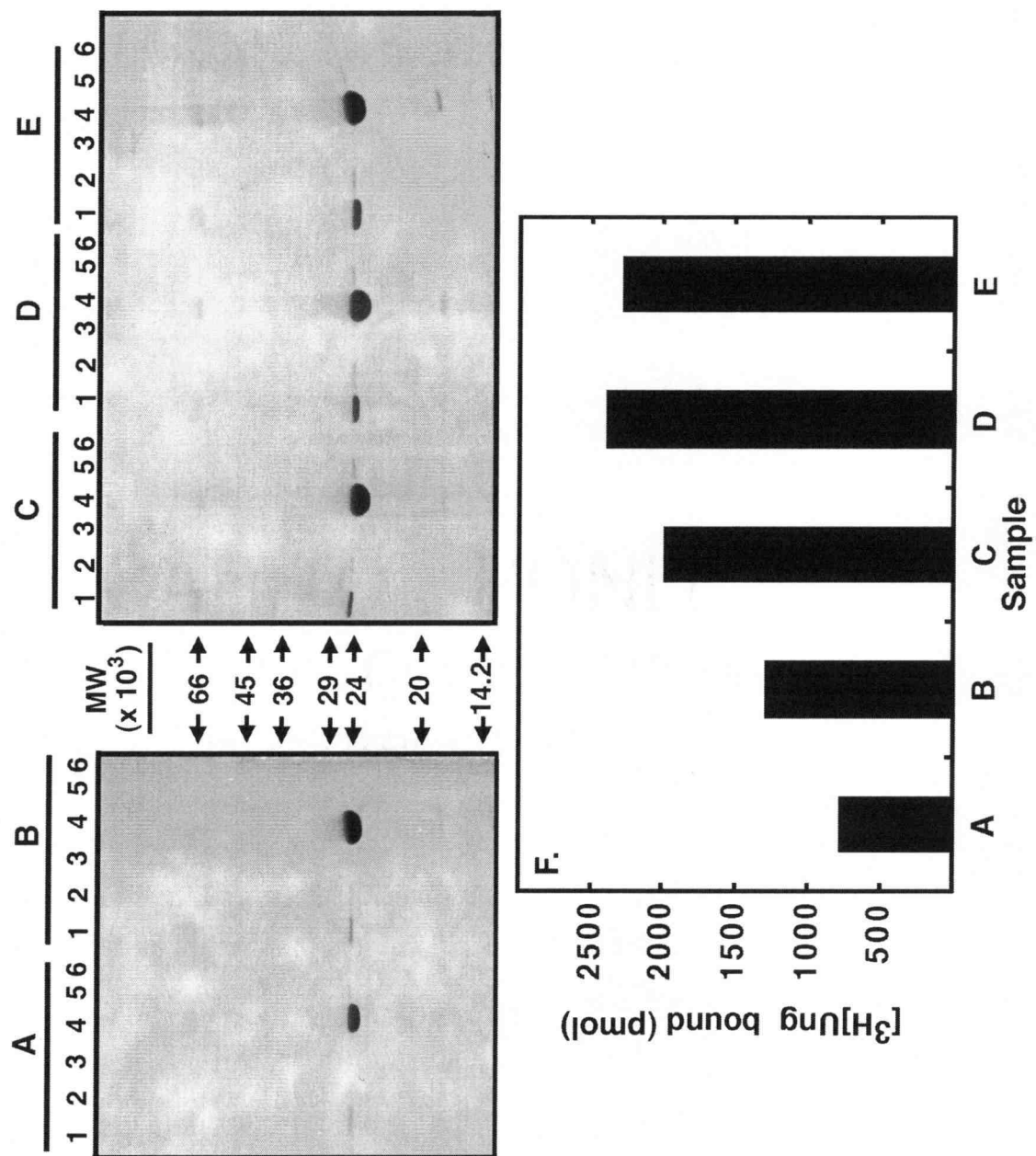
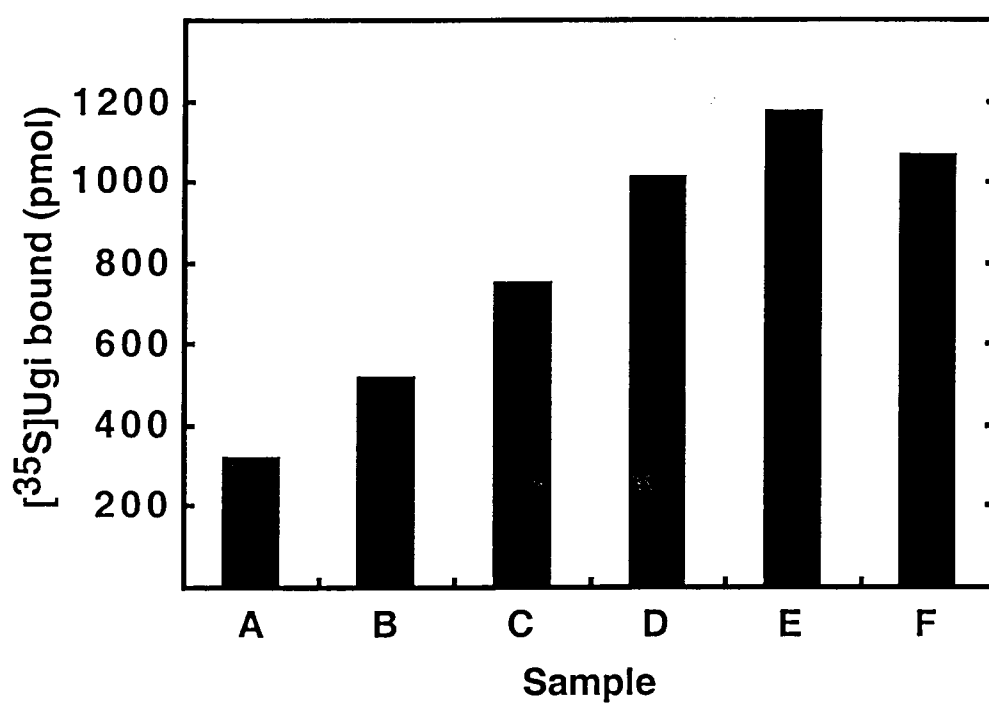


Figure 25. Binding capacity of Ung-Sepharose. The binding capacity of Ung-Sepharose was determined as described in Figure 23 by incubating 390 (A), 780 (B), 1170 (C), 1560 (D), 1950 (E), or 3900 (F) pmol of [35 S]Ugi (28 cpm/pmol) with 100 μ l of a 25% (v/v) resin slurry in DAB buffer for 10 min at 25°C as described under "Experimental Procedures". The resin was washed three times with 200 μ l of DAB buffer and the [35 S]Ugi was eluted by the addition of SDS sample buffer (50 μ l) and incubating at 100°C for 10 min. Aliquots of flow through (100 μ l), wash (100 μ l), and SDS sample buffer eluted fractions (25 μ l) and the resin were quantitated for [35 S] radioactivity by liquid scintillation counting using Formula 989 fluor. The total amount of bound [35 S]Ugi was determined by summing the amount of radioactivity detected in SDS sample buffer eluted fractions and resin.

Figure 25



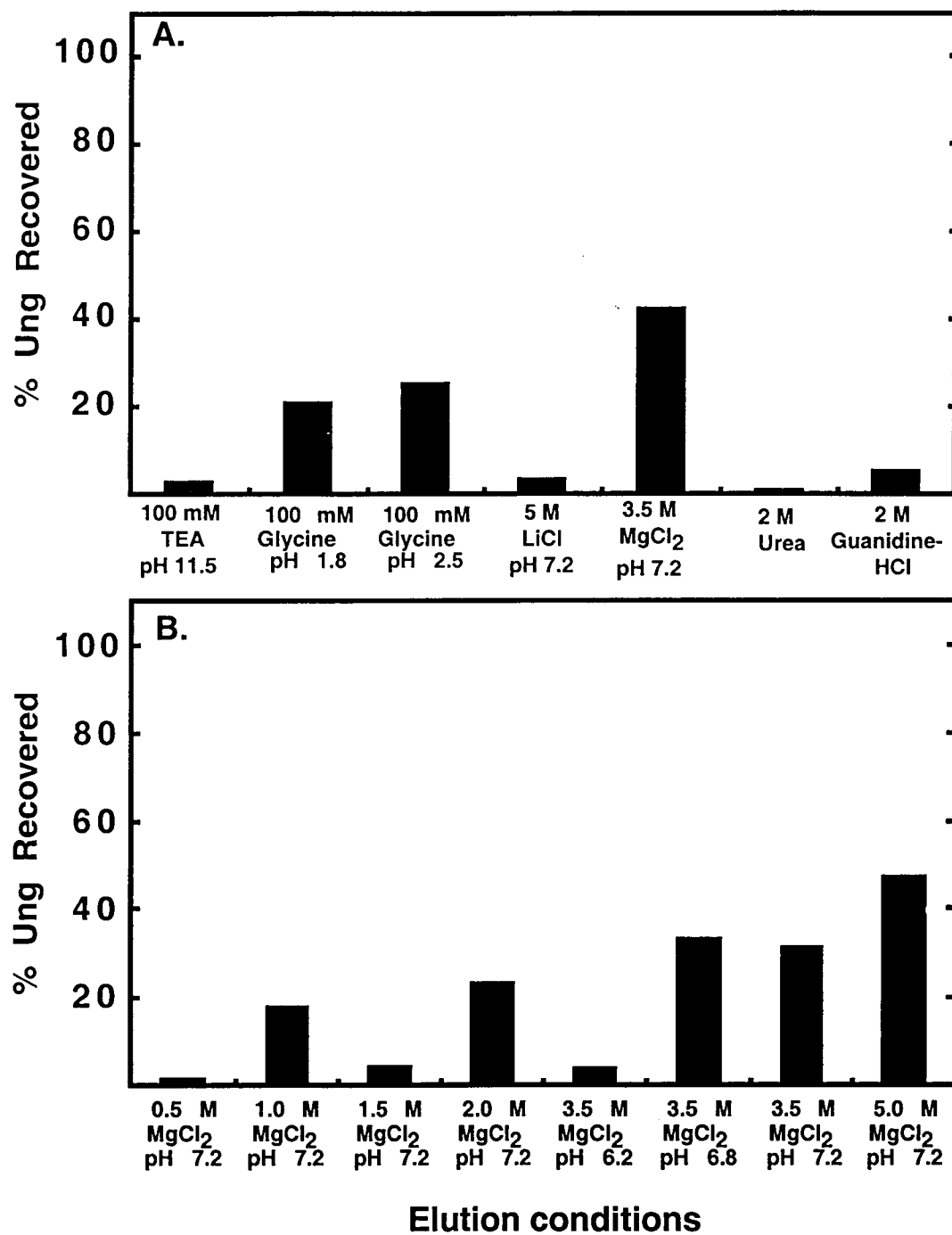
bound proteins were eluted with gel loading dye containing SDS. Aliquots of flow through, wash, and elution fractions were analyzed by SDS-polyacrylamide gel electrophoresis. Although no detectable Ung was recovered when Ugi-Sepharose was incubated with cell extract alone (Figure 26, lane 14), protein bands corresponding to Ung were visualized when the extract was supplemented with purified *E. coli* Ung (Figure 26, lanes 15 and 16).

In order to optimize elution conditions, Ugi-Sepharose resin was incubated with 1950 pmol of [³H]Ung and washed. Buffers of varying pH and ionic strengths were tested as elutants. In some cases, the elutant was collected into 10 µl of neutralizing buffer as described in Table 3. The efficiency of elution was determined by quantitating the amount of recovered [³H]Ung by liquid scintillation counting. Buffers composed of 100 mM TEA (pH 11.5), 10 mM potassium phosphate buffer (pH 7.2) and 5 M LiCl (pH 7.2), and 2 M guanidine-HCl eluted ≤5% of the bound [³H]Ung (Figure 27A). The 100 mM glycine buffers (pH 1.8 and 2.5) removed ~20-25% of the bound [³H]Ung. In contrast, buffer containing 10 mM potassium phosphate buffer (pH 7.2) and 3.5 M MgCl₂ eluted ~43% of the bound Ung. The concentration of MgCl₂ and pH of the potassium phosphate buffer were then varied as described in Figure 27B in an attempt to increase total recovery of bound Ung. The amount of [³H]Ung eluted increased with increasing MgCl₂; 5 M MgCl₂ recovered nearly twice as much Ung versus 2 M MgCl₂ and 34 times more Ung than 0.5 M MgCl₂ (Figure 27B). While the recovery of bound Ung was enhanced ~8-fold by increasing the buffer pH from 6.2 to 6.8, there was no significant change in recovery when the pH was increased to 7.2 (Figure 27B). Consequently, 10 mM potassium phosphate buffer (pH 7.2) and 5 M MgCl₂ was adopted as the standard elution conditions for recovery of Ung utilizing Ugi-Sepharose chromatography.

Figure 26. Recovery of Ung from *E. coli* cell extracts by Ugi-Sepharose chromatography. Cell-free extract (95 μ g) was prepared, mixed with 0-50 μ g of purified *E. coli* Ung, then incubated with 100 μ l of Ugi-Sepharose or Sepharose 4B resin (25% (v/v) slurries) for 10 min at 25°C. The extract was removed by centrifugation as described under "Experimental Procedures". The resin was washed three times with 200 μ l of DAB buffer and bound proteins were removed with 100 μ l of SDS sample buffer and heating at 100°C for 10 min. Aliquots (50 μ l) of each flow through, wash and elution fraction were prepared for 12.5% SDS polyacrylamide gel electrophoresis. Lanes 1-3 contain flow through fractions of Ugi-Sepharose incubated with cell-free extract containing 0, 5, or 50 μ g of Ung, respectively. Lane 4 contains flow through of cell-free extract incubated with Sepharose 4B control resin. Wash fractions of Ugi-Sepharose plus cell-free extract supplemented with 0, 5, or 50 μ g Ung are shown in lanes 5-7, respectively. The second and third washes of Ugi-Sepharose plus cell-free extract supplemented with Ung are likewise shown in lanes 8-10 and 11-13. Lanes 14-16 contain fractions eluted with SDS sample buffer from Ugi-Sepharose incubated with cell-free extract containing 0, 5, or 50 μ g of Ung, respectively, and lane 17 contains cell-free extract incubated with Sepharose 4B control resin and eluted with SDS sample buffer. The locations of Ung and tracking dye (TD) are indicated by *arrows*. The molecular weight standards for bovine serum albumin, ovalbumin, glyceraldehyde-3-phosphate dehydrogenase, carbonic anhydrase, trypsinogen, and trypsin inhibitor are indicated by *arrows* from *top* to *bottom*.

Figure 27. Elution of *E. coli* Ung from Ugi-Sepharose. [^3H]Ung (1950 pmol, 13.5 cpm/pmol) was incubated with 100 μl of Ugi-Sepharose slurry (25% v/v) at 25°C for 10 min. The resin was washed as described under "Experimental Procedures" then bound [^3H]Ung was eluted with various buffer conditions (A) or varying concentrations of MgCl_2 and pH (B) as indicated. The total amount of [^3H]Ung recovered in each elution fraction was quantitated by liquid scintillation counting as described under "Experimental Procedures".

Figure 27



3.2.4 Affinity Purification of Polyclonal Antibody to Uracil-DNA Glycosylase

Antiserum was incubated with Ung-Sepharose to determine optimum elution conditions for the affinity purification of polyclonal antibody to Ung. The resin was washed and eluted with various buffer conditions as previously described for the affinity purification of Ung ("Section 2.2.15", Table 3). Eluted antibody was detected by 12.5% SDS-polyacrylamide gel electrophoresis and silver staining (Figure 28). The amount of purified IgG recovered was estimated by comparing the relative intensity of the bands corresponding to heavy chain (~55 kDa) and light chain (~25 kDa) polypeptides with other serum proteins detected in the elution fractions. Although 100 mM glycine (pH 2.0) and 100 mM TEA (pH 11.5) appeared to recover the greatest quantity of bound antibody (Figure 28, samples 1 and 3, respectively), buffer containing a 3.5 M MgCl_2 concentration also eluted a reasonable amount of antibody from the resin (Figure 28, sample 4). Thus, 3.5 M MgCl_2 in 10 mM potassium phosphate buffer (pH 7.2) was selected for the elution buffer because it dissociated a large quantity of bound antibody yet did not require additional steps to neutralize extremes of pH.

Large-scale purification of anti-Ung antibody was performed by incubating 12.5 ml of serum with 25 ml of Ung-Sepharose slurry (25% (v/v)). After washing the resin with potassium phosphate buffer (pH 7.2), Ung antibody was eluted with 3.5 M MgCl_2 in 10 mM potassium phosphate (pH 7.2). The purification profile is shown in Figure 29. The flow through fractions contained large amounts of serum protein which were not immunoreactive to Ung in ELISA. The minor protein peak at fraction 70 produced a strong reaction against Ung in ELISA and was enriched for the 55 kDa and 25 kDa protein species corresponding to the heavy and light IgG polypeptides. In addition, ELISA for total IgG produced a strong response across fractions 68-80.

Figure 28. Determining elution conditions for affinity purification of polyclonal antibody to Ung using Ung-Sepharose. Optimum conditions for the elution of anti-Ung antibody from Ung-Sepharose resin were identified by incubating polyclonal antiserum (50 μ l) immunized to *E. coli* Ung with 100 μ l of Ung-Sepharose for 10 min at 25°C. The resin was washed and eluted with (1) 100 mM glycine (pH 2.0), (2) 100 mM glycine (pH 1.8), (3) 100 mM TEA (pH 11.5), (4) 3.5 M $MgCl_2$ and 10 mM potassium phosphate (pH 7.2), or (5) 5 M LiCl and 10 mM potassium phosphate (pH 7.2) as described under "Experimental Procedures". Aliquots (1.25 μ l) of the two elution fractions (A and B) from each sample were analyzed by 12.5% SDS-polyacrylamide gel electrophoresis followed by silver staining. The location of IgG heavy and light chains are denoted by *H* and *L*, respectively. The molecular weight standards for bovine serum albumin, ovalbumin, glyceraldehyde-3-phosphate dehydrogenase, carbonic anhydrase, trypsinogen, and trypsin inhibitor are indicated by arrows from *top* to *bottom*.

Figure 28

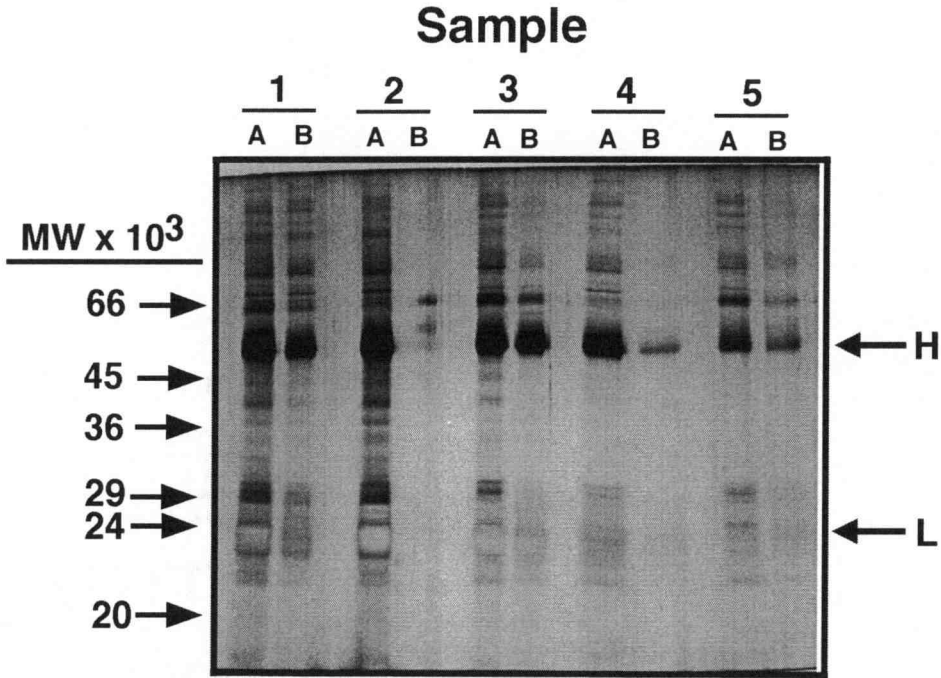
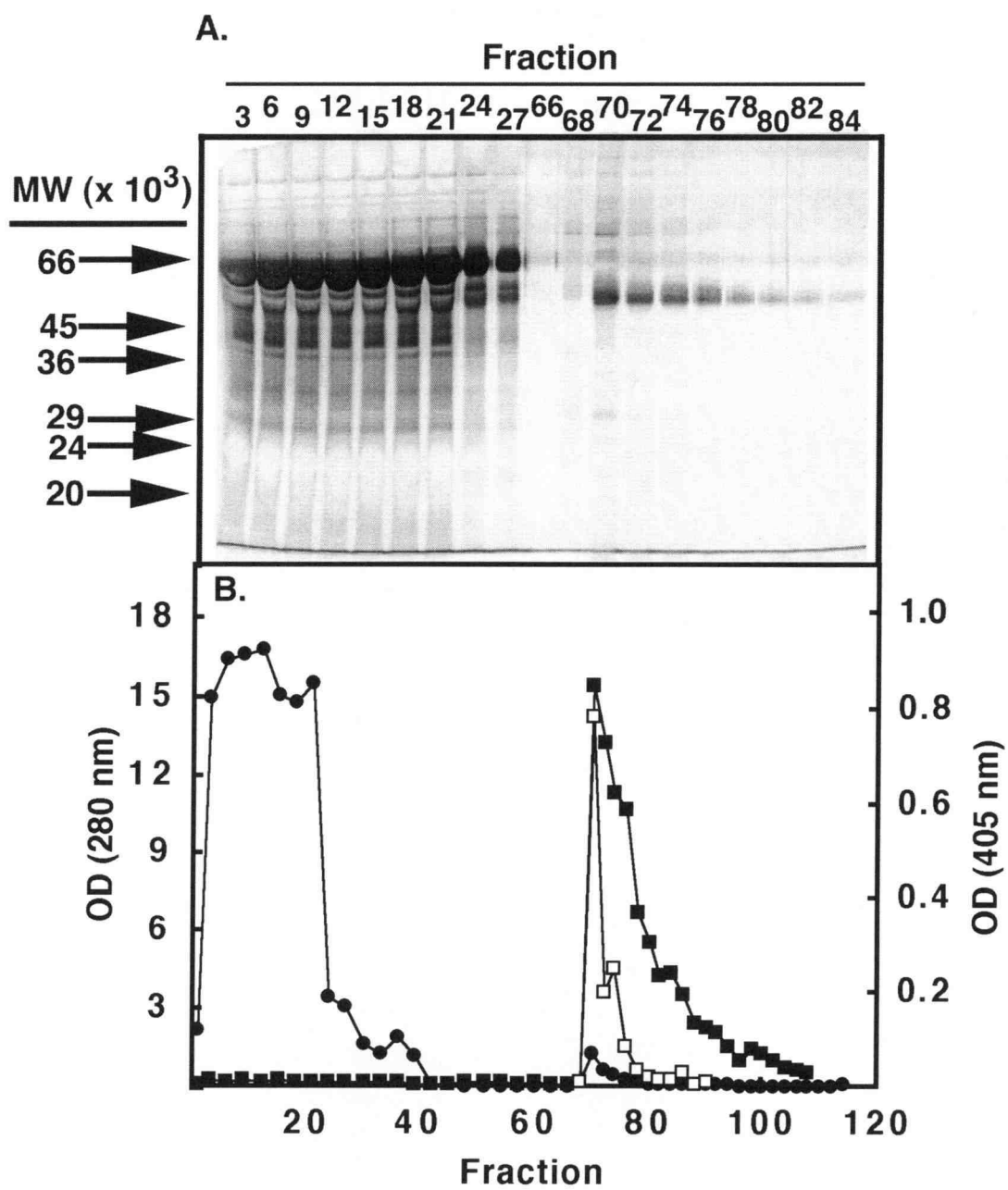


Figure 29. Affinity purification of anti-Ung polyclonal antibody.

Purification of anti-Ung polyclonal antibody was performed by mixing 25 ml Ung-Sepharose with 12.5 ml of immunized rabbit serum for 30 min at 25°C. The slurry was transferred to a 1.5 cm diameter BioRad column, the resin was washed with 10 mM potassium phosphate buffer (pH 7.2), and eluted with 3.5 M MgCl_2 in 10 mM potassium phosphate buffer (pH 7.2). (A) Fractions (1 ml) were collected and selected fractions were analyzed by 12.5% SDS polyacrylamide gel electrophoresis and silver staining as described under "Experimental Procedures". The molecular weight standards for bovine serum albumin, ovalbumin, glyceraldehyde-3-phosphate dehydrogenase, carbonic anhydrase, trypsinogen, and trypsin inhibitor are indicated by *arrows* from *top* to *bottom*. (B) Fractions were assayed for total protein (●) by absorbance spectroscopy at 280 nm and for total (□) and anti-Ung (■) IgG by detecting the product of the horseradish peroxidase reaction with ABTS in an ELISA at 405 nm as described under "Experimental Procedures".

Figure 29



3.2.5 Purification of Ung from Mitochondrial Extracts

In order to determine whether polyclonal antiserum to *E. coli* Ung was capable of cross-reacting with mitochondrial uracil-DNA glycosylase, Western blot analysis was performed on samples containing mitochondrial crude extract or purified *E. coli* Ung. Additionally, mixtures of mitochondrial extract and *E. coli* Ung were analyzed to determine whether mitochondrial proteins interfered with the detection of Ung in the event that immunoreactive bands were not visualized in mitochondrial samples. No immunoreactive bands were detected in the mitochondrial crude extract (Figure 30A), although the specific uracil-DNA glycosylase activity of the extract was determined to be ~6.4 units/mg protein. *E. coli* Ung was detected by Western blot analysis to ≥6.25 ng, in purified form and when mixed with mitochondrial extract (Figure 30B and C, respectively). A protein species that migrated faster than *E. coli* Ung was also observed (Figure 30B and C, lanes 6 and 7). The smaller apparent molecular weight, cross-reactivity with Ung specific antibody, and the increasing intensity of the band with increasing concentrations of Ung, suggests a degradation product in the purified Ung preparation.

The process of base excision repair in mitochondria has not been extensively studied. Although reconstitution of mitochondrial BER has been attempted, these studies utilized AP site containing DNA (105) or a truncated form of human UDG (72) rather than purified mitochondrial uracil-DNA glycosylase to catalyze the first step of the repair reaction. In order to fully understand this pathway in mitochondria, a source of mitochondrial uracil-DNA glycosylase free of contaminating nuclear activity would be desirable. Thus, a protocol was devised for purifying Ung activity from mitochondrial extracts (Figure 31). Rat or pig liver mitochondria were disrupted by grinding with alumina powder and the crude extract was recovered by centrifugation as described previously. The proteins that precipitated between 35% and 65% (saturation) ammonium sulfate were recovered, resuspended, and subjected to Ugi-Sepharose affinity chromatography. Fractions from each step of the purification were analyzed by SDS-polyacrylamide gel electrophoresis and

Figure 30. Detection of Ung in mitochondrial extracts using Western blot analysis. Samples containing (A) 10, 20, 30, 40, 60, 80 or 100 μ g of rat liver mitochondrial extract (lanes 1-7), (B) 0.05, 0.25, 1.25, 6.25, 31, 156 or 781 ng of *E. coli* Ung (lanes 1-7), or (C) a mixture of \sim 30 μ g of mitochondrial extract with 0.05, 0.25, 1.25, 6.25, 31, 156 or 781 ng of *E. coli* Ung (lanes 1-7) were prepared for 12.5% SDS polyacrylamide gel electrophoresis. Western blot analysis was performed as described under "Experimental Procedures". The proteins were transferred to nitrocellulose and probed with anti-Ung antiserum (1:5000 dilution). After the addition of alkaline phosphatase-conjugated secondary antibody (1:2000 dilution) the Western blot was developed with 100 mM NaHCO_3 (pH 9.8), 10 mM MgCl_2 , 3 mg nitro blue tetrazolium in 70% dimethyl formamide, and 15 mg bromochloroindolyl phosphate in 100% dimethyl formamide. The prestained molecular weight standards for phosphorylase B, bovine serum albumin, carbonic anhydrase, soybean trypsin inhibitor, and lysozyme are indicated by *arrows from top to bottom*.

Figure 30

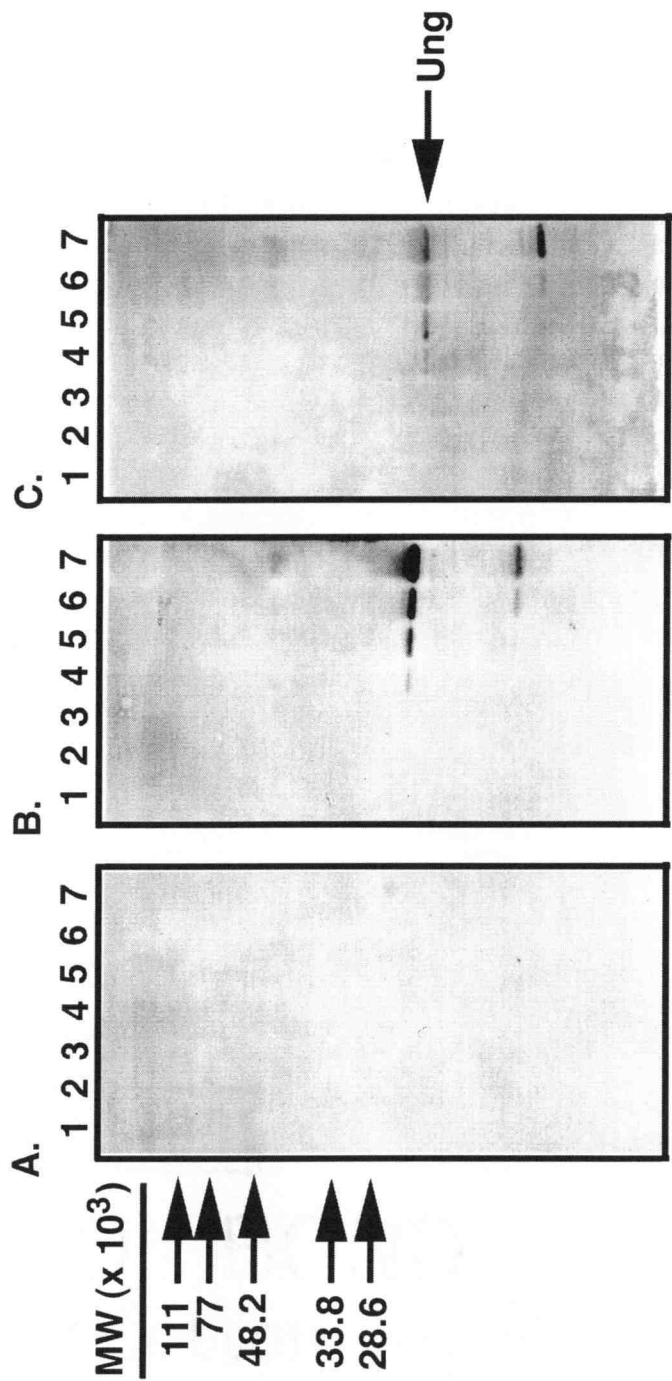
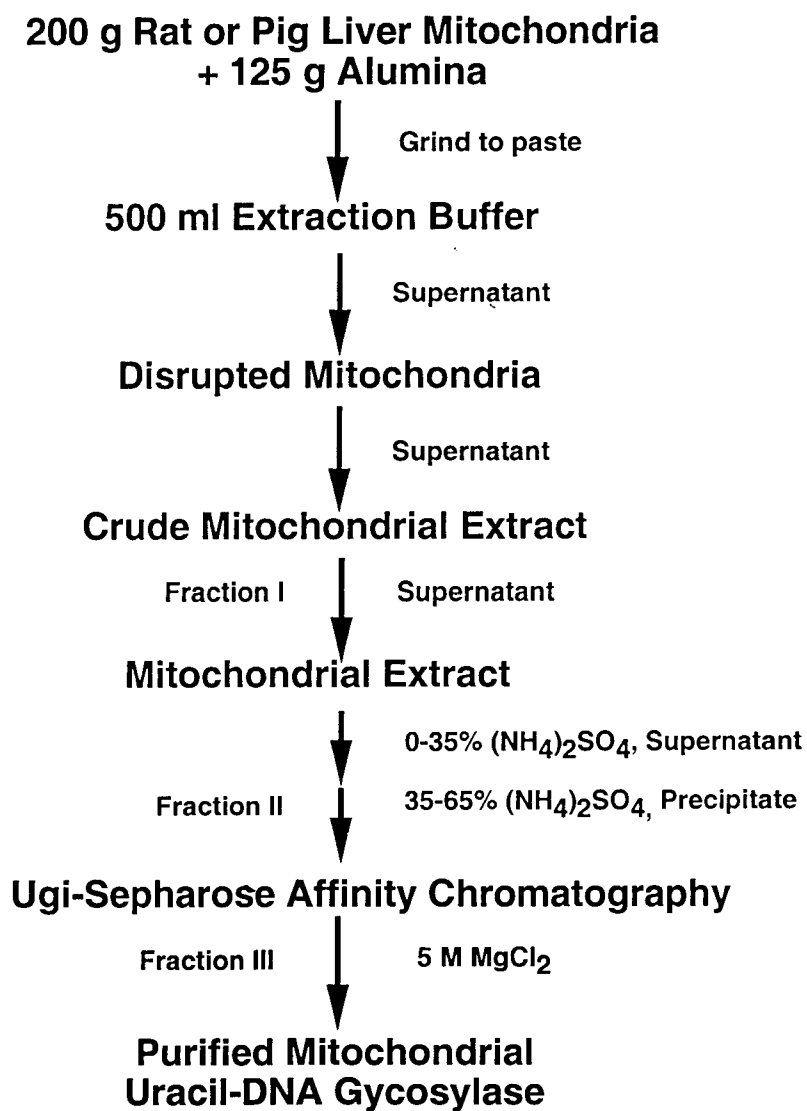


Figure 31. Scheme for purification of rat or pig liver mitochondrial Ung.

Uracil-DNA glycosylase was purified from rat or pig liver mitochondria by grinding mitochondria frozen in liquid N₂ with alumina powder and extraction buffer (50 mM Tris-HCl (pH 8.0), 5 mM β-mercaptoethanol, 1 mM EDTA, 1 M NaCl, 1 mM PMSF). The sample was centrifuged at 5,000 x g for 10 min to remove the alumina, followed by centrifugation at 10,000 x g for 10 min to remove unbroken mitochondria. The mitochondrial membranes were removed by ultracentrifugation at 100,000 x g for 1 h and the supernatant (Fraction I) was recovered. Ammonium sulfate precipitations were performed as described under "Experimental Procedures". The ammonium sulfate-insoluble fraction was resuspended in TDEG buffer and designated Fraction II after dialysis into the same buffer. Fraction II was applied to a Ugi-Sepharose column (100 μl) and serial washes (100 μl) of 10 mM potassium phosphate (pH 7.2), 0.5 M NaCl, and 10 mM potassium phosphate (pH 7.2) were performed as described under "Experimental Procedures". The column was eluted step-wise with three 50 μl washes of 10 mM potassium phosphate (pH 7.2) containing 5 M MgCl₂.

Figure 31



silver staining. From the rat source, the final purification step yielded a sample greatly enriched for a single protein slightly smaller than *E. coli* Ung (Figure 32A). When the proteins contained within the polyacrylamide gel were transferred to nitrocellulose and Western blot analysis was performed, elution fractions produced anti-Ung antibody immunoreactive bands which stained with an intensity similar to that of a sample containing 6 ng (0.2 pmol) of purified *E. coli* Ung (Figure 32B). Purification of porcine mitochondrial Ung resulted in two major protein bands, one similar in size to *E. coli* Ung, which had an apparent molecular weight of ~29,000, and a second of ~48,000 (Figure 33A). The 28,000 molecular weight species was immunoreactive to affinity-purified anti-Ung antibody while the 48,000 molecular weight species was relatively unreactive (Figure 33B).

Figure 32. Purification of uracil-DNA glycosylase from rat liver mitochondrial extracts. Aliquots of fraction I (1 μ l), II (1 μ l), and wash and elution fractions (2 μ l each) from Ugi-Sepharose chromatography were prepared for 12.5% SDS polyacrylamide gel electrophoresis as described under "Experimental Procedures". After electrophoresis, protein bands were visualized by silver staining (A) or Western blotting (B) using anti-Ung antibody as described under "Experimental Procedures". Lane 1, Fraction I; lane 2, Fraction II; lane 3, 10 mM potassium phosphate buffer (pH 7.2) wash; lanes 4-6, 0.5 M NaCl washes; lane 7, 10 mM phosphate buffer (pH 7.2) wash; lanes 8-10, 10 mM potassium phosphate (pH 7.2) and 5 M $MgCl_2$ elution fractions. A titration series of 0.01, 0.05, 0.23, 1.2, 5.8, and 29 pmol of *E. coli* Ung is shown in lanes 11-17, respectively. The location of *E. coli* Ung is indicated by *arrows*.

Figure 32

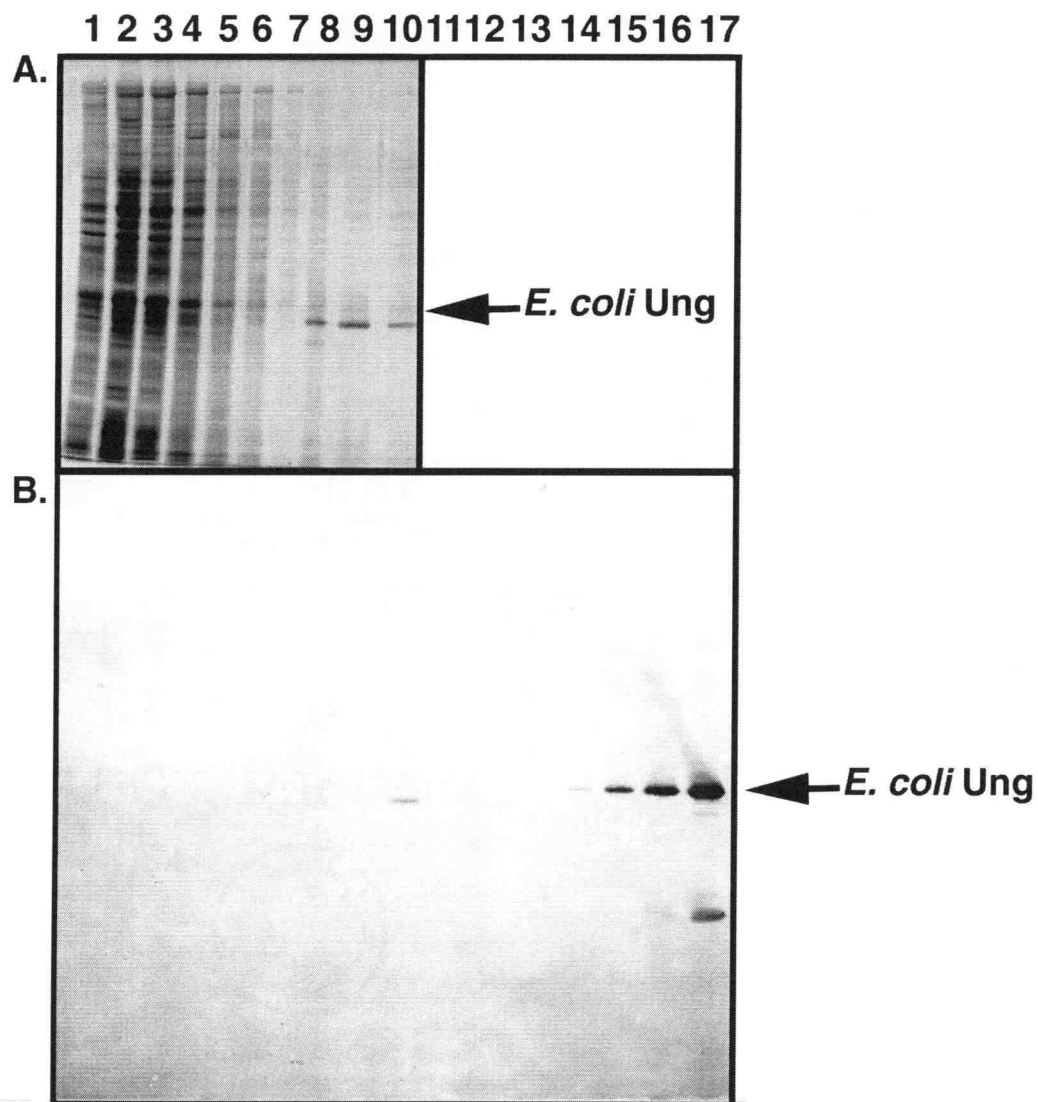
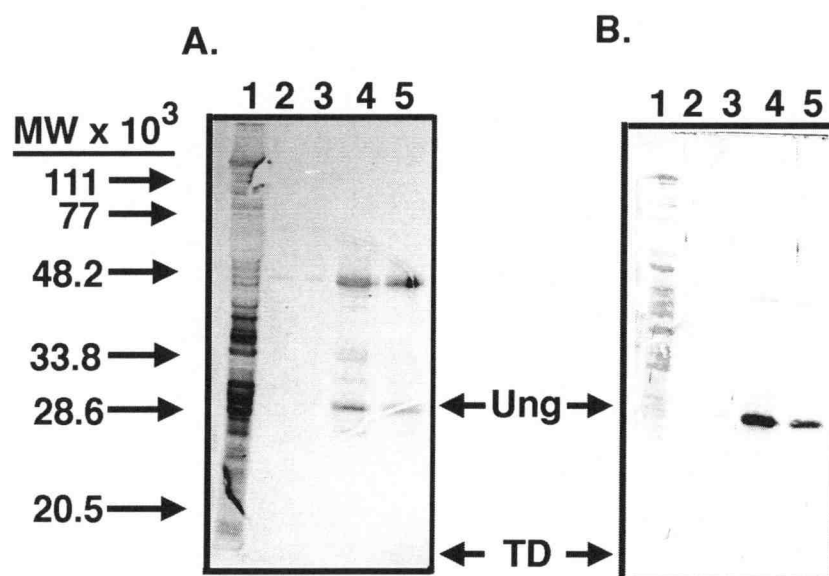


Figure 33. Purification of uracil-DNA glycosylase from pig liver mitochondrial extracts. Aliquots of Fraction II (1 μ l), and wash and elution fractions (2 μ l each) from Ugi-Sepharose chromatography were prepared for 12.5% SDS polyacrylamide gel electrophoresis as described under "Experimental Procedures". After electrophoresis, protein bands were visualized by silver staining (A) or Western blot analysis (B) using anti-Ung antibody as described under "Experimental Procedures". Lane 1, Fraction II; lane 2, 10 mM potassium phosphate buffer (pH 7.2) wash; lanes 3-5, 10 mM potassium phosphate (pH 7.2) and 5 M $MgCl_2$ elution fractions. The prestained molecular weight standards for phosphorylase B, bovine serum albumin, ovalbumin, carbonic anhydrase, soybean trypsin inhibitor, and lysozyme are indicated by *arrows* from *top* to *bottom*. The locations of *E. coli* Ung and tracking dye (TD) are indicated by *arrows*.

Figure 33



4. DISCUSSION

4.1 Overproduction and Characterization of Uracil-DNA Glycosylase H187D

Site-directed mutagenesis was performed to examine the role of an active site amino acid residue (His-187) in uracil-DNA recognition and excision by *E. coli* uracil-DNA glycosylase. After verifying the construction of the overexpression vectors containing the *ung* and *ungH187D* genes by *Bam*H I digestion of plasmid DNA recovered from *E. coli* JM105, transformation of pSB1051 and pUngH187D into an *E. coli ung* background was attempted. However, neither *E. coli* strains BW310 (*ung-1*) nor BD2314 (*ung-152::Tn10*) stably maintained the overexpression vectors. None of the pSB1051 or pUngH187D isolates from *E. coli* BD2314 or BW310 displayed the expected restriction fragments upon digestion with *Bam*H I restriction endonuclease. Some isolates appeared to have lost their *Bam*H I recognition sites as they were incapable of being cleaved by the restriction enzyme. The remaining isolates produced restriction fragments that could not be identified relative to the known plasmid maps of pSB1051 and pUngH187D. Thus, the restriction patterns observed suggested that deletions and/or rearrangements occurred on the plasmids.

The reason for the instability was not determined, although it was hypothesized that the *ung* and *ungH187D* gene products may be toxic to *E. coli ung* strains. The *E. coli ung* strains transformed with pSB1051 or pUngH187D formed smaller colonies and grew more slowly when compared to the same strains transformed with the control vector that lacked an insert. The Ung and Ung H187D proteins themselves did not appear to cause toxicity as both plasmids were stable in *E. coli* JM105. Thus, the instability appeared to arise from the *ung*⁻ genotype in concert with the *ung*- or *ungH187D*-containing vector. It is likely the BW310 and BD2314 genomes had higher concentrations of uracil residues in DNA than wild type *E. coli* due to the absence of Ung activity in these strains. Thus, some of the uracil may have been incorporated

in close proximity to uracil residues on the opposite DNA strand. This phenomenon might offer a possible explanation for the genetic instability. The presence of closely spaced uracil residues on opposing DNA strands has been demonstrated to increase the rate of double-strand breaks and deletion formation in *ung*⁺ *E. coli* (24). Expression of *ung* after transformation of *E. coli* BW310 and BD2314 with pSB1051 would make these strains *ung*⁺ and capable of excising uracil residues from their genomes. Transformants harboring pUngH187D would also be capable of uracil excision if the *ungH187D* gene product retained some catalytic activity despite the mutation. Thus plasmid rearrangements may have resulted from the introduction of uracil-DNA glycosylase activity in these strains as a mechanism to prevent potentially lethal double-strand breaks or deletion mutations resulting from the excision of numerous uracil residues. Recombination may have occurred between copies of the plasmid or between plasmid and homologous regions of the chromosomal *ung* sequences.

To address the potential problem of gene rearrangement and recombination, *E. coli* BW310 was made *recA* defective by P1vir transduction. The resulting transductant was designated *E. coli* MJS100. *E. coli* MJS100 appeared to be defective in *recA* by virtue of its sensitivity to UV radiation, which was phenotypically equivalent to the parent strain *E. coli* JC10289 from which the transducing phage was created. Although the *recA* mutation allowed pSB1051 to be stably maintained in *E. coli* MJS100 cells, pUngH187D remained unstable. It is not clear why the plasmid containing the mutant *ungH187D* gene would be less stable than wild type *ung*. Rather than attempt to further address this instability, the Ung H187D protein was overproduced in wild type *E. coli* and purification was undertaken to isolate the Ung H187D protein and to resolve it from wild type Ung.

The activity of crude cell extracts containing overproduced Ung H187D suggested that the H187D mutation compromised the enzyme's catalytic activity. While pSB1051 containing crude extracts demonstrated a 930-fold increase in Ung activity with IPTG-induction, extracts containing overproduced Ung H187D had only 1.5 times more uracil-DNA glycosylase

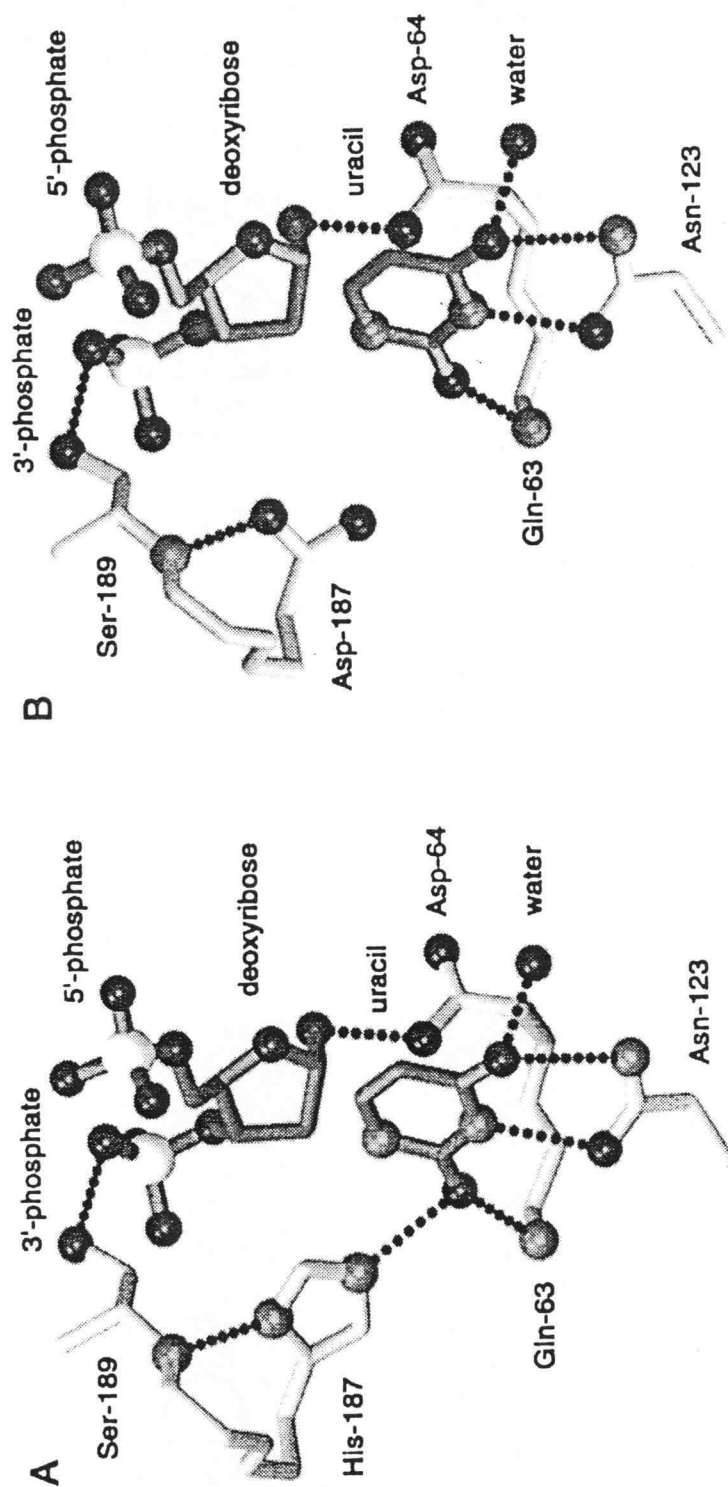
activity relative to cell extracts containing the pKK223-3 control vector. Thus it appeared that the H187D mutation reduced the enzyme's activity by at least 620-fold.

During the purification of Ung H187D, it was observed that, unlike the endogenous wild type enzyme, the H187D mutant failed to bind single-stranded DNA agarose under conditions conducive to stable binding by wild type Ung. In contrast, Ung H187D was observed to stably bind to poly(U) Sepharose. These findings suggested that the His to Asp substitution interfered with the ability of the mutant enzyme to form a persistent complex with single-stranded DNA. However, one may infer both from the low, but detectable, catalytic activity and from the observed inhibition by free uracil that Ung H187D conserved, to some extent, the native uracil nucleotide interaction. A structural comparison of the active sites by Tainer and coworkers (110) implies that steric constraints should not dramatically affect uracil binding by Ung H187D (Figure 34). Furthermore, the experimental findings indicating altered DNA substrate specificity of Ung H187D suggested that the negative charge of the Asp-187 side chain may repel the phosphate backbone of the single-stranded DNA, which is less constrained than in double-stranded DNA. This interpretation was consistent with the close proximity of the Asp-187 carboxyl group to the 3'- and 5'-phosphates of the target uracil nucleotide in DNA (Figure 34B). In addition, when the equivalent histidine residue in human uracil-DNA glycosylase (His-268) was mutated to Leu, significantly lowered affinity to DNA was not observed (80), presumably because the Leu side chain lacked the long range interactions of the Ung Asp-187 carboxylate. In the case of binding to poly(U)-Sepharose, perhaps the negative Asp-187 carboxylate:phosphate interaction in DNA is mitigated in part by hydrogen bonding between the ribose 2' hydroxyl and the Asp side chain.

E. coli Ung was purified to apparent homogeneity, as evidenced by the presence of a single protein band coincident with the Ung H187D activity eluted from poly(U)-Sepharose when fractions were analyzed by SDS-polyacrylamide gel electrophoresis. A low level of uracil-DNA glycosylase

Figure 34. Model of *E. coli* Ung binding to uracil-containing DNA. The location of Ung (A) and Ung H187D (B) active site amino acid residues are shown as determined by Tainer and coworkers using high resolution X-ray crystallography (110). The position of the cleaved uracil nucleotide was modeled into the uracil recognition pocket by superimposing the Ung structure onto the human uracil-DNA glycosylase:U/G-DNA co-crystal structure (103). Alignment was performed by the program CKWHENCE (110). The active site residues portrayed are absolutely conserved between *E. coli* and human uracil-DNA glycosylase. The proposed interactions between various residues, uracil, deoxyribose phosphates, and water are indicated. Protein is shaded in light gray, DNA in dark gray; heteroatoms are nitrogen (*gray*), oxygen (*black*), and phosphorus (*white*).

Figure 34



activity was detected in the Ung H187D preparation. This activity was reduced approximately 55,000-fold relative to that of wild type Ung as indicated by a specific activity of 37 units/mg. Based on this observation, Ung H187D was calculated to have a turnover rate of 0.95 uracil/h. Several observations indicated that the activity of the Ung H187D preparation was inherent to the mutant protein and not the result of very low-level contamination by wild type Ung: 1) a preparation of Ung H187D deliberately contaminated with Ung was effectively resolved into two distinct peaks (mutant and wild type Ung) using DNA-agarose affinity chromatography, which was applied to the separation procedure during the final step in the purification protocol; 2) the pH optimum of Ung H187D (pH 7.0) was distinct from that of Ung (pH 8.0); and 3) the substrate specificity of Ung H187D differed from that of Ung. From these observations it was concluded that the Ung H187D mutant enzyme preparation was sufficiently pure to warrant further characterization.

Recently, the structures of both Ung and Ung H187D in complex with the uracil-DNA glycosylase inhibitor protein were determined by X-ray crystallography at 2.4 Å and 2.6 Å resolution, respectively (110). Ung is the first full-length uracil-DNA glycosylase for which crystal structure information is available (110, 111, 153). Overlay of the Ung and Ung H187D structures indicated that the mutant protein is properly folded with respect to the wild type enzyme, and the principal amino acid residues that form the uracil binding pocket and active site (Asp-64, Pro-65, Tyr-66, Phe-77, Asn-123, His/Asp-187) of Ung and Ung H187D are nearly superimposable when the two structures are compared (110). Moreover, structural comparison of *E. coli* Ung with both the human (79) and HSV-1 (117) uracil-DNA glycosylase homologs has indicated that the major structural motifs implicated in enzyme function and specificity have been conserved, specifically the Leu intercalation loop (*E. coli* residues 187-HPSPLSAHR-195), the Pro-rich loop (84-AIPPS-88), the Gly-Ser loop (165-GS-166), the uracil specificity region (120-LLLN-123), and the catalytic water-activating loop (63-QDPYH-67) (103, 110). Thus, conclusions concerning the catalytic role of Ung His-187 are most likely

applicable to the various members of the uracil-DNA glycosylase protein family for which this amino acid is an absolutely conserved residue.

In addition to structural analysis, the Ung H187D enzyme was subjected to biochemical characterization. As previously shown, uracil-DNA glycosylases display a marked preference for single-stranded uracil-containing DNA, and favor U/G mispairs over U/A basepairs in double-stranded DNA (9, 102). Under conditions optimal for wild type Ung (pH 8.0), the substrate preference of Ung H187D was U/G-25-mer > single-stranded U-25-mer > U/A-25-mer. However, Ung H187D processed these same DNA substrates at pH 7.0 with comparable rates, although single-stranded U-25-mer was slightly preferred. Furthermore, activity on the single-stranded uracil-DNA substrate increased about three-fold at pH 7.0 compared to that at pH 8.0. That the substrate specificity and specific activity of Ung H187D were pH-dependent suggested that the protonation state of the Asp-187 γ -carboxylate may affect various aspects of the uracil-excision reaction including: the extent and duration of DNA-binding, uracil nucleotide flipping, and stabilization of the uracil/deoxyribose transition state. In this regard it was interesting that the effect of pH on uracil inhibition of both Ung and Ung H187D was small, and that Ung H187D was less susceptible than Ung to uracil inhibition. In addition, the mutant enzyme was not inhibited by 5-fluorouracil at any of the concentrations tested. Taken together, these results imply that the mutation reduced the affinity of the active site for uracil. This can be explained from a structural basis as caused by loss of hydrogen bonding and repulsive electrostatic interactions with the permanent electric dipole at uracil O2 (Figure 34). In the case of 5-fluorouracil, steric interference and like-charge repulsion by the 5-fluorine moiety with the Asp-187 side chain were apparently sufficient to preclude binding. If like-charge repulsion is a major factor in 5-fluorouracil binding, one might expect that nonpolar substitutions at residue 187, such as Leu, would not affect 5-fluorouracil inhibition due to the presence of a neutral aliphatic side chain in the active site.

Previously, biochemical characterization of the Ugi inhibitor protein revealed that Ugi binds Ung in a 1:1 stoichiometry (8). Crystallographic data

further demonstrate that both Ung and Ung H187D bind Ugi to form a 1:1 Ung•Ugi complex (110). Because mutant and wild type Ung bind Ugi in a 1:1 ratio, one would expect [^{35}S]Ugi to form complex with Ung and Ung H187D in a manner directly proportional to the molar ratio of inhibitor to enzyme. However, it was observed that only 2/3 and 7/8 of [^{35}S]Ugi was detected in complex with Ung and Ung H187D, respectively, at equal molar ratios. Several factors may account for this discrepancy. The concentrations of Ung and Ung H187D may have been overestimated or the enzyme preparations may have been heterogeneous, with a subpopulation incapable of binding to Ugi. When purified [^3H]Ung was incubated with Ugi-Sepharose, a fraction of the preparation was refractory to Ugi-binding even in excess of resin. This suggests that the purification process may inactivate a subpopulation of the enzyme. However, even at a 5-fold molar excess of enzyme to Ugi it was not possible to complex 100% of the [^{35}S]Ugi. This may be a product of experimental error and may reflect the limits of detection of this assay. Alternatively, it may indicate that a fraction of the inhibitor is also rendered incapable of complex formation during the purification process. The Ugi purification includes a heat denaturation step; it is likely that some fraction of this heat-resistant Ugi protein does not fully renature and thus become incapable of complex formation. Regardless, both the mobility shift assay and crystallographic analysis indicate that the H187D mutant is able to complex with Ugi. Ugi forms a complex with Ung by inserting its $\beta 1$ edge over the DNA binding groove of the enzyme and sequestering the active site pocket (79, 110). Although Ung His-187 makes a water-mediated hydrogen bond with Ugi Glu-28 and hydrophobic contacts with Ile-22 and Met-56 (110), the other interactions between Ung and the Ugi $\beta 1$ edge appear to be so extensive that the Asp-187 mutation has little to no effect on complex formation.

By using UV-catalyzed protein/DNA cross-linking as a measure of DNA binding affinity, the efficiency of Ung His187D cross-linking to the oligonucleotide dT₂₀ was determined to be about the same as to dT₁₉-U. Thus, the presence of uracil in the 20-mer did not increase the DNA binding affinity

of Ung H187D. Since the turnover rate of the Ung H187D mutant was very low (~ 1 uracil/h), it seemed unlikely that very many AP-sites were created during the 30 minute UV-irradiation. Moreover, the extent of UV-catalyzed cross-linking to an AP-site-containing oligonucleotide (dT₁₉-AP) was reduced about 50% relative to the rate on dT₁₉-U. These results suggested that the main factor affecting the uracil-DNA binding affinity of Ung H187D was not the recognition of uracil but the Asp-187 γ -carboxylate/DNA phosphate electrostatic repulsion. This led to speculation that the negative electrostatic interaction was more pronounced when the DNA substrate contained an abasic site, as the 3' and 5' deoxyribose phosphates were more accessible.

Unexpectedly, the wild type enzyme was cross-linked by UV-irradiation less efficiently to the uracil-containing substrate (dT₁₉-U) than to the abasic site-containing substrate (dT₁₉-AP) or even to the non-specific substrate, dT₂₀. Since the turnover rate of Ung (800 uracils/min) is rapid compared to Ung H187D it might be expected that a significant fraction of uracil had been excised from dT₁₉-U during the UV-irradiation reaction containing Ung. When human uracil-DNA glycosylase was co-crystallized with a 10-basepair double-stranded DNA containing either a U/A basepair or a U/G mismatch, free uracil and a deoxyribose C1' OH were bound in the active site (103). Thus, it is conceivable that a portion of the Ung molecules cross-linked to a uracil base bound in the active site rather than to the thymine-DNA; such enzyme molecules may not be capable of binding DNA.

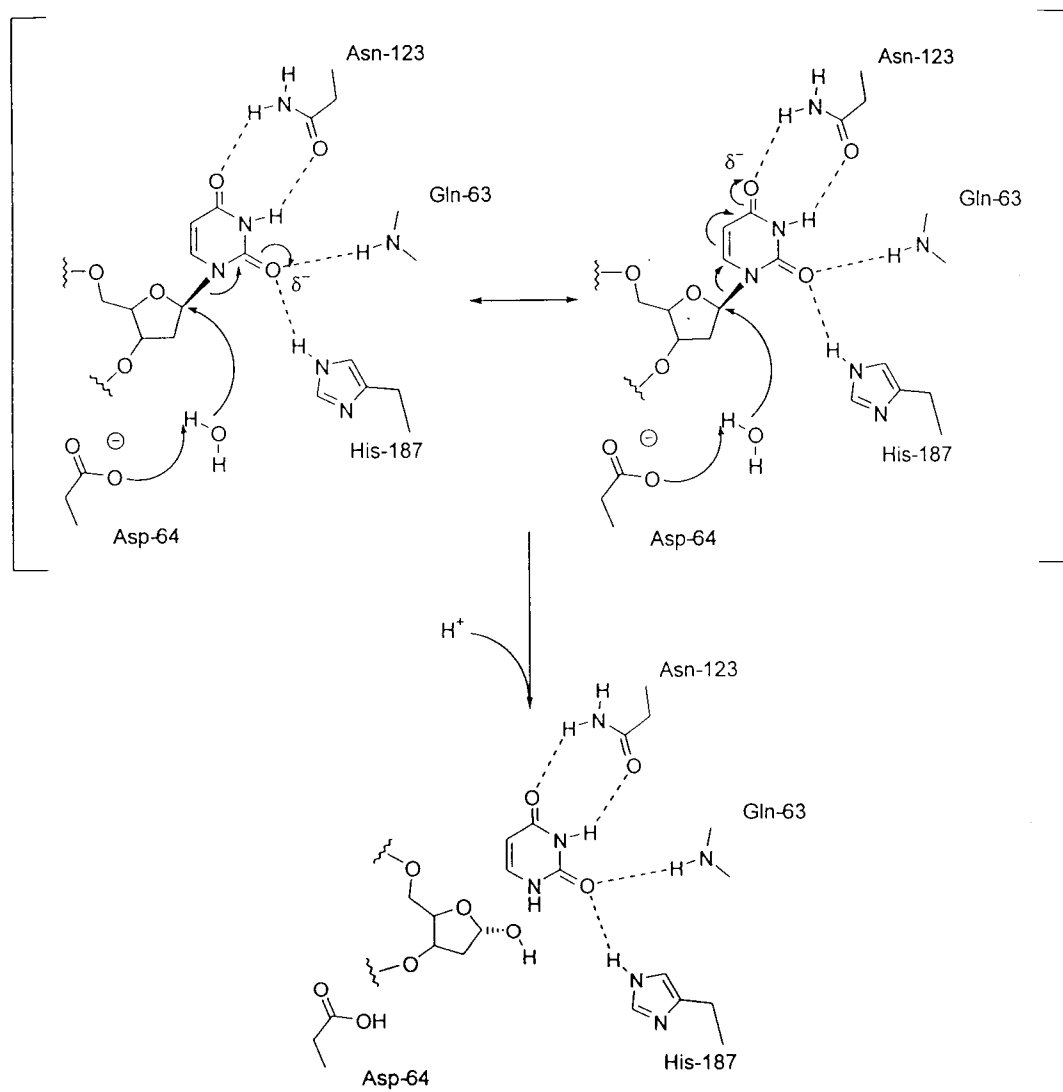
Addition of 2 mM uracil to the cross-linking reactions had no effect on the efficiency of Ung \times dT₂₀ cross-linking, but the efficiency of Ung H187D \times dT₂₀ cross-linking was reduced several fold. These results demonstrated that the affinity of Ung was considerably greater for DNA than for uracil, as even 2 mM uracil did not disrupt Ung/dT₂₀ binding. These results show further that the His to Asp mutation has a greater effect on DNA affinity than on uracil binding, assuming that uracil bound in the active site prevents DNA binding.

A comparison of the reaction kinetics of mutant and wild type enzyme demonstrated that the H187D mutation had a minor effect on V_{\max}/K_m . At standard reaction pH, the values of V_{\max}/K_m for Ung and Ung H187D were 4.4×10^{-4} and $1.9 \times 10^{-4} \text{ sec}^{-1}$, respectively. In contrast, k_{cat} was reduced 48,000-fold from 12 to 0.00025 sec^{-1} . The data for V_{\max}/K_m suggested that the processes involved from binding to the first irreversible step of uracil-DNA glycosylase action were not affected by the Asp-187 mutation because this value remained essentially unchanged. In contrast the large impact of the mutation on k_{cat} suggested that the rate limiting step of the reaction had been disrupted. Kinetic measurements using a double-stranded 2-aminopurine-containing 27-mer confirmed this observation. The k_{cat} of Ung was reduced from 0.59 to 0.00068 sec^{-1} . During the process of this work, Xiao *et al.* (153) reported the kinetic analysis of an Ung H187Q mutant utilizing a similar substrate. By using a double-stranded 19-mer containing a 2-APu·U pair, the k_{cat} for Ung H187Q was reduced 160-fold relative to wild type Ung (153). These observations suggest that substrate binding and uracil base flipping are independent of His-187 while a subsequent reaction step such as catalysis or product release involves this active site residue.

Based on the collection of biochemical and structural data for *E. coli* Ung, it is proposed that His-187 participates in glycosylic bond scission as illustrated in Figure 35. Stable active site geometry suggests that His-187 N δ 1 is a hydrogen bond acceptor to the Ser-189 main chain amide. In the 'closed' conformation, movement of the Leu intercalation loop (amino acid residues 187-195) brings the His-187 N ϵ 2 $\sim 2 \text{ \AA}$ closer to the uracil O2 where it can act as a hydrogen bond donor (103, 110, 127), as previously suggested by Savva *et al.* (116). Delocalization of electron density across the His-187 imidazole side chain contributes to catalysis by stabilization of the oxyanion form of the uracil O2 carbonyl and the attendant polarization of the N1-C1' glycosylic bond. The side chain of Asn-123 and the main chain of Gln-63 act to further stabilize electron delocalization in the uracil ring by forming hydrogen bonds with N3 and O4. In addition, the O4' of the deoxyribose, because of its

Figure 35. Scheme of the reaction mechanism for cleavage of the N1-C1' glycosylic bond by *E. coli* Ung. Resonance forms of the proposed hydrolysis intermediates in the uracil-excision are illustrated. The N1-C1' glycosylic bond is polarized by electron density withdrawal from the deoxyribose C1' through N1 into the uracil ring. The developing negative charge is distributed about the uracil ring by resonance effects involving oxyanion formation at O2 and O4 and stabilized by hydrogen bonding with the side chains of His-187 and Asn-123, and the main chain Gln-63 amide. The catalytic water is bound by Asp-64 in the water-activating loop formed by 64-Asp-Pro-Tyr-His-67 (103).

Figure 35



electron-withdrawing nature, is proposed to participate in forming a reactive, electrophilic C1' since substitution of the less electronegative sulfur atom for O4' resulted in a uracil nucleotide refractory to hydrolysis as reported by Parikh *et al.* (103). As observed in both the human (103, 127) and the HSV-1 (116) uracil-DNA glycosylase structures, the side chain of the conserved Asp-64 appears properly positioned in *E. coli* Ung to bind the catalytic water (110, 111). Electron density withdrawal from the deoxyribose C1' renders the N1-C1' bond vulnerable to nucleophilic attack by the water activated by the γ -carboxylate of Asp-64. In addition, the developing negative charge of the uracil base, stabilized by resonance effects and hydrogen bonding to active site residues (Gln-63, Asn-123, His-187), makes uracil a good leaving group. Abstraction of a proton from solvent by N1 also enhances uracil departure and restores electrostatic neutrality to the free uracil base following glycosylic bond scission.

The mechanism proposed here differs from previous proposals in several important respects. Recent structural information derived from the co-crystallization of human uracil-DNA glycosylase with uracil-DNA (103, 127) shows that His-268 (Ung His-187) is on the wrong side of the uracil to carry out either a direct nucleophilic attack on C1' or to mediate an indirect attack by serving as a general base to activate a nucleophilic water, as previously proposed (80). Unlike previously proposed mechanisms (116), it is unnecessary to require protonation of uracil O2 in order to improve the leaving group quality of the base under the current mechanism. Rather, the developing negative charge that characterizes the transition state is not posited solely in the O2 oxyanion but is distributed among N1, O2 and O4 on the uracil ring by the effects of resonance and hydrogen bonding (Figure 34). The proximity of the Ser-189 NH to the His-187 imidazole N δ 1 in both open and closed conformations indicates that N δ 1 acts as a hydrogen bond acceptor to the main chain amide; accordingly, the His-187 N ϵ 2 is a hydrogen bond donor to O2. In this scenario, it is unlikely that the His-187 imidazole binds two hydrogens, carries a full positive charge, and protonates O2 to return to

electronic neutrality, as was proposed (116). The aromaticity of the imidazole side chain seems uniquely suitable to stabilize any partial charge associated with electrostatic interactions with the uracil nucleotide backbone and hydrogen bonding with uracil O2.

The relatively bulky nature of the imidazole side chain of His-187 may also contribute to the steric selectivity of the active site. This selectivity pocket is thought to distort the N1-C1' glycosylic bond, since an intact extrahelical uracil residue in DNA does not easily 'fit' into the active site without torsional strain (103, 110). In contrast, the Asp-187 side chain is too small to contribute much to steric selectivity.

Substitution of Asp for His-187 has profound effects on the cleavage of the N1-C1' glycosylic bond. Asp-187 does not extend far enough into the specificity pocket to allow a protonated side chain to hydrogen bond with uracil O2. On the other hand, it is too long to allow a water molecule to act as a bridge between the Asp-187 side chain carboxylate and uracil O2 (110). In removing the hydrogen bonding interaction of His-187 with uracil O2, the Asp-187 mutation not only hampers uracil binding, it also influences the stabilization of developing negative charge at O2 that is requisite for N1-C1' bond cleavage. Simple removal of the hydrogen bond, as observed in the human H268L mutant, reduced the specific activity ~300-fold (80); however, the specific activity of the *E. coli* H187D mutant enzyme decreased an additional two orders of magnitude. The large effect of the Asp-187 mutation on specific activity most likely results from the destabilization of the hydrolytic transition state caused by electrostatic repulsion of the developing negative charge at uracil O2 by the Asp-187 carboxylate. Reduction of this electrostatic repulsion by partial protonation of the Asp-187 side chain may be the fundamental influence that shifts the pH optimum of the mutant enzyme from 8.0 to 7.0. Hence, the Asp-187 mutation provides a subtle probe of the Ung reaction mechanism, indicating how an amino acid residue whose side chain is ~4.5 Å from the nearest atom of the scissile bond can reduce the reaction rate by ~55,000-fold.

In summary, it is proposed that the imidazole side chain of Ung His-187 1) facilitates uracil nucleotide flipping by 'pulling' the uracil residue into the active site through favorable electrostatic interactions with the 3' and 5' uracil deoxyribose phosphates; 2) contributes sterically to the fit and selectivity of the uracil binding pocket; and 3) stabilizes the hydrolytic transition state by hydrogen-bonding with uracil O2. The reaction mechanism advanced here provides a realistic explanation of the properties of the Ung H187D mutant enzyme. However, how the release of the uracil-excision reaction products, free uracil and AP-site DNA, affects the catalytic efficiency of uracil-DNA glycosylase remains to be established.

4.2 Ugi-Affinity Purification of Mitochondrial Uracil-DNA Glycosylases

Polyclonal antibody was raised to both Ung and Ugi proteins. In addition, Ung- and Ugi-affinity chromatography methods were developed for use in conjunction with anti-Ung antibody to purify uracil-DNA glycosylases from mitochondrial extracts of mammalian liver tissue. Serum from rabbits immunized with Ung or Ugi was able to inhibit enzyme or inhibitor, respectively, in a functional assay although complete inhibition of protein activity was not achieved. The immune response to Ugi was variable, with one sample of antiserum capable of only 16% inhibition. In contrast, a second animal had an initially strong response but subsequent injections may have induced tolerance. It was observed that the nearly complete inhibition detected after the second boost was reduced by approximately 1/3 after 4 additional injections. As expected due to the greater than 50% amino acid identity between human and *E. coli* uracil-DNA glycosylase, polyclonal antiserum raised to Ung inhibited a substantial fraction (52%) of human Δ 84UDG activity. This suggested that uracil-DNA glycosylases from different species contain similar immunogenic determinants and these anti-Ung antiserum preparations would allow for the detection of uracil-DNA glycosylase from diverse biological sources.

Ung-Sepharose was utilized for the affinity purification of polyclonal antibody to Ung. Serum proteins, including nonspecific IgG, were recovered in the flow through and wash fractions. Proteins consistent with the size of IgG large and small chains were recovered following a 3.5 M MgCl₂ elution of the Ung-Sepharose column. This recovered antibody preparation was reactive to *E. coli* Ung in immunoassays. Similarly, Ugi-Sepharose affinity resin was used to purify uracil-DNA glycosylase from extracts. While Ung and Ugi bind very tightly under physiological conditions, it was possible to remove Ung bound to Ugi-Sepharose with extremes of pH and salt. The use of 100 mM glycine (pH 2.5) for the elution of Ung from Ugi-Sepharose had previously been reported by Caradonna and coworkers (15). The results presented here indicated that 5 M MgCl₂ (in 10 mM potassium phosphate (pH 7.2)) was nearly twice as effective at dissociating the enzyme from the resin. Concentrations of NaCl as high as 1 M had no effect on Ung-Ugi-Sepharose interactions, an observation that allowed for the reduction of nonspecific protein binding.

CNBr-activated Sepharose 4B was coupled to enzyme and inhibitor to produce Ung- and Ugi-Sepharose affinity resins. It was estimated that 220 nmol of Ugi coupled per ml of packed Sepharose 4B resin. Because Ung complexes with Ugi in a 1:1 stoichiometry, the maximum binding capacity for the Ugi-Sepharose resin would be 220 nmol of Ung per ml of Ugi-Sepharose. However, upon incubation of Ugi-Sepharose with [³H]Ung, it was observed that 90 nmol of enzyme bound per ml of resin. Similarly, the estimate for Ung coupling to Sepharose 4B was 97 nmol protein/ml of resin but only 40 nmol of [³⁵S]Ugi was observed to bind per ml of Ung-Sepharose. In both instances, the amount of protein determined to bind to the affinity resin experimentally was 2.4-fold less than the amount of protein predicted to bind if 100% of the coupled ligand was capable of productive Ung•Ugi complex formation. This is not surprising due to the nature of the coupling reaction. CNBr-activated Sepharose 4B couples to proteins by reacting with primary amines residing in various locations on the coupling ligand. Ung contains nineteen primary amines, while Ugi contains six. The reaction between an activated Sepharose

bead and an amine group results in a heterogeneous population of Ung- or Ugi-conjugated Sepharose beads with ligand coupled such that the active site face of the molecule is presented many different orientations. Some orientations may preclude Ung•Ugi complex formation due to steric interference with the Sepharose bead. In a similar fashion, the coupling of multiple ligand molecules to a single Sepharose bead may result in steric interference between ligands which prevents one or all of the conjugated molecules from forming Ung•Ugi complex. Ugi interacts with Ung primarily through interactions on the Ugi β 1-strand and α 2-helix (79, 110). Ugi Gln-19, Glu-20, Ser-21, and Leu-23 of the β 1-strand form hydrogen bonds with the Ung DNA binding groove (110). The α 2-helix and β 1-sheet also form a hydrophobic cavity which sequesters the conserved Leu-loop and plays an important role in Ung•Ugi complex stability (110). Thus, coupling conformations that interfere with the formation of these structures are expected to reduce the number of ligands capable of forming Ung•Ugi complex. From the data presented, it appears that under the coupling conditions used only 41% of the ligand molecules coupled in such a way that they were capable of productive complex formation. In determining the amount of resin required to purify uracil-DNA glycosylase from crude extracts, the experimentally determined binding capacity of 90 nmol/ml of packed Ugi-Sepharose was used in order to maximize recovery.

Ugi-affinity chromatography was utilized to purify *E. coli* Ung from 95 μ g of whole cell extracts. The SDS-eluted samples were analyzed by 12.5% SDS-polyacrylamide gel electrophoresis. Protein bands were not visualized upon Coomassie Brilliant Blue staining of the polyacrylamide gel unless the extracts were supplemented with 200 pmol of purified *E. coli* Ung. Based on the specific activity of the cell extracts, it is estimated the samples contained 0.3 pmol of Ung, which is ~600-fold lower than the levels of Ung detected in the supplemented system. Likewise, when mitochondrial extracts were subjected to Ugi-affinity chromatography and the fractions that bound the matrix were examined by Western blot analysis, it was not possible to detect background

levels of UDG in the extract samples. However, by this method 0.24 pmol of *E. coli* Ung was detected in purified form or when mixed with mitochondrial extract. These results indicated that factors in the mitochondrial extract did not inhibit recognition of Ung by Ung antiserum. When the specific activity of the mitochondrial extracts is taken into consideration, 100 µg of extract was estimated to contain only 0.12 pmol of UDG which is 2-fold lower than the limits of detection by the Western blot system described. It appears that Western blot analysis is the more sensitive method to detect uracil-DNA glycosylase in extracts at physiological concentrations, provided the starting material is abundant.

By using large quantities of mammalian liver tissue (1200 g) as starting material, it was possible to purify uracil-DNA glycosylase from mitochondrial extracts by Ugi-affinity chromatography. The rat and pig mitochondrial sources were greatly enriched for UDG, although the end products were not homogeneous. Unlike the rat mitochondrial sample, which contained one major band, similar in size (MW ~25,000) to *E. coli* Ung, the porcine sample appeared to contain two polypeptide species with apparent molecular weights of 28,000 and 48,000. Western blot analysis revealed that the 48,000 molecular weight protein was not reactive with Ung antibody; thus, it was unlikely to be a uracil-DNA glycosylase. This species may be a protein that co-purified with porcine mitochondrial UDG as part of a multi-protein repair complex or it may be a protein unrelated to UDG that coincidentally was able to bind Ugi-Sepharose. Further characterization of this protein is required to determine its identity. Previous purification of UDG from rat liver mitochondria resolved two distinct activity peaks, designated form I and form II, with virtually identical kinetic properties (27). Form I, a single polypeptide with an apparent molecular weight of 24,000, constituted approximately 85% of the total activity (27). The molecular weight of form II was ~29,000 (27).

The purification of mitochondrial UDG may be useful in the study of uracil-initiated BER in mitochondria. The process of BER has been reconstituted with mitochondrial enzymes using AP site-containing DNA as a substrate for repair (71, 105), but the full pathway, beginning with a uracil

lesion, has not been examined. The methods described here provide a source of purified mitochondrial UDG to catalyze the first step of a reconstituted repair pathway.

The current understanding of the mammalian system is that nuclear and mitochondrial forms of UDG are encoded by a single gene, share a common catalytic domain, and differ in their N-terminal amino acid sequences (95, 100). To date, most of the data supporting these predictions has been indirect in the form of immunolocalization (89, 125, 126) and cytofluorescence (87, 101) studies and analysis of the *UNG* gene promoter and splicing consensus sequences (95, 101). Caradonna and coworkers utilized Ugi-affinity chromatography to purify nuclear UDG and the purified protein was subjected to direct protein microsequencing (87). The derived amino acid sequence indicated that the nuclear UDG corresponded to UNG2, as predicted by Nilsen *et al.* (87, 95). However definitive identification of the mitochondrial UDG in the form of direct amino acid sequence determination has not been accomplished. The approach described here for the purification of mitochondrial UDG lays the groundwork for this analysis.

Together, Ugi-Sepharose and Ung antibodies are tools which can be utilized for the rapid screening of cell or organelle extracts to determine the presence, number, size, and activity of uracil-DNA glycosylases from various species. Extracts could be depleted of Ung activity by incubation with Ugi-Sepharose, permitting the study of DNA repair processes in phenotypically *ung⁻* samples. Using less stringent purification methods, it may be possible to analyze protein-protein interactions between Ung and other base excision repair enzymes by probing crude extracts with Ugi-Sepharose similar to the process used by Prasad and colleagues to affinity purify a multiprotein repair complex from bovine testis extracts (107). In this regard, Ugi-affinity purification has been successfully used to identify a physical interaction between PCNA and the cyclin-like UDG in HeLa cell extracts (88), suggesting that this procedure may allow for the identification of proteins that make physical associations with uracil-DNA glycosylase.

BIBLIOGRAPHY

1. Anderson, C. T., and Friedberg, E. C. (1980) The presence of nuclear and mitochondrial uracil-DNA glycosylase in extracts of human KB cells. *Nucleic Acids Res.* **8**, 875-888.
2. Asahara, H., Wistort, P. M., Bank, J. F., Bakerian, R. H., and Cunningham, R. P. (1989) Purification and characterization of *Escherichia coli* endonuclease III from the cloned nth gene. *Biochemistry* **28**, 4444-4449.
3. Au, K. G., Clark, S., Miller, J. H., and Modrich, P. (1989) *Escherichia coli* mutY gene encodes an adenine glycosylase active on G-A mispairs. *Proc. Natl. Acad. Sci. U.S.A.* **86**, 8877-8881.
4. Bailly, V., and Verly, W. G. (1987) *Escherichia coli* endonuclease III is not an endonuclease but a beta- elimination catalyst. *Biochem J.* **242**, 565-572.
5. Barrett, T. E., Savva, R., Panayotou, G., Barlow, T., Brown, T., Jiricny, J., and Pearl, L. H. (1998) Crystal structure of a G:T/U mismatch-specific DNA glycosylase: mismatch recognition by complementary-strand interactions. *Cell* **92**, 117-129.
6. Bennett, S. E. (1995) Characterization of the *Escherichia coli* uracil-DNA glycosylase•inhibitor complex. *Thesis*. Oregon State University, Corvallis, Oregon.
7. Bennett, S. E., Jensen, O. N., Barofsky, D. F., and Mosbaugh, D. W. (1994) UV-catalyzed cross-linking of *Escherichia coli* uracil-DNA glycosylase to DNA. *J. Biol. Chem.* **269**, 21870-21879.
8. Bennett, S. E., and Mosbaugh, D. W. (1992) Characterization of the *Escherichia coli* uracil-DNA glycosylase/inhibitor protein complex. *J. Biol. Chem.* **267**, 22512-22521.
9. Bennett, S. E., Sanderson, R. J., and Mosbaugh, D. W. (1995) Processivity of *Escherichia coli* and rat liver mitochondrial uracil-DNA glycosylase is affected by NaCl concentration. *Biochemistry* **34**, 6109-6119.
10. Bennett, S. E., Schimerlik, M. I., and Mosbaugh, D. W. (1993) Kinetics of the uracil-DNA glycosylase/inhibitor protein association. *J. Biol. Chem.* **268**, 26879-26885.
11. Berkner, K. L., and Folk, W. R. (1979) The effects of substituted pyrimidines in DNAs on cleavage by sequence-specific endonucleases. *J. Biol. Chem.* **54**, 2551-2602.

12. Bessman, M. J., Lehman, I. R., Adler, J., Zimmerman, S. B., Simms, E. S., and Kornberg, A. (1958) Enzymatic synthesis of deoxyribonucleic acid. III. The incorporation of pyrimidine and purine analogues into deoxyribonucleic acid. *Proc. Natl. Acad. Sci. U.S.A.* **44**, 633-640.
13. Biade, S., Sobol, R. W., Wilson, S. H., and Matsumoto, Y. (1998) Impairment of proliferating cell nuclear antigen-dependent apurinic/apyrimidinic site repair on linear DNA. *J. Biol. Chem.* **273**, 898-902.
14. Bradford, M. M. (1976) A rapid and sensitive method for the quantitation of microgram quantities of protein utilizing the principle of protein-dye binding. *Anal. Biochem.* **72**, 248-254.
15. Caradonna, S., Ladner, R., Hansbury, M., Kosciuk, M., Lynch, F., and Muller, S. (1996) Affinity purification and comparative analysis of two distinct human uracil-DNA glycosylases. *Exp. Cell. Res.* **222**, 345-359.
16. Caradonna, S. J., and Cheng, Y.-C. (1980) Uracil DNA-glycosylase. Purification and properties of this enzyme isolated from blast cells of acute myelocytic leukemia patients. *J. Biol. Chem.* **255**, 2293-2300.
17. Chen, H., and Shaw, B. R. (1993) Kinetics of bisulfite-induced cytosine deamination in single-stranded DNA. *Biochemistry* **32**, 3535-3539.
18. Chen, H., and Shaw, B. R. (1994) Bisulfite induces tandem double CC to TT mutations in double-stranded DNA. 2. Kinetics of cytosine deamination. *Biochemistry* **33**, 4121-4129.
19. Csonka, L. N., and Clark, A. J. (1979) Deletions generated by the transposon Tn10 in the srl recA region of the Escherichia coli K-12 chromosome. *Genetics* **93**, 321-343.
20. Dianov, G., and Lindahl, T. (1994) Reconstitution of the DNA base excision-repair pathway. *Curr. Biol.* **4**, 1069-1076.
21. Dianov, G., Price, A., and Lindahl, T. (1992) Generation of single-nucleotide repair patches following excision of uracil residues from DNA. *Mol. Cell. Biol.* **12**, 1605-1612.
22. Dianov, G., Sedgwick, B., Daly, G., Olsson, M., Lovett, S., and Lindahl, T. (1994) Release of 5'-terminal deoxyribose-phosphate residues from incised abasic sites in DNA by the *Escherichia coli* RecJ protein. *Nucleic Acids Res.* **22**, 993-998.
23. Dianov, G. L., Prasad, R., Wilson, S. H., and Bohr, V. A. (1999) Role of DNA polymerase beta in the excision step of long patch mammalian base excision repair. *J. Biol. Chem.* **274**, 13741-13743.

24. Dianov, G. L., Timchenko, T. V., Sinitsina, O. I., Kuzminov, A. V., Medvedev, O. A., and Salganik, R. I. (1991) Repair of uracil residues closely spaced on the opposite strands of plasmid DNA results in double-strand break and deletion formation. *Mol. Gen. Genet.* **225**, 448-452.
25. Doetsch, P. W., and Cunningham, R. P. (1990) The enzymology of apurinic/apyrimidinic endonucleases. *Mutat. Res.* **236**, 173-201.
26. Domena, J. D., and Mosbaugh, D. W. (1985) Purification of nuclear and mitochondrial uracil-DNA glycosylase from rat liver. Identification of two distinct subcellular forms. *Biochemistry* **24**, 7320-7328.
27. Domena, J. D., Timmer, R. T., Dicharry, S. A., and Mosbaugh, D. W. (1988) Purification and properties of mitochondrial uracil-DNA glycosylase from rat liver. *Biochemistry* **27**, 6742-6751.
28. Dube, D. K., Kunkel, T. A., Seal, G., and Loeb, L. A. (1979) Distinctive properties of mammalian DNA polymerases. *Biochim. Biophys. Acta* **561**, 369-382.
29. Duncan, B. K. (1981) "DNA Glycosylases." in *The Enzymes* (Boyer, P. D., ed) Vol. XIV, 3rd Ed., pp. 565-586, Academic Press, New York, NY.
30. Duncan, B. K. (1985) Isolation of insertion, deletion, and nonsense mutations of the uracil- DNA glycosylase (ung) gene of *Escherichia coli* K-12. *J. Bacteriol.* **164**, 689-695.
31. Duncan, B. K., and Chambers, J. A. (1984) The cloning and overproduction of *Escherichia coli* uracil-DNA glycosylase. *Gene* **28**, 211-219.
32. Duncan, B. K., and Miller, J. H. (1980) Mutagenic deamination of cytosine residues in DNA. *Nature* **287**, 560-561.
33. Duncan, B. K., Rockstroh, P. A., and Warner, H. R. (1978) *Escherichia coli* K-12 mutants deficient in uracil-DNA glycosylase. *J. Bacteriol.* **134**, 1039-1045.
34. Duncan, B. K., and Weiss, B. (1982) Specific mutator effects of ung (uracil-DNA glycosylase) mutations in *Escherichia coli*. *J. Bacteriol.* **151**, 750-755.
35. Eden, S., and Cedar, H. (1994) Role of DNA methylation in the regulation of transcription. *Curr. Opin. Genet. Dev.* **4**, 255-259.

36. Ehrlich, M., Zhang, X. Y., and Inamdar, N. M. (1990) Spontaneous deamination of cytosine and 5-methylcytosine residues in DNA and replacement of 5-methylcytosine residues with cytosine residues. *Mutat. Res.* **238**, 277-286.
37. Fisher, E. F., and Caruthers, M. H. (1979) Studies on gene control regions XII. The functional significance of a lac operator constitutive mutation. *Nucleic Acids Res.* **7**, 401-416.
38. Fortini, P., Pascucci, B., Parlanti, E., Sobol, R. W., Wilson, S. H., and Dogliotti, E. (1998) Different DNA polymerases are involved in the short- and long-patch base excision repair in mammalian cells. *Biochemistry* **37**, 3575-3580.
39. Franklin, W. A., and Lindahl, T. (1988) DNA deoxyribosephosphodiesterase. *EMBO J.* **7**, 3617-3622.
40. Frederico, L. A., Kunkel, T. A., and Shaw, B. R. (1990) A sensitive genetic assay for the detection of cytosine deamination: determination of rate constants and the activation energy. *Biochemistry* **29**, 2532-2537.
41. Friedberg, E. C., Ganesan, A. K., and Minton, K. (1975) N-glycosidase activity in extracts of *Bacillus subtilis* and its inhibition after infection with bacteriophage PBS2. *J. Virol.* **16**, 315-321.
42. Frosina, G., Fortini, P., Rossi, O., Carrozzino, F., Raspaglio, G., Cox, L. S., Lane, D. P., Abbondandolo, A., and Dogliotti, E. (1996) Two pathways for base excision repair in mammalian cells. *J. Biol. Chem.* **271**, 9573-9578.
43. Gallinari, P., and Jiricny, J. (1996) A new class of uracil-DNA glycosylases related to human thymine-DNA glycosylase. *Nature* **383**, 735-738.
44. Griffin, S., Branch, P., Xu, Y. Z., and Karran, P. (1994) DNA mismatch binding and incision at modified guanine bases by extracts of mammalian cells: implications for tolerance to DNA methylation damage. *Biochemistry* **33**, 4787-4793.
45. Gupta, P. K., and Sirover, M. A. (1984) Altered temporal expression of DNA repair in hypermutable Bloom's syndrome cells. *Proc. Natl. Acad. Sci. U.S.A.* **81**, 757-761.
46. Hang, B., Medina, M., Fraenkel-Conrat, H., and Singer, B. (1998) A 55-kDa protein isolated from human cells shows DNA glycosylase activity toward 3,N4-ethenocytosine and the G/T mismatch. *Proc. Natl. Acad. Sci. U.S.A.* **95**, 13561-13566.

47. Haug, T., Skorpen, F., Aas, P. A., Malm, V., Skjelbred, C., and Krokan, H. E. (1998) Regulation of expression of nuclear and mitochondrial forms of human uracil-DNA glycosylase. *Nucleic Acids Res.* **26**, 1449-1457.
48. Haug, T., Skorpen, F., Lund, H., and Krokan, H. E. (1994) Structure of the gene for human uracil-DNA glycosylase and analysis of the promoter function. *FEBS Lett.* **353**, 180-184.
49. Haushalter, K. A., Todd Stukenberg, M. W., Kirschner, M. W., and Verdine, G. L. (1999) Identification of a new uracil-DNA glycosylase family by expression cloning using synthetic inhibitors. *Curr. Biol.* **9**, 174-185.
50. Hayatsu, H. (1976) Bisulfite modification of nucleic acids and their constituents. *Prog. Nucleic Acids Res. Mol. Biol.* **16**, 75-124.
51. Horst, J. P., and Fritz, H. J. (1996) Counteracting the mutagenic effect of hydrolytic deamination of DNA 5- methylcytosine residues at high temperature: DNA mismatch N-glycosylase Mig.Mth of the thermophilic archaeon *Methanobacterium thermoautotrophicum* THF. *EMBO J.* **15**, 5459-5469.
52. Hunter, B. I., Yamagishi, H., and Takahashi, I. (1967) Molecular weight of bacteriophage PBS1 deoxyribonucleic acid. *J. Virol.* **9**, 841-842.
53. Kahan, F. M. (1963) Novel enzymes formed by *Bacillus subtilis* infected with bacteriophage. *Fed. Proc.* **22**, 406.
54. Karran, P., Cone, R., and Friedberg, E. C. (1981) Specificity of the bacteriophage PBS2 induced inhibitor of uracil-DNA glycosylase. *Biochemistry* **20**, 6092-6096.
55. Kavli, B., Slupphaug, G., Mol, C. D., Arvai, A. S., Petersen, S. B., Tainer, J. A., and Krokan, H. E. (1996) Excision of cytosine and thymine from DNA by mutants of human uracil-DNA glycosylase. *EMBO J.* **15**, 3442-3447.
56. Kelman, Z. (1997) PCNA: structure, functions and interactions. *Oncogene* **14**, 629-40.
57. Kim, J., and Linn, S. (1988) The mechanisms of action of *E. coli* endonuclease III and T4 UV endonuclease (endonuclease V) at AP sites. *Nucleic Acids Res.* **16**, 1135-1141.
58. Klungland, A., and Lindahl, T. (1997) Second pathway for completion of human DNA base excision-repair: reconstitution with purified proteins and requirement for DNase IV (FEN1). *EMBO J.* **16**, 3341-3348.

59. Koulis, A., Cowan, D. A., Pearl, L. H., and Savva, R. (1996) Uracil-DNA glycosylase activities in hyperthermophilic micro-organisms. *FEMS Microbiol. Lett.* **143**, 267-271.
60. Krokan, H. (1981) Preferential association of uracil-DNA glycosylase activity with replicating SV40 mini-chromosomes. *FEBS Lett.* **133**, 89.
61. Krokan, H., and Wittwer, C. U. (1981) Uracil DNA-glycosylase from HeLa cells: general properties, substrate specificity and effect of uracil analogs. *Nucleic Acids Res.* **9**, 2599-2613.
62. Krokan, H. E., Standal, R., and Slupphaug, G. (1997) DNA glycosylases in the base excision repair of DNA. *Biochem. J.* **325**, 1-16.
63. Kubota, Y., Nash, R. A., Klungland, A., Schar, P., Barnes, D. E., and Lindahl, T. (1996) Reconstitution of DNA base excision-repair with purified human proteins: interaction between DNA polymerase beta and the XRCC1 protein. *EMBO J.* **15**, 6662-6670.
64. Laemmli, U. K. (1970) Cleavage of structural proteins during the assembly of the heads of bacteriophage T4. *Nature* **227**, 680-685.
65. Leblanc, J.-P., and Laval, J. (1982) Comparison at the molecular level of uracil-DNA glycosylases from different origins. *Biochimie* **64**, 735-738.
66. Lindahl, T. (1974) An N-glycosidase from *Escherichia coli* that releases free uracil from DNA containing deaminated cytosine residues. *Proc. Natl. Acad. Sci. U.S.A.* **71**, 3649-3653.
67. Lindahl, T. (1976) New class of enzymes acting on damaged DNA. *Nature* **259**, 64-66.
68. Lindahl, T. (1980) Uracil-DNA glycosylase from *Escherichia coli*. *Methods Enzymol.* **65**, 284-290.
69. Lindahl, T., Ljungquist, S., Siebert, W., Nyberg, B., and Sperens, B. (1977) DNA N-glycosidases. Properties of a uracil-DNA glycosidase from *Escherichia coli*. *J. Biol. Chem.* **252**, 3286-3294.
70. Lindahl, T., and Nyberg, B. (1974) Heat-induced deamination of cytosine residues in deoxyribonucleic acid. *Biochemistry* **13**, 3405-3410.
71. Longley, M. J., Pierce, A. J., and Modrich, P. (1997) DNA polymerase delta is required for human mismatch repair in vitro. *J. Biol. Chem.* **272**, 10917-10921.

72. Longley, M. J., Prasad, R., Srivastava, D. K., Wilson, S. H., and Copeland, W. C. (1998) Identification of 5'-deoxyribose phosphate lyase activity in human DNA polymerase gamma and its role in mitochondrial base excision repair in vitro. *Proc. Natl. Acad. Sci. U.S.A.* **95**, 12244-12248.
73. Longley, M. J., Ropp, P. A., Lim, S. E., and Copeland, W. C. (1998) Characterization of the native and recombinant catalytic subunit of human DNA polymerase gamma: identification of residues critical for exonuclease activity and dideoxynucleotide sensitivity. *Biochemistry* **37**, 10529-10539.
74. Lundquist, A. J., Beger, R. D., Bennett, S. E., Bolton, P. H., and Mosbaugh, D. W. (1997) Site-directed mutagenesis and characterization of uracil-DNA glycosylase inhibitor protein. *J. Biol. Chem.* **272**, 21408-21419.
75. Maniatis, T., Fritsch, E. F., and Sambrook, J. (1982) *Molecular cloning: a laboratory manual.*, Cold Spring Harbor Laboratory, Cold Spring Harbor, NY.
76. Matsumoto, Y., and Kim, K. (1995) Excision of deoxyribose phosphate residues by DNA polymerase beta during DNA repair. *Science* **269**, 699-702.
77. Matsumoto, Y., Kim, K., and Bogenhagen, D. F. (1994) Proliferating cell nuclear antigen-dependent abasic site repair in *Xenopus laevis* oocytes: an alternative pathway of base excision DNA repair. *Mol. Cell Biol.* **14**, 6187-6197.
78. Merchant, K., Chen, H., Gonzales, T. C., Keefer, L. K., and Shaw, B. R. (1996) Deamination of single-stranded DNA cytosine residues in aerobic nitric oxide solution at micromolar total NO exposures. *Chem. Res. Toxicol.* **9**, 891-896.
79. Mol, C. D., Arvai, A. S., Sanderson, R. J., Slupphaug, G., Kavli, B., Krokan, H. E., Mosbaugh, D. W., and Tainer, J. A. (1995) Crystal structure of human uracil-DNA glycosylase in complex with a protein inhibitor: protein mimicry of DNA. *Cell* **82**, 701-708.
80. Mol, C. D., Arvai, A. S., Slupphaug, G., Kavli, B., Alseth, I., Krokan, H. E., and Tainer, J. A. (1995) Crystal structure and mutational analysis of human uracil-DNA glycosylase: structural basis for specificity and catalysis. *Cell* **80**, 869-878.
81. Mosbaugh, D. W., and Bennett, S. E. (1994) Uracil-excision DNA repair. *Prog. Nucleic Acid Res. Mol. Biol.* **48**, 315-370.

82. Mosbaugh, D. W., and Linn, S. (1980) Further characterization of human fibroblast apurinic/apyrimidinic DNA endonucleases. The definition of two mechanistic classes of enzyme. *J. Biol. Chem.* **255**, 11743-11752.
83. Mosbaugh, D. W., and Linn, S. (1982) Characterization of the action of *Escherichia coli* DNA polymerase I at incisions produced by repair endodeoxyribonucleases. *J. Biol. Chem.* **257**, 575-583.
84. Mosbaugh, D. W., and Linn, S. (1983) Excision repair and DNA synthesis with a combination of HeLa DNA polymerase beta and DNase V. *J. Biol. Chem.* **258**, 108-118.
85. Muller, S. J., and Caradonna, S. (1991) Isolation and characterization of a human cDNA encoding uracil-DNA glycosylase. *Biochim. Biophys. Acta* **1088**, 197-207.
86. Muller, S. J., and Caradonna, S. (1993) Cell cycle regulation of a human cyclin-like gene encoding uracil-DNA glycosylase. *J. Biol. Chem.* **268**, 1310-1319.
87. Muller-Weeks, S., Mastran, B., and Caradonna, S. (1998) The nuclear isoform of the highly conserved human uracil-DNA glycosylase is an M_r 36,000 phosphoprotein. *J. Biol. Chem.* **273**, 21909-21917.
88. Muller-Weeks, S. J., and Caradonna, S. (1996) Specific association of cyclin-like uracil-DNA glycosylase with the proliferating cell nuclear antigen. *Exp. Cell Res.* **226**, 346-355.
89. Nagelhus, T. A., Slupphaug, G., Lindmo, T., and Krokan, H. E. (1995) Cell cycle regulation and subcellular localization of the major human uracil-DNA glycosylase. *Exp. Cell. Res.* **220**, 292-297.
90. Nealon, K., Nicholl, I. D., and Kenny, M. K. (1996) Characterization of the DNA polymerase requirement of human base excision repair. *Nucleic Acid Res.* **24**, 3763-3770.
91. Neddermann, P., Gallinari, P., Lettieri, T., Schmid, D., Truong, O., Hsuan, J. J., Wiebauer, K., and Jiricny, J. (1996) Cloning and expression of human G/T mismatch-specific thymine-DNA glycosylase. *J. Biol. Chem.* **271**, 12767-12774.
92. Neddermann, P., and Jiricny, J. (1993) The purification of a mismatch-specific thymine-DNA glycosylase from HeLa cells. *J. Biol. Chem.* **268**, 21218-21224.

93. Neddermann, P., and Jiricny, J. (1994) Efficient removal of uracil from G.U mispairs by the mismatch-specific thymine DNA glycosylase from HeLa cells. *Proc. Natl. Acad. Sci. U.S.A.* **91**, 1642-1646.
94. Nicholl, I. D., Nealon, K., and Kenny, M. K. (1997) Reconstitution of human base excision repair with purified proteins. *Biochemistry* **36**, 7557-7566.
95. Nilsen, H., Otterlei, M., Haug, T., Solum, K., Nagelhus, T. A., Skorpen, F., and Krokan, H. E. (1997) Nuclear and mitochondrial uracil-DNA glycosylases are generated by alternative splicing and transcription from different positions in the *UNG* gene. *Nucleic Acids Res.* **25**, 750-755.
96. Nilsen, H., Yazdankhah, S. P., Eftedal, I., and Krokan, H. E. (1995) Sequence specificity for removal of uracil from U:A pairs and U:G mismatches by uracil-DNA glycosylase from *Escherichia coli*, and correlation with mutational hotspots. *FEBS Lett.* **362**, 205-209.
97. O'Connor, T. R., and Laval, J. (1989) Physical association of the 2,6-diamino-4-hydroxy-5N- formamidopyrimidine-DNA glycosylase of *Escherichia coli* and an activity nicking DNA at apurinic/apyrimidinic sites. *Proc. Natl. Acad. Sci. U.S.A.* **86**, 5222-5226.
98. O'Donovan, G. A., Edlin, G., Fuchs, J. A., Neuhaard, J., and Thomassen, E. (1971) Deoxycytidine triphosphate deaminase: characterization of an *Escherichia coli* mutant deficient in the enzyme. *J. Bacteriol.* **105**, 666-672.
99. Olivera, B. M. (1978) DNA intermediates at the *Escherichia coli* replication fork: effect of dUTP. *Proc. Natl. Acad. Sci. U.S.A.* **75**, 238-242.
100. Olsen, L. C., Aasland, R., Wittwer, C. U., Krokan, H. E., and Helland, D. E. (1989) Molecular cloning of human uracil-DNA glycosylase, a highly conserved DNA repair enzyme. *EMBO J.* **8**, 3121-3125.
101. Otterlei, M., Haug, T., Nagelhus, T. A., Slupphaug, G., Lindmo, T., and Krokan, H. E. (1998) Nuclear and mitochondrial splice forms of human uracil-DNA glycosylase contain a complex nuclear localisation signal and a strong classical mitochondrial localisation signal, respectively. *Nucleic Acids Res.* **26**, 4611-4617.
102. Panayotou, G., Brown, T., Barlow, T., Pearl, L. H., and Savva, R. (1998) Direct measurement of the substrate preference of uracil-DNA glycosylase. *J. Biol. Chem.* **273**, 45-50.
103. Parikh, S. P., Mol, C.D., Slupphaug, G., Bharati, S., Krokan, H.E., and Tainer, J.A. (1998) Base excision repair initiation revealed by crystal structures and binding kinetics of human uracil-DNA glycosylase with DNA. *EMBO J.* **17**, 5214-5226.

104. Pelletier, H., Sawaya, M. R., Wolfle, W., Wilson, S. H., and Kraut, J. (1996) Crystal structures of human DNA polymerase beta complexed with DNA: implications for catalytic mechanism, processivity, and fidelity. *Biochemistry* **35**, 12742-12761.
105. Pinz, K. G., and Bogenhagen, D. F. (1998) Efficient repair of abasic sites in DNA by mitochondrial enzymes. *Mol. Cell Biol.* **18**, 1257-1265.
106. Podust, L. M., Podust, V. N., Floth, C., and Hubscher, U. (1994) Assembly of DNA polymerase delta and epsilon holoenzymes depends on the geometry of the DNA template. *Nucleic Acids Res.* **22**, 2970-2975.
107. Prasad, R., Singhal, R. K., Srivastava, D. K., Molina, J. T., Tomkinson, A. E., and Wilson, S. H. (1996) Specific interaction of DNA polymerase beta and DNA ligase I in a multiprotein base excision repair complex from bovine testis. *J. Biol. Chem.* **271**, 16000-16007.
108. Price, A. R., and Fogt, S. M. (1973) Deoxythymidylate phosphohydrolase induced by bacteriophage PBS2 during infection of *Bacillus subtilis*. *J. Biol. Chem.* **248**, 1372-1380.
109. Price, A. R., and Frato, J. (1975) *Bacillus subtilis* deoxyuridinetriphosphatase and its bacteriophage PBS2- induced inhibitor. *J. Biol. Chem.* **250**, 8804-8811.
110. Putnam, C. D., Shroyer, M. J. N., Lundquist, A. J., Mol, C. D., Arvai, A. S., Mosbaugh, D. W., and Tainer, J. A. (1999) Protein mimicry of DNA from crystal structures of the uracil-DNA glycosylase inhibitor protein and its complex with *Escherichia coli* uracil-DNA glycosylase. *J. Mol. Biol.* **287**, 331-346.
111. Ravishankar, R., Bidya Sagar, M., Roy, S., Purnapatre, K., Handa, P., Varshney, U., and Vijayan, M. (1998) X-ray analysis of a complex of *Escherichia coli* uracil DNA glycosylase (*EcUDG*) with a proteinaceous inhibitor. The structure elucidation of a prokaryotic UDG. *Nucleic Acids. Res.* **26**, 4880-4887.
112. Sanderson, R. J., and Mosbaugh, D. W. (1998) Fidelity and mutational specificity of uracil-initiated base excision DNA repair synthesis in human glioblastoma cell extracts. *J. Biol. Chem.* **273**, 24822-24831.
113. Sandigursky, M., and Franklin, W. A. (1999) Thermostable uracil-DNA glycosylase from *Thermotoga maritima* a member of a novel class of DNA repair enzymes. *Curr. Biol.* **9**, 531-534.

114. Sandigursky, M., Freyer, G. A., and Franklin, W. A. (1998) The post-incision steps of the DNA base excision repair pathway in *Escherichia coli*: studies with a closed circular DNA substrate containing a single U:G base pair. *Nucleic Acids Res.* **26**, 1282-1287.
115. Saparbaev, M., and Laval, J. (1998) 3,N4-ethenocytosine, a highly mutagenic adduct, is a primary substrate for *Escherichia coli* double-stranded uracil-DNA glycosylase and human mismatch-specific thymine-DNA glycosylase. *Proc. Natl. Acad. Sci. U.S.A.* **95**, 8508-8513.
116. Savva, R., McAuley-Hecht, K., Brown, T., and Pearl, L. (1995) The structural basis of specific base-excision repair by uracil-DNA glycosylase. *Nature* **373**, 487-493.
117. Savva, R., and Pearl, L. H. (1995) Nucleotide mimicry in the crystal structure of the uracil-DNA glycosylase-uracil glycosylase inhibitor protein complex. *Nat. Struct. Biol.* **2**, 752-757.
118. Schuster, H. (1960) The reaction of nitrous acid with deoxyribonucleic acid. *Biochem. Biophys. Res. Commun.* **2**, 320-323.
119. Shapiro, R., and Klein, R. S. (1966) The deamination of cytidine and cytosine by acidic buffer solutions. Mutagenic implications. *Biochemistry* **5**, 2358-2362.
120. Shlomai, J., and Kornberg, A. (1978) Deoxyuridine triphosphatase of *Escherichia coli*. Purification, properties, and use as a reagent to reduce uracil incorporation into DNA. *J. Biol. Chem.* **253**, 3305-3312.
121. Shroyer, M. J., Bennett, S. E., Putnam, C. D., Tainer, J. A., and Mosbaugh, D. W. (1999) Mutation of an active site residue in *Escherichia coli* uracil-DNA glycosylase: effect on DNA binding, uracil inhibition and catalysis. *Biochemistry* **38**, 4834-4845.
122. Sibghat, U., Gallinari, P., Xu, Y. Z., Goodman, M. F., Bloom, L. B., Jiricny, J., and Day, R. S. r. (1996) Base analog and neighboring base effects on substrate specificity of recombinant human G:T mismatch-specific thymine DNA-glycosylase. *Biochemistry* **35**, 12926-12932.
123. Singhal, R. K., Prasad, R., and Wilson, S. W. (1995) DNA polymerase beta conducts the gap-filling step in uracil-initiated base excision repair in a bovine testis nuclear extract. *J. Biol. Chem.* **270**, 949-957.
124. Singhal, R. K., and Wilson, S. H. (1993) Short gap-filling synthesis by DNA polymerase beta is processive. *J. Biol. Chem.* **268**, 15906-15911.

125. Slupphaug, G., Eftedal, I., Kavli, B., Bharati, S., Helle, N. M., Haug, T., Levine, D. W., and Krokan, H. E. (1995) Properties of a recombinant human uracil-DNA glycosylase from the *UNG* gene and evidence that *UNG* encodes the major uracil-DNA glycosylase. *Biochemistry* **34**, 128-138.
126. Slupphaug, G., Markussen, F.-H., Olsen, L. C., Aasland, R., Aarsaether, N., Bakke, O., Krokan, H. E., and Helland, D. E. (1993) Nuclear and mitochondrial forms of human uracil-DNA glycosylase are encoded by the same gene. *Nucleic Acids Res.* **21**, 2579-2584.
127. Slupphaug, G., Mol, C. D., Kavli, B., Arvai, A. S., Krokan, H. E., and Tainer, J. A. (1996) A nucleotide-flipping mechanism from the structure of human uracil-DNA glycosylase bound to DNA. *Nature* **384**, 87-92.
128. Slupphaug, G., Olsen, L. C., Helland, D., Aasland, R., and Krokan, H. E. (1991) Cell cycle regulation and *in vitro* hybrid arrest analysis of the major human uracil-DNA glycosylase. *Nucleic Acids Res.* **19**, 5131-5137.
129. Sobol, R. W., Horton, J. K., Kuhn, R., Gu, H., Singhal, R. K., Prasad, R., Rajewsky, K., and Wilson, S. H. (1996) Requirement of mammalian DNA polymerase-beta in base excision repair. *Nature* **379**, 183-186.
130. Stucki, M., Pascucci, B., Parlanti, E., Fortini, P., Wilson, S. H., Hubscher, U., and Dogliotti, E. (1998) Mammalian base excision repair by DNA polymerases delta and epsilon. *Oncogene* **17**, 835-843.
131. Takahashi, I., and Marmur, J. (1963) Replacement of thymidylic acid by deoxyuridylic acid in the deoxyribonucleic acid of a transducing phage for *Bacillus subtilis*. *Nature* **197**, 794-795.
132. Tessman, I., and Kennedy, M. A. (1991) The two-step model of UV mutagenesis reassessed: deamination of cytosine as the likely source of the mutations associated with deamination. *Mol. Gen. Genet.* **227**, 144-148.
133. Timmer, R. T. (1989) *In vitro* rat liver mitochondrial DNA repair: Examination of the product inhibition of uracil-DNA glycosylase and demonstration of an apurinic/apyrimidinic endonuclease. *Thesis*. University of Texas at Austin, Austin, Texas.
134. Tomita, F., and Takahashi, I. (1969) A novel enzyme, dCTP deaminase, found in *Bacillus subtilis* infected with phage PBS1. *Biochim. Biophys. Acta* **179**, 18-27.

135. Tsai-Wu, J. J., Liu, H. F., and Lu, A. L. (1992) *Escherichia coli* MutY protein has both N-glycosylase and apurinic/apyrimidinic endonuclease activities on A.C and A.G mispairs. *Proc. Natl. Acad. Sci. U.S.A.* **89**, 8779-8783.
136. Tye, B.-K., Chien, J., Lehman, I. R., Duncan, B. K., and Warner, H. R. (1978) Uracil incorporation: a source of pulse-labeled DNA fragments in the replication of the *Escherichia coli* chromosome. *Proc. Natl. Acad. Sci. U.S.A.* **75**, 233-237.
137. Tye, B.-K., and Lehman, I. R. (1977) Excision repair of uracil incorporated in DNA as a result of a defect in dUTPase. *J. Mol. Biol.* **117**, 293-306.
138. Tye, B.-K., Nyman, P.-O., Lehman, I. R., Hochhauser, S., and Weiss, B. (1977) Transient accumulation of Okazaki fragments as a result of uracil incorporation into nascent DNA. *Proc. Natl. Acad. Sci. U.S.A.* **74**, 154-157.
139. Ullman, J. S., and McCarthy, B. J. (1973) Alkali deamination of cytosine residues in DNA. *Biochim. Biophys. Acta* **294**, 396-404.
140. Upton, C., Stuart, D. T., and McFadden, G. (1993) Identification of a poxvirus gene encoding a uracil DNA glycosylase. *Proc. Natl. Acad. Sci. U.S.A.* **90**, 4518-4522.
141. Varshney, U., Hutcheon, T., and van de Sande, J. H. (1988) Sequence analysis, expression, and conservation of *Escherichia coli* uracil-DNA glycosylase and its gene (ung). *J. Biol. Chem.* **263**, 7776-7784.
142. Varshney, U., and van de Sande, J. H. (1991) Specificities and kinetics of uracil excision from uracil-containing DNA oligomers by *Escherichia coli* uracil DNA glycosylase. *Biochemistry* **30**, 4055-4061.
143. Wang, Z., and Mosbaugh, D. W. (1989) Uracil-DNA glycosylase inhibitor gene of bacteriophage PBS2 encodes a binding protein specific for uracil-DNA glycosylase. *J. Biol. Chem.* **264**, 1163-1171.
144. Wang, Z., Smith, D. G., and Mosbaugh, D. W. (1991) Overproduction and characterization of the uracil-DNA glycosylase inhibitor of bacteriophage PBS2. *Gene* **99**, 31-37.
145. Ward, D. C., Reich, E., and Stryer, L. (1969) Fluorescence studies of nucleotides and polynucleotides. I. Formycin, 2-aminopurine riboside, 2,6-diaminopurine riboside, and their derivatives. *J. Biol. Chem.* **244**, 1228-1237.

146. Warner, H. R., Demple, B. F., Deutsch, W. A., Kane, C. M., and Linn, S. (1980) Apurinic/apyrimidinic endonucleases in repair of pyrimidine dimers and other lesions in DNA. *Proc. Natl. Acad. Sci. U.S.A.* **77**, 4602-4606.
147. Warner, H. R., Duncan, B. K., Garrett, C., and Neuhaud, J. (1981) Synthesis and metabolism of uracil-containing deoxyribonucleic acid in *Escherichia coli*. *J. Bacteriol.* **145**, 687-695.
148. Waters, T. R., Gallinari, P., Jiricny, J., and Swann, P. F. (1999) Human thymine DNA glycosylase binds to apurinic sites in DNA but is displaced by human apurinic endonuclease 1. *J. Biol. Chem.* **274**, 67-74.
149. Waters, T. R., and Swann, P. F. (1998) Kinetics of the action of thymine DNA glycosylase. *J. Biol. Chem.* **273**, 20007-20014.
150. Wiebauer, K., and Jiricny, J. (1989) In vitro correction of G.T mispairs to G.C pairs in nuclear extracts from human cells. *Nature* **339**, 234-236.
151. Wiebauer, K., and Jiricny, J. (1990) Mismatch-specific thymine DNA glycosylase and DNA polymerase beta mediate the correction of G.T mispairs in nuclear extracts from human cells. *Proc. Natl. Acad. Sci. U.S.A.* **87**, 5842-5845.
152. Winters, T. A., and Williams, M. V. (1990) Use of the PBS2 uracil-DNA glycosylase inhibitor to differentiate the uracil-DNA glycosylase activities encoded by herpes simplex virus types 1 and 2. *J. Virol. Methods* **29**, 233-242.
153. Xiao, G., Tordova, M., Jagadeesh, J., Drohat, A. C., Stivers, J. T., and Gilliland, G. L. (1999) Crystal structure of *Escherichia coli* uracil DNA glycosylase and its complexes with uracil and glycerol: structure and glycosylase mechanism revisited. *Proteins* **35**, 13-24.
154. Yanisch-Perron, C., Vieira, J., and Messing, J. (1985) Improved M13 phage cloning vectors and host strains: nucleotide sequence of the M13mp18 and pUC19 vectors. *Gene* **33**, 103-119.